Universitat
de les Illes Balears

COMPLEX DYNAMICS IN POWER GRIDS

Eder Batista Tchawou Tchuisseu

Doctoral Thesis

Universitat de les Illes Balears

2018

Universitat
de les Illes Balears

COMPLEX DYNAMICS IN POWER GRIDS

Thesis submitted by

Eder Batista Tchawou Tchuisseu

to the

Doctoral Program in Physics

of the

Universitat de les Illes Balears

for the degree of

Doctor in *Physics*

Doctoral advisors:

Dr. Damià Gomila

Prof. Pere Colet

Doctoral Tutor:

Prof. Claudio Mirasso

Universitat de les Illes Balears

2018

COMPLEX DYNAMICS IN POWER GRIDS

Eder Batista Tchawou Tchuisseu
Instituto de Física Interdisciplinar y Sistemas Complejos (IFISC)
Universitat de les Illes Balears (UIB)
Consejo Superior de Investigaciones Científicas (CSIC)

PhD Thesis

Doctoral advisors: Dr. Damià Gomila and Prof. Pere Colet

For an updated version of this document, please visit http://ifisc.uib-csic.es/ or contact the author at ederbatista@ifisc.uib-csic.es or tchawou@gmail.com

Document typeset in *Latin Modern* using LaTeX 2ε

WE,

Damià Gomila and Pere Colet,
Professors of the Universitat de les Illes Balears,

DECLARE

that the thesis entitled "*COMPLEX DYNAMICS IN POWER GRIDS*", submitted by Eder Batista Tchawou Tchuisseu to the Doctoral Program in Physics of the Universitat de les Illes Balears in partial fulfillment of the requirements for the degree of Doctor in Physics, has been completed under our supervision and meets the requirements for the International Mention.

Palma de Mallorca, 27th July 2018.

Dr. Damià Gomila
Advisor

Prof. Pere Colet
Advisor

Eder Batista Tchawou Tchuisseu
Candidate

Abstract

The electric power grid is a complex interconnected network designed to deliver electricity from suppliers to consumers. It is the largest human-made infrastructure ever built, and it is at the center of our daily life. The complexity of the electric grid comes from the number of components interacting directly or indirectly in the network, such as generators, consumers, transformers, circuit breakers, relays, transmission lines, retailers, nature and the environment. The electric grid can be seen as the circulatory system of the society. The electricity (blood) is produced at the generators (heart) which pushes it (pumps) into the transmission lines (arteries and veins), which transport and distribute it to the end users or consumers (organs). The modern electric network increasingly combines new types of generation units powered by renewable energy sources (wind, water, and solar), which are all dependent of the weather and therefore unpredictable and fluctuating. As an important and essential part of our lives the electric network should be well understood and analyzed, in order to make it reliable, robust and safe for the users. It is well known that instabilities in the electric grid can arise through frequency or voltage unbalances, or due to a line breaking. Much research has been devoted to the modeling and control of the stability of the grid. Most of it it's focused on the frequency and voltage angle stabilization using diverse algorithms and control methods. Other works built up methods for understanding and analyzing the propagation of blackouts in the electric network.

The main purpose of this thesis is first to understand the dynamics of the grid in presence of decentralized frequency control directly included in the electric devices. We first consider the case of a single power plant and then extend the study to the case of a network. Second, this thesis aims to analyze the propagation of either blackouts or line outages in a situation where the electric consumption is controlled. To these ends, we model a realistic electric power grid using mathematical tools and computational methods.

The first step to model the power grid is the modeling of the power plant, which roughly speaking is composed of a generator and frequency and voltage regulators. The power plant model is based on the second Newton's law for a rotating body. The obtained equation, also known as swing equation, gives the time variation of the frequency of the grid as a result of the unbalance between the mechanical and the electrical power. The swing equation is then combined with the frequency regulator model. The frequency regulation considered here is composed by the load frequency control (LFC) which is the primary control and the automatic generation control (AGC), also referred to as secondary control. It is shown that after any deviation the frequency is brought back to its reference value thanks to the LFC and the AGC. The voltage regulation is not considered in this thesis and the voltage is assumed to be always constant. Second, we propose a very simple stochastic demand model able to reproduce the main statistical properties of real demand fluctuations. This stochastic model corresponds exactly to a Markov process for a system composed of N particles, each one making transitions between two states (on, off) with a certain rate p. The frequency fluctuations arising from such model adjusting only the switching rate p are close enough to the real frequency fluctuations measured in the Balearic island grid as to validate the model.

The power grid frequency control is a demanding task requiring expensive idle power plants to adapt the supply to the fluctuating demand. An alternative approach is controlling the demand side in such a way that certain appliances modify their operation to adapt to the power availability. This is especially important to enable a high penetration of renewable energy sources. A number of methods to manage the demand side have been proposed. In this work we focus on dynamic demand control (DDC), where smart appliances can delay their switchings depending on the frequency of the system. We first introduce DDC in the proposed simple model to study its effects on the frequency of the power grid. We find that DDC can reduce small and medium-size fluctuations but it can also increase the probability of observing large frequency peaks due to the necessity of recovering pending tasks. Although these events (large frequency peaks) are very rare they can potentially trigger a failure of the system, and therefore strategies to avoid them have to be addressed. We then introduce a new method including communication among DDC devices belonging to a given group, such that they can coordinate opposite actions to keep the group demand more stable. We show that for this method the amount of pending tasks decreases by a factor 10 while large frequency fluctuations are significantly reduced or even completely avoided. Extending the study to the case of a simple network, we show that in addition to the reduction of the frequency fluctuations observed in each node, DDC smooths out the fluctuations of the phase differences between generators. Furthermore, we show that in the case of a sudden breaking of a line, smart devices adapt their consumption according to the outage in the network. This is not the case in the

uncontrolled network.

Regarding the effects of control on a network, we have also studied how secondary control may help to prevent an effect called Braess' paradox. Nowadays, the integration of renewable energy sources requires grid extensions and sophisticated control actions on different time scales to cope with short-term fluctuations and a long-term power imbalance. Braess' paradox constitutes a counterintuitive collective phenomenon that occurs if adding a new transmission line to a network increases loads on some other lines, effectively reducing the system's performance and potentially even entirely halting its operating state. Combining simple analytical considerations with numerical investigations on a simple network, we study the dynamical consequences of secondary control in a AC power grid model. We show that control applied to all nodes provides dynamical stability to the system and cures Braess' paradox, while control applied only to generator nodes has a limited efficiency which depends on the grid topology. Our results highlight the importance of demand control in conjunction with grid topology for stable operation and reveal a new functional benefit of secondary control.

Finally we address the issue of cascading failures in a realistic model for the electricity dispatch in the power grid. The components of the power grid are interconnected in such a way that any failure can propagate, affecting neighboring elements of the network if nothing is done to isolate the faulty element or the affected region. The understanding of cascading failures constitutes an important challenge in the electric network control community, and it is primordial for the grid's safety and the economic development of a society. Several models have been proposed to address this problem. Among them, the ORNL-Pserc-Alaska (OPA) model, which is a model proposed by researchers and engineers from Oak Ridge National Laboratory (ORNL), Power System Engineering Research Center of Wisconsin University (PSerc), and Alaska University (Alaska) to study and understand cascading failures and blackouts. We study here the cascading failures on a small network of hundred nodes using the OPA model in which we introduce power fluctuations and DDC. We observe that the complementary cumulative distribution function of the blackout sizes has a tail showing a power law characteristic, both with and without DDC. We also observe a reduction in the number of overloaded lines and blackouts in presence of DDC as compared to the case without control. DDC shifts blackouts from peak hours to valley time, where pending tasks are recovered. Although the number of blackouts is reduced, the probability of observing a large one at valley time is higher than without control, a similar phenomena to that observed in the case of the AC network.

Resumen

La red eléctrica es un complejo interconectado diseñado para entregar electricidad de los proveedores a los consumidores. Es la infraestructura humana más grande jamás construida, y está en el centro de nuestra vida diaria. La complejidad de la red eléctrica proviene del número de componentes que interactúan directa o indirectamente en la red, como generadores, consumidores, transformadores, relés, líneas de transmisión, comercializadoras, naturaleza y el medioambiente. La red eléctrica se puede ver como el sistema circulatorio de la sociedad. La electricidad (sangre) se produce en los generadores (corazón) que la empujan (bombas) hacia las líneas de transmisión (arterias y venas), que la transportan y la distribuyen a los usuarios finales o consumidores (órganos). La red eléctrica moderna combina cada vez más un nuevo tipo de unidades de generación alimentadas por fuentes de energía renovables (eólica, solar y de agua), todas ellas dependientes del clima y, por lo tanto, impredecibles y fluctuantes. Como parte importante y esencial de nuestras vidas, la red eléctrica debe ser bien comprendida y analizada para que sea confiable, robusta y segura para los usuarios. Es bien sabido que las inestabilidades en la red eléctrica pueden aparecer a través de desequilibrios de frecuencia o voltaje, o debido a la ruptura de una línea u otro componente. Se han dedicado muchas investigaciones al modelado y al control de la estabilidad de la red. La mayor parte se centra en la frecuencia y la estabilización del voltaje utilizando diversos algoritmos y métodos de control. Otros trabajos construyen métodos para comprender y analizar la propagación de apagones en la red eléctrica.

El objetivo principal de esta tesis es, primero, comprender la dinámica de la red en presencia de control de frecuencia descentralizado incluido directamente en los dispositivos eléctricos. Primero consideramos el caso de una sola central eléctrica y luego ampliamos el estudio al caso de una red. En segundo lugar, esta tesis tiene como objetivo analizar la propagación de apagones o cortes de línea en una situación en la que se controla el consumo eléctrico. Para estos fines, modelamos una red eléctrica realista utilizando herramientas matemáticas y métodos computacionales.

El primer paso para modelar la red eléctrica es el modelado de la central eléctrica, que en términos generales está compuesta por un generador y los reguladores de frecuencia y voltaje. El modelo de la central eléctrica se basa en la segunda ley de Newton para un cuerpo en rotación. La ecuación obtenida, también conocida como "swing equation", relaciona la variación de la frecuencia de la red con el desequilibrio entre la potencia eléctrica y la mecánica. Esta ecuación se combina luego con el modelo del regulador de frecuencia. La regulación de frecuencia considerada aquí está compuesta por el control de frecuencia de carga (LFC) que es el control primario y el control de generación automático (AGC), también considerado como control secundario. Se muestra que después de cualquier desviación la frecuencia vuelve a su valor de referencia gracias al LFC y al AGC. La regulación de voltaje no se considera en esta tesis y se supone que la tensión es siempre constante. En segundo lugar proponemos un modelo de demanda estocástica muy simple capaz de reproducir las principales propiedades estadísticas de las fluctuaciones de la demanda real. Este modelo estocástico corresponde exactamente a un proceso de Markov para un sistema compuesto por N partículas, cada una haciendo transiciones entre dos estados (encendido, apagado) con una cierta tasa p. Las fluctuaciones de frecuencia que crea dicho modelo ajustando únicamente la tasa de encendido y apagado p son lo suficientemente similares a las fluctuaciones de frecuencia reales medidas en la red de islas de Baleares mediante como para considerarlo un modelo válido.

El control de frecuencia de la red eléctrica es una tarea exigente que requiere costosas plantas de generación de reserva para adaptar el suministro a la demanda fluctuante. Un enfoque alternativo es controlar el lado de la demanda de tal manera que ciertos dispositivos modifiquen su funcionamiento para adaptarse a la disponibilidad de energía. Esto es especialmente importante para lograr una alta penetración de fuentes de energía renovables. Se han propuesto varios métodos para gestionar el lado de la demanda. En este trabajo nos centramos en el control dinámico de la demanda (DDC por sus siglas en inglés), donde los dispositivos inteligentes pueden retrasar sus conmutaciones dependiendo de la frecuencia del sistema. Primero introducimos DDC en el modelo simple propuesto para estudiar sus efectos en la frecuencia de la red eléctrica. Encontramos que el DDC puede reducir las fluctuaciones de tamaño pequeño y mediano, pero también puede aumentar la probabilidad de observar grandes picos de frecuencia debido a la necesidad de recuperar tareas pendientes. Aunque estos eventos (grandes picos de frecuencia) son muy raros, pueden desencadenar un fallo del sistema y, por lo tanto, deben abordarse estrategias para evitarlos. Después, presentamos un nuevo método que incluye comunicación entre dispositivos DDC pertenecientes a un grupo determinado, de forma que puedan coordinar acciones opuestas para mantener la demanda del grupo más estable. Mostramos que para este método la cantidad de tareas pendientes disminuye en un factor de 10, mientras que las grandes fluctuaciones de frecuencia se reducen significativamente o incluso se evi-

tan por completo. Extendiendo el estudio al caso de una red simple, mostramos que además de la reducción de las fluctuaciones de frecuencia observadas en cada nodo, el DDC suaviza las fluctuaciones de las diferencias de fase entre los generadores. Además, mostramos que en el caso de una interrupción repentina de una línea, los dispositivos inteligentes adaptan su consumo de acuerdo con la interrupción en la red. Esto no sucede en la red sin control.

Con respecto a los efectos del control en una red, también hemos estudiado cómo el control secundario puede ayudar a prevenir la llamada paradoja de Braess. Hoy en día la integración de las fuentes de energía renovables requiere extensiones de la red y acciones de control sofisticadas en diferentes escalas de tiempo para hacer frente a las fluctuaciones a corto plazo y el desequilibrio de potencia a largo plazo. La paradoja de Braess constituye un fenómeno colectivo contraintuitivo que se produce si al agregar una nueva línea de transmisión a una red aumenta la carga en otras líneas, lo que reduce de manera efectiva el rendimiento del sistema o incluso puede impedir completamente su funcionamiento. Combinando consideraciones analíticas con investigaciones numéricas en una red simple, estudiamos las consecuencias dinámicas del control secundario en un modelo de red eléctrica de corriente alterna. Demostramos que aplicando control a todos los nodos proporciona estabilidad dinámica al sistema y cura la paradoja de Braess, mientras que si el control se aplica sólo a los nodos generadores su eficacia es limitada y depende de la topología de la red. Nuestros resultados resaltan la importancia del control de la demanda junto con la topología de la red para un funcionamiento estable, y revelan un nuevo beneficio funcional del control secundario.

Finalmente abordamos el problema de los fallos en cascada en un modelo realista del despacho de electricidad en la red eléctrica. Los componentes de la red eléctrica están interconectados de forma tal que cualquier fallo puede propagarse, afectando los elementos vecinos de la red si no se hace nada para aislar el elemento defectuoso o la región afectada. La comprensión de los fallos en cascada constituye un desafío importante en la comunidad de control de la red eléctrica, y es primordial para la seguridad de la red y el desarrollo económico de una sociedad. Se han propuesto varios modelos para abordar este problema. Entre ellos, el modelo ORNL-PSerc-Alaska (OPA), que es un modelo propuesto por investigadores e ingenieros del Oak Ridge National Laboratory (ORNL), Power System Engineering Research Center de la Universidad de Wisconsin (PSerc) y la Universidad de Alaska (Alaska) para estudiar y comprender fallos y apagones en cascada. Aquí estudiamos los fallos en cascada en una pequeña red de cientos de nodos utilizando el modelo OPA en el que hemos añadido fluctuaciones de potencia y DDC. Observamos que la función de distribución acumulativa complementaria del tamaño de los apagones tiene una cola que muestra una característica de la ley de potencia, ambos con y sin DDC. También observamos una reducción del número de lineas sobrecargadas y apagones en presencia de DDC en comparación

con el caso sin control. DDC desplaza los apagones de las horas pico a las horas valle, donde se recuperan las tareas pendientes. Aunque se reduce el número de apagones, la probabilidad de observar uno grande en horas valle es mayor que sin control, un fenómeno similar al observado en el caso de la red de corriente alterna.

Resum

La xarxa elèctrica és un complex interconnectat dissenyat per lliurar electricitat dels proveïdors als consumidors. És la infraestructura humana més gran mai construïda, i està al centre de la nostra vida diària. La complexitat de la xarxa elèctrica prové del nombre de components que interactuen directament o indirectament a la xarxa, com a generadors, consumidors, transformadors, relés, línies de transmissió, comercialitzadores, la naturalesa i el medi ambient. La xarxa elèctrica es pot veure com el sistema circulatori de la societat. L'electricitat (sang) es produeix en els generadors (cor) que l'empenyen (bombes) cap a les línies de transmissió (artèries i venes), que la transporten i la distribueixen als usuaris finals o consumidors (òrgans). La xarxa elèctrica moderna combina cada vegada més un nou tipus d'unitats de generació alimentades per fonts d'energia renovables (eòlica, solar i d'aigua), totes elles dependents del clima i, per tant, impredictibles i fluctuants. Com a part important i essencial de les nostres vides, la xarxa elèctrica ha de ser ben compresa i analitzada perquè sigui fiable, robusta i segura per als usuaris. És ben sabut que les inestabilitats a la xarxa elèctrica poden aparèixer a través de desequilibris de freqüència o voltatge, o causa de la ruptura d'una línia o altres components. S'han dedicat moltes investigacions al modelat i al control de l'estabilitat de la xarxa. La major part se centra en la freqüència i l'estabilització del voltatge utilitzant diversos algoritmes i mètodes de control. Altres treballs construeixen mètodes per comprendre i analitzar la propagació d'apagades a la xarxa elèctrica.

L'objectiu principal d'aquesta tesi és, primer, comprendre la dinàmica de la xarxa en presència de control de freqüència descentralitzat inclòs directament en els dispositius elèctrics. Primer considerem el cas d'una sola central elèctrica i després ampliam l'estudi al cas d'una xarxa. En segon lloc, aquesta tesi té com a objectiu analitzar la propagació d'apagades o talls de línia en una situació on es controla el consum elèctric. Per a aquests fins, modelem una xarxa elèctrica realista utilitzant eines matemàtiques i mètodes computacionals.

El primer pas per a modelar la xarxa elèctrica és el modelatge de la central elèctrica, que en termes generals està composta per un generador i els reguladors de freqüència i voltatge. El model de la central elèctrica es basa en la segona llei de Newton per a un cos en rotació. L'equació obtinguda, també coneguda com a "swing equation", relaciona la variació de la freqüència de la xarxa amb el desequilibri entre la potència elèctrica i la mecànica. Aquesta equació es combina després amb el model del regulador de freqüència. La regulació de freqüència considerada aquí està composta pel control de freqüència de càrrega (LFC) que és el control primari i el control de generació automàtic (AGC), també considerat com a control secundari. Es mostra que després de qualsevol desviació, la freqüència torna al seu valor de referència gràcies al LFC i al AGC. La regulació de voltatge no es considera en aquesta tesi i se suposa que la tensió és sempre constant. En segon lloc proposem un model de demanda estocàstica molt simple capaç de reproduir les principals propietats estadístiques de les fluctuacions de la demanda real. Aquest model estocàstic correspon exactament a un procés de Markov per a un sistema compost per N partícules, cadascuna fent transicions entre dos estats (encès, apagat) amb una certa taxa p. Les fluctuacions de freqüència que crea aquest model ajustant únicament la taxa d'encesa i apagada p són prou similars a les fluctuacions de freqüència reals mesurades a la xarxa de les Illes Balears com per considerar-lo un model vàlid.

El control de freqüència de la xarxa elèctrica és una tasca exigent que requereix tenir costoses plantes d'energia preparades per adaptar el subministrament a la demanda fluctuant. Un enfocament alternatiu és controlar el costat de la demanda de tal manera que certs dispositius modifiquin el seu funcionament per adaptar-se a la disponibilitat d'energia. Això és especialment important per aconseguir una alta penetració de fonts d'energia renovable. S'han proposat diversos mètodes per gestionar el costat de la demanda. En aquest treball ens centrem en el control dinàmic de la demanda (DDC per les seves sigles en anglès), on els dispositius intel · ligents poden retardar les seves commutacions depenent de la freqüència del sistema. Primer introduïm DDC en el model simple proposat per estudiar els seus efectes en la freqüència de la xarxa elèctrica. Trobem que el DDC pot reduir les fluctuacions de mida petita i mitjana, però també pot augmentar la probabilitat d'observar grans pics de freqüència a causa de la necessitat de recuperar tasques pendents. Tot i que aquests esdeveniments (grans pics de freqüència) són molt rars, poden desencadenar una fallada del sistema i, per tant, s'han d'abordar estratègies per evitar-los. Després, presentem un nou mètode que inclou comunicació entre dispositius DDC pertanyents a un grup determinat, de manera que puguin coordinar accions oposades per mantenir la demanda del grup més estable. Mostrem que per aquest mètode la quantitat de tasques pendents disminueix en un factor de 10, mentre que les grans fluctuacions de freqüència es redueixen significativament o fins i tot s'eviten completament. Estenent l'estudi al cas d'una xarxa simple, mostram que a més de la reducció de les fluctuacions

de freqüència observades en cada node, el DDC suavitza les fluctuacions de les diferències de fase entre els generadors. A més, mostram que en el cas d'una interrupció sobtada d'una línia, els dispositius intel · ligents adapten el seu consum d'acord amb la interrupció a la xarxa. Això no succeeix a la xarxa sense control.

Pel que fa als efectes del control en una xarxa, també hem estudiat com el control secundari pot ajudar a prevenir l'anomenada paradoxa de Braess. Avui dia la integració de les fonts d'energia renovables requereix extensions de la xarxa i accions de control sofisticades a diferents escales de temps per fer front a les fluctuacions a curt termini i el desequilibri de potència a llarg termini. La paradoxa de Braess constitueix un fenomen col · lectiu contraintuïtiu que es produeix si l'agregar una nova línia de transmissió a una xarxa augmenta la càrrega en altres línies, el que redueix de manera efectiva el rendiment del sistema o fins i tot pot impedir completament el seu funcionament. Combinant consideracions analítiques amb investigacions numèriques en una xarxa simple, estudiem les conseqüències dinàmiques del control secundari en un model de xarxa elèctrica de corrent altern. Demostram que aplicant control a tots els nodes proporciona estabilitat dinàmica al sistema i cura la paradoxa de Braess, mentre que si el control s'aplica només als nodes generadors la seva eficàcia es limitada i depèn de la topologia de la xarxa. Els nostres resultats ressalten la importància del control de la demanda juntament amb la topologia de la xarxa per a un funcionament estable, i revelen un nou benefici funcional del control secundari.

Finalment abordem el problema de les fallades en cascada en un model realista del despatx d'electricitat a la xarxa elèctrica. Els components de la xarxa elèctrica estan interconnectats de manera que qualsevol error pot propagar-se, afectant als elements veïns de la xarxa si no es fa res per aïllar l'element defectuós o la regió afectada. La comprensió de les fallades en cascada constitueix un desafiament important en la comunitat científica que estudia el control de la xarxa elèctrica, i és primordial per a la seguretat de la xarxa i el desenvolupament econòmic d'una societat. S'han proposat diversos models per abordar aquest problema. Entre ells, el model ORNL-PSerc-Alaska (OPA), que és un model proposat per investigadors i enginyers de l'Oak Ridge National Laboratory (ORNL), Power System Engineering Research Center de la Universitat de Wisconsin (PSerc) i la Universitat d'Alaska (Alaska) per estudiar i comprendre errors i apagades en cascada. Aquí estudiam les fallades en cascada en una petita xarxa de centenars de nodes utilitzant el model OPA en el qual hem afegit fluctuacions de potència i DDC. Observem que la funció de distribució acumulativa complementària de la mida de les apagades té una cua que mostra característiques de llei de potència, tots dos amb i sense DDC. També observem una reducció del nombre de línies sobrecarregades i apagades en presència de DDC en comparació amb el cas sense control. DDC desplaça les apagades de les hores punta a les hores vall, on es recuperen les tasques pendents. Encara que es redueix el nombre d'apagades, la

probabilitat d'observar-ne una de gran en hores vall és més gran que sense control, un fenomen similar a l'observat en el cas de la xarxa de corrent altern.

List of publications

- Tchawou Tchuisseu, E.B., and Woafo, P., (2014). Harvesting energy using a magnetic mass and a sliding behaviour. *Nonlinear Engineering*, 3(2): 89–97.
- Oumbe Tekam, G.T., Tchawou Tchuisseu, E.B., Kitio Kwuimy, C.A., and Woafo, P., (2014). Analysis of an electromechanical energy harvester system with geometric and ferroresonant nonlinearities. *Nonlinear Dynamics*, 76: 1561.
- Tchawou Tchuisseu, E.B., Gomila, D., Brunner, D., and Colet, P., (2017). Effects of dynamic-demand-control appliances on the power grid frequency. *Physical Review E*, 96, 022302.
- Tchawou Tchuisseu, E.B., Gomila, D.,Colet, P., Witthaut, D., Timme, M. and Schäfer, B. (2018). Curing Braess' Paradox by Secondary Control in Power Grids. *New Journal of Physics*, 20 083005.
- Tchawou Tchuisseu, E.B., Gomila, D.,Colet, P. (2018). Reduction of power grid fluctuations by communication between smart devices. *arxiv.org*, 1805.07432

Dedication

This Thesis is dedicated to:
My lovely mother Yvonne Nguenkoua Nkwayep Tchawou, for all the education you provide to me and to my siblings, for your encouragement when I had doubts and your permanent support. Mama Yvonne, many thanks may God gives you long life, to enjoy all what you sowed in us.
To the loving memory of my father Daniel Denis Tchawou. Thank you to have existed and to have given everything you could for my education despite the difficulties of the life, you have always been present for my siblings and me. Thank you Papa.

Acknowledgements

This Thesis has been possible thanks to my supervisors Prof. Pere Colet and Dr. Damià Gomila. I would like particularly to thank Damià, for his patience, availability, advices and guidance during the past last 4 years. You have been always proposing your help when I have been in difficulty. Thank you so much Damià to have believed in me and to have accepted to lead this Thesis. I would like also to express my gratitude to Pere, despite your really busy schedule, you were always finding some time to listen to me, and you never hesitated to give me advice and encouragement. I enjoyed all the meetings with you and I'm always fascinated by the ease you have to make me understand my work. Today, I can say that I really started to make a mature step in research thanks to both of you. This work would not have been possible without the FPI-MINECO fellowship, and without the validation of Prof. Maxi San Miguel, to whom I would like to express my gratitude. Thanks Maxi to have allowed my presence in this illustrious Institute you are directing. By extension, I would like to thank all the IFISC staff, the IFISC PhD students, the administration and technical members in particular, who have been working hard clearing up my mistakes and teaching me how to easily manage with the servers. Many thanks to have kept the machines alive.

I would like also express my gratitude to Prof. Benjamin Carreras from the BACV Solution Inc., Oak Ridge for his availability in teaching me the secrets of the OPA Model used in this thesis, despite the difficulty of the understanding of this model, you have been so patient with me. Thank you for the the energy you have put to let me understand the Physics and the complexity behind this model.

I would like to thank Prof. Marc Timme, Prof. Dirk Witthaut and Dr. Benjamin Schaefer for having opened the door of the Nonlinear Dynamic and Network group of the Max Planck Institute for Dynamics and self-organization. My stay in that illustrious Institute has added a value to my knowledge. Thanks to you I deeply understood the electric network dynamics. By extension I would like to thank the ensemble of researchers with whom I have exchanged knowledge, and from whom I have learned a lot. I would like to thank then Dr. Jose Casadiego,

Dr. Debshanka, Dr. Malte Shröeder, Dimitra Maousa, Dimult and many others.
My first academic and research steps had been initiated in my homeland Cameroon, under the wings of Prof. Paul Woafo and Dr. Samuel Noubissié. I would like to thank them for my initiation in the research which gave me the possibility to enroll to this PhD program. I would like in particular to acknowledge Prof. Paul Woafo, who always fight to provide not just to me, but to several young researchers precious advices and support to carry out their study and research. Thank you for all you have done to us Prof. Woafo.
I would like to thank my family, my precious queens my grandmother mama Meta and my mother mama Yvonne, who have made everything to provide us with accommodation, education even in difficult moments I have always had your support Thanks for all. Many thanks to my eights siblings, Aymerich, Armand, Charline, Donald, Laurine, Syntych, Daphenel and Ivan, thank you for your prayers and your support. I would like in particular express my gratitude to my brother Dr. Tchawou Wandji Armand, who has been sponsoring my academic studies and who had deeply played the role of the father that we lost back in 2005. Thanks to have always believed in me, thank you for your unwavering support. By extension I would like to thank my brother's wife Dr. Nina Luisa-Michels for her support to me and my family. I would like to thank Mr. Tchatchouang my former professor of Physics at the secondary school who has inspired me and encouraged me during my academic studies.
Living in this beautiful island would not be the same without those people who talk to us, who planed some Mallorca tours and party, and who make our integration easier. I would like to thank the Cameroonian community of Mallorca, particularly Mr. Fumba Rigobert and its wife Mrs Ameline, Mr. Luiz Maria, Ivan Bacthom,Mr. Patrick Salomon Kalla, Mr. Thatcha Merlin, Mr. Julio, Mr. Kamdem Williams and many others, for their support during the good and bad moments.
Last but not least, thank you to my little family, to my wife Karla Vaneckova and to my treasure, my son Lenny Armand for existing. Karla, from the day you entered in my life, I knew that you were the missed piece of the puzzle. Thank you for your love, your patience and support, for the nights you have been waiting for me until late. Thank You for being part of my live, I love you. I would also like to thanks my wife's family for its hospitality.

Contents

CHAPTER 1

Introduction

ELECTRICITY is one of the most important human discoveries. It is used in various fields of human activity: lighting rooms, cooking, heating, fans, domestic appliances, television, motors, machines, computers, tramway, metro, electric vehicles, etc. All this provides comfort to people and makes electricity so important for our day to day lives. This importance is better understood during the few minutes of a blackout or power outage. During the last decade, several blackouts affecting million of people occurred around the world. That includes among those, the November 9, 1965 Northeast blackout that left over 30 million people without power, the July 13–14 blackout in New York City which affects 9 million of people and the November 4 2006 blackout that affected several European countries like Germany, France, Italy, Belgium, Spain, and Portugal and which left over 15 million households without power [24, 65, 116]. All the people's social life almost break down during electrical blackouts. Indeed, during blackouts, all activities, devices and services requiring electricity are interupted, and security systems fail. This induces a change in behaviour of people, which is characterized by anxiety, frustrations, nervousness, global increase of the rate of criminality and vandalism [70]. In contrast to those blackouts, it had been noticed in the 13-14 July New York City blackout, property looses resulting from looting and arson [49].

The infrastructure enabling production and consumption of electricity is called power grid. It is composed by generation stations, power lines and consumers. Electricity is produced at power plants by synchronous generators, which transform a primary source of energy into electricity. Electrical power is then carried by power lines and served to consumers which are the end-users. Depending on the primary energy converted one can find nuclear, thermal, coal, wind, solar and hydro power plants. All these power plants have a negative impact on the environment but those using fossil fuels have bigger consequences than the others.

Indeed, according to the U.S. Energy Information Administration [115], about 40% of the total energy consumed is in the form of electricity. Among that, 68% is generated burning fossil fuels (gas, oil, coal) which emit a huge amount of greenhouse gases such as Carbone dioxide (CO_2), methane, nitrous oxide, fluorinated gases into the atmosphere, contributing then to the global warming which should be kept well below 2 °C according the Intergovernmental Panel on Climate Change (IPCC) [84]. These environmental contaminations and greenhouse gas emissions induce climate change which increases the level of water in the oceans and the probability of strong storms and hurricanes which can cause power failures and blackouts. Nuclear power plants, on the other hand, do not produce greenhouse gases, but they leave dangerous radioactive waste. The waste can cause a disaster at any accident which would put them in contact with the environment. That is what happened after the 2011 Fukushima nuclear disaster where about 50000 households have been displaced after the contamination of the air, soil and sea by nuclear waste which destroys the environment [16]. Furthermore, nuclear power plants use water from a river or ocean for their cooling systems, which is returned warmer than the water was before. That impact the environment by killing some species of fish and vegetation [16]. An efficient solution to limit or even suppress the impact of electricity generation in the environment is to switch electricity production from fossil fuels to renewable energy sources (RES) such as water, wind and solar. That will help to reduce greenhouse gas emissions and dangerous nuclear waste.

The electric power grid is based on a permanent balance between the power production and the power consumption in all the network. Due to the limitation of storage electricity for a long time, the power plants have to generate exactly what is consumed at any time and keep the generators synchronized. Any power imbalance induces variations on the frequency of the system and implicitly on the voltage and current. The control of the grid frequency is therefore one of the most important tasks of the system operator to ensure global stability, reliability and efficiency of the power electric grid operation. In the traditional grid, this is achieved by several control methods and suitable management that includes demand forecasting, technical maintenances, generation and transmission planning, etc. But, the global increase in demand (which fluctuates) of about 2% per year [115], necessitates a higher and increasing integration of renewable energy power plants due to environmental concerns. Power fluctuations from renewable energy coupled to the ones coming from demand increase the difficulty to stabilize the electric system from only the supply side. This issue (power fluctuations on the supply side) triggered a new control philosophy aimed to allow consumers to adapt their power consumption to the state of the grid in order to balance the power generation at all times and therefore ensure the grid stability.
This philosophy called demand side management (DSM), consists in the plan-

ning, implementation and monitoring through initiatives (financial incentive and consumers education) and technologies (smart meter, smart appliances, digital communication and Internet) that encourage consumers to optimize their energy use by reducing their consumption during peak hours or to move the energy use to off-peak time such as nighttime or the week-end. All this combined to the communication systems allowing two ways communication between utility companies and consumers is transforming the traditional power grid into a smart grid.
A smart grid is defined as an electricity supply network that uses digital communications technology to detect and react to local changes in consumption and generation [27].
In the following, we review a brief history of the electricity network and some basic notions on electricity, we describe the structure of a modern electric network as well as the control methods used to manage electricity.

1.1

Brief history of the electric power network

Most of the electricity we use is generated by generators based on the electromagnetic induction principle, which was discovered way back in the 1830's by Michael Faraday, who noticed during his experiments that when he moved a permanent magnet in and out of a coil or a single loop of wire it induced an Electromotive Force or a voltage, consequently an induced current flowing across the wire. That is basically the foundation of the generator. In the 1860s and 1870s, from Faraday's principle, severals inventors worked and thought on ways to generate electricity mechanically, that led to the emergence of two types of generators: a generator of direct current (dc) electricity and the generator of alternating current (ac) electricity. In the dc generator, the electric charge only flows in one direction and the electricity which is produced with a constant voltage can not be easily converted from low to high voltage. On the other hand, alternating current reverses direction periodically and the voltage can be changed easily via transformers.
At the end of the year 1882, a brilliant engineer, Thomas Edison through his illuminating company, constructed the first electric power grid at the Pearl street station in New York in the United States of America. It was a low voltage (110 volts) electricity served to about 85 consumers (for about 400 lamps) and powered by a dc generator and distributed by underground cables. Due to the increase in demand and to the fact that the dc current produced could not be transmitted for long distance (because of the excessive power losses at low voltage), Edison company increased its production by adding more than three generators

for providing electricity to around 500 consumers (for about 10150 lamps). Simultaneously similar power grids were developed under Edison's patents across the U.S such in Shamokin, PA; Sunbuny, PA; Brockon, MA; Mount Carmel, PA and so on. The problem of transmitting electricity over long distances was solved with the invention of the transformer in 1885 by William Stanley which allows to step up or down the ac voltage for transmission and distribution [90]. The invention by Tesla in 1888 of the 1-phase, 2-phases and 3-phases induction motor some years later to replace the dc generators, posed the basis of the first ac power grid. Using the ac generator combined with the transformer allowed to produce and transport over long distances high-voltage electricity, and reduce ohmic losses. It is in 1891, during the International Electro-Technical Exhibition held in Frankfurt, that the first long distance transmission of three-phase AC, which powered lights and motors was experimented. Then, in 1893 the first ac 3 phases hydroelectric power plant was built at the Niagarra falls to power and transmit electricity to residences in Bufallo, NY, USA. By November 1896 ac power started to power industries in Buffalo and that was the beginning of the decline of the dc power. Many companies developed throughout U.S and began to operate at different frequencies from 25 Hz to 133 Hz. There were several power grids across U.S operating at different frequencies and due to the need of interconnection, a standard frequency of 60 Hz and standard voltage 120 volts were chosen. Europe adopted an ac standard of 220-240 volts at 50 Hz.

1.2

Basic definitions and notions

To understand how the electric power system works, it is important to define some basic notions on electricity such as conductor, resistance, inductance, capacitance, reactance, impedance and power.

- **Electric current**: It measures the rate of flow of charge. It is expressed in Ampere (A)
- **Voltage**: also referred to as potential, is a measure of the capacity of a device connected to two points to perform work per unit of charge that flows between those points. The differences of potential between two points generates an electric field, contrary to the current whose variation generates a magnetic field. The voltage (or potential) is measured in volt (V).

- **An electric conductor**: It is often an object allowing the flow of electric charge or current from one or many directions. It is characterized by two specific electrical properties: resistance and inductance.
  The measure of the difficulty that a current has to flow through that conductor is called resistance. The inverse quantity is electrical conductance, and it is the ease with which an electric current passes. The resistance of a conductor depends on its length, cross section and its resistivity, and it is expressed by $R = \rho l/S$. Where l is the conductor length in m, S its cross section in m^2, ρ the resistivity of the conductor material in Ωm and R the resistance (Ω).
  Varying the direction of the flow of the current through a conductor produces a magnetic flux, and consequently **an inductance**, which is defined as the number of magnetic flux linkage (product of magnetic flux through a coil of wire and the number of turns of the wire) produced per ampere of current flowing through the line, and is expressed by: $L = \lambda/I$ Where L is the inductance given in Henry (H), I is the electrical current measuring the rate of flow of charge through the conductor and it is expressed in Ampere (A), and λ is the flux linkage in weber-turns (Wb-turn). An electric conductor is then characterized by its resistance and inductance as illustrated in figure 1.1.

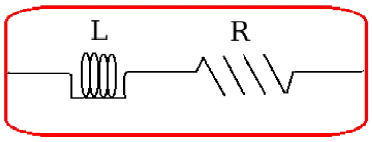

Figure 1.1: conductor

- **Capacitance**: The capacitance is defined as the ability of an object to store electric charge. That object, called capacitor, is composed of one or more pairs of conductors separated by an insulator. The capacitance only depends on the geometry of the design and the permissibility of the dielectric material between the plates of the capacitor. It is expressed by: $C = q/V$, where C is the capacitance in $Faraday$ (F), q is the electric charge on the capacitor expressed in $Coulomb$ (C) and V is the voltage measured in volt (V).

- **Impedance**: It is a property of a conducting device, that represents the impediment it poses to the flow of the current through it. It has two components: a resistance and reactance. The last is a measure of the flow of power caused by the creation a magnetic and electric fields. The Impedance and reactance are also expressed in Ohm (Ω).

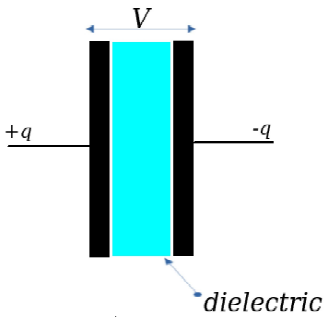

Figure 1.2: Capacitor

- **Electric power of a device**: It is the rate at which work is being done. The instantaneous power supplied to a device in either dc or ac circuit is the product of the instantaneous voltage across its terminals times the instantaneous current flowing through it. It is given by the well-known Equation

$$p(t) = v(t) * i(t) \tag{1.1}$$

where $p(t)$ is the instantaneous power measured in watts (W), $v(t)$ and $i(t)$ are the instantaneous voltage and current respectively. In general the voltage and current are constant in a dc circuit or system, while they can vary in ac circuit as we will see in the next paragraph.

Power in an alternating current circuit

As we already developed previously, in dc system or circuits the current flows in one direction and the generator (battery) supplies the circuit with constant voltage. In ac systems on the other hand, the current and the voltage are changing periodically following a sine function. Thus, the current $i(t)$ and the voltage $v(t)$ with amplitude I_m and V_m are time dependent with frequency ω, phases ϕ_u, ϕ_v respectively. Lets consider a circuit, composed by a load with resistance R, supplied by an ac voltage source. So let denote by

$$i(t) = I_m \cos(\omega t + \phi_i) \tag{1.2}$$

the instantaneous current. The instantaneous voltage $v(t)$ is given by the equation

$$v(t) = V_m \cos(\omega t + \phi_v). \tag{1.3}$$

Then, the instantaneous power delivered to the load R defined as the product of the current times the voltage is given by:

$$p(t) = v(t)i(t) = V_m I_m \cos(\omega t + \phi_v) \cos(\omega t + \phi_i). \tag{1.4}$$

Simplifying equation (1.4) using some trigonometry properties and using the root-mean-square (rms) value of $v(t)$ ($|V| = V_m/\sqrt{2}$) and $i(t)$ ($|I| = I_m/\sqrt{2}$), we obtain the instantaneous power in terms of the rms values given by the equation

$$p(t) = |V||I|\cos(\phi)[1 + \cos(2(\omega t + \phi_v))] + |V||I|\sin(\phi)sin(2(\omega t + \phi_v)) \quad (1.5)$$

, where $\phi = (\phi_v - \phi_i)$. The power has been divided into two components X and Y:

$$X = |V||I|\cos(\phi)[1 + \cos(2(\omega t + \phi_v))] \quad (1.6)$$

$$Y = |V||I|\sin(\phi)\sin(2(\omega t + \phi_v)). \quad (1.7)$$

The first component X accounts for the energy flow into the circuit and consumed by resistive components of the node. The power delivered to the load is obtained by averaging over time the instantaneous power. Since the average of the time dependent sinusoidal function is zero, the average power delivered to the load is given by

$$P = |V||I|\cos(\phi), \quad (1.8)$$

which is just the energy absorbed by the resistive components of the load. P is also called *real or active power*. The product of rms voltage and rms current $|V||I|$ is known as *apparent power*.
The second component Y accounts for the energy borrowed and returned by the circuit due to the presence of capacitive and inductive components of load or *reactive* components. It is a pulsating power and its amplitude is called reactive power and is designated by Q and is given by:

$$Q = |V||I|sin(\phi) \quad (1.9)$$

The active and reactive power P and Q are the real and imaginary parts of the complex power S, which is defined as the product of the complex effective voltage V ($V = |V|e^{j\phi_v}$) and the complex effective conjugate current I^*($I^* = |I|e^{-j\phi_i}$),

$$S = VI^* = P + jQ \quad (1.10)$$

where the complex conjugate is indicated by the asterisk (*) and the letter j identifies the imaginary unit.

1.3

Modern electric power system structure

The modern electric power system is a complex interconnected network for delivering electricity from generation to consumers. It does so by converting

a natural and available primary source of energy (fuel, nuclear, water, sun, wind) into electricity which is transported to the points of consumption.
Fig. 1.3 shows a schematic representation of an electric grid, which is composed by: generation stations, transformers, power lines (transmission and distribution), loads or consumers and a control center. All these components are indispensable for the reliable operation of the grid.

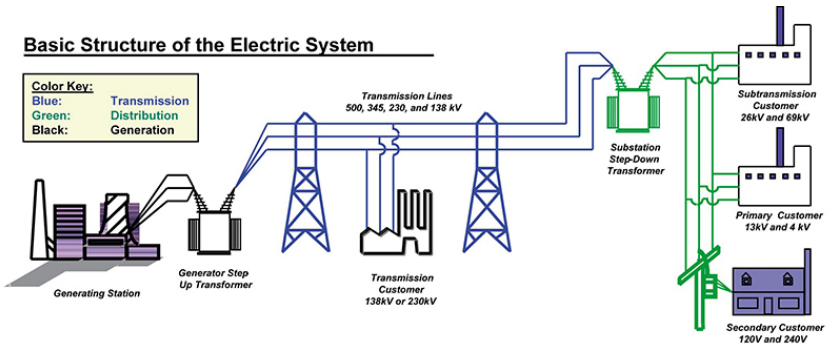

Figure 1.3: Schematic diagram of the traditional electric grid. Source:http://www.webpages.uidaho.edu/sustainability/chapters/ch06/ch06-p3a.asp

Generation stations

The generation station is the place where electrical power is produced by three-phases ac synchronous generators. Indeed, the prime movers (hydro-turbine at waterfalls, steam turbine or gas turbine) known as sources of mechanical power, convert a primary source of energy (wind, fossil, thermal, gas, nuclear and hydraulic) into mechanical energy which is, in turn converted to electrical energy by synchronous generators.
The three-phases synchronous generator is an electromechanical device constituted by two main elements, a stator and a rotor coupled magnetically:

- The stator which is the stationary part of the generator, carries the three armature windings separated each other by 120° producing an ac voltage output.
- The rotor is the rotating part of the generator. It is a large magnet or an excited (with an external dc current powered by dc generator or other dc sources) electromagnet attached on the generator shaft, carrying the magnetic field and rotating with a constant speed.

The three-phase synchronous generator operates under the electromagnetic induction principle. In fact, driven by the turbine on which it (rotor) is connected through a shaft, the rotor then produces a rotating magnetic field which induces a current in each stator winding to form the three phases ac voltage at the terminal output. In general synchronous generators (producing electricity) and motors (consuming electricity) operating under the same principle are referred to as synchronous machines. Fig.1.4 illustrates a schematic of the cross section of a three-phase, 2-poles synchronous machine.

Nowadays, due to environmental and sustainability concerns, the traditional power plants using synchronous machines are progressively replaced by renewable energy sources generation (wind turbine and solar power plants) interfaced with power electronic converters [6, 87]. Solar or photovoltaics power plants generate dc output, which, to be fed into the existing grid requires a dc to ac converter. The power converter transforms the dc output into ac suitable for injecting into the electric grid, generally at 50 Hz and at the needed voltage [6]. Indeed, the connection of renewable energy sources to the grid via inverters increases the difficulty for studying the dynamic stability of the whole network. Several works have addressed the analysis of electric networks including renewable energy sources and their power converters [6, 11, 74, 112, 113].

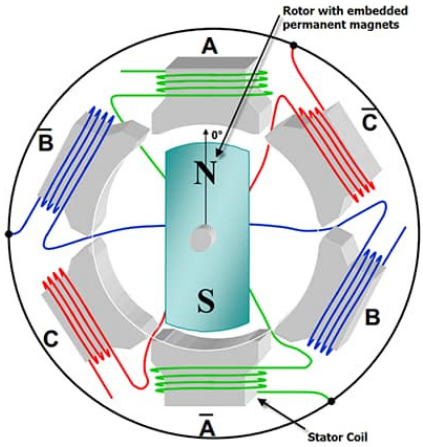

Figure 1.4: Schematic diagram of a three-phase synchronous generator. source: https://eu.mouser.com/applications/stepper-motors-smart-drivers/

Transformers

A voltage transformer, is an electric device which is used to step-up the electric voltage from the generator output and therefore reduce the current. Consequently reduced losses in the line make the transmission of power over long distances possible. It is also used for stepping-down the electric voltage by reducing it to a suitable for residential consumers, industry and commercial loads. Fig. 1.5

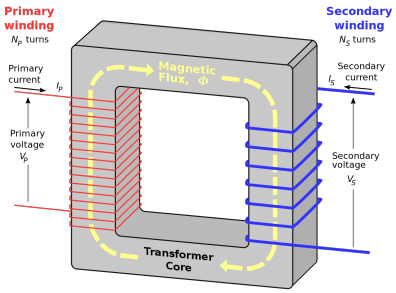

Figure 1.5: Schematic diagram of a single-phase transformer. Source:http://webcampresence.com/transformer-diagram/hybrid-switching-step-down-converter-with-a-transformer-diagram-circuit-20120249102-08/

shows a schematic representation of a single-phase transformer, which contains two windings, one on the primary and the other on the secondary side. The primary voltage is the voltage which has to be stepped up or down and the resulting voltage is called secondary voltage.

Transmission network

The synchronous generator at the generation station produces low AC voltage which is then stepped up by a transformer and carried through the high-voltage transmission lines from the generation station to substations, where it is stepped down and taken to the consumers by the distribution lines. Thus, the transmission lines and the distribution lines compose the transmission network which connects all the generating stations and major load centers in the power system. The transmission and distribution lines are resistive, inductive and capacitive.
First of all, when the electricity flows through a power line, it experiences a resistance to the current flow. Such resistance depends on the temperature and on the electric power through the Ohm law given by : $R = \frac{v}{i}$, where v and i are respectively electric voltage and current. The conductor is then subjected to the *Joule* effect known also as resistive heating which is the process by which the passage

of an electric current through a conductor produces heat. Hence the conductor temperature increases as electricity flows. Furthermore, for many materials the intrinsic resistivity increases with the temperature as $R = R_0[1+\alpha(T-T_0)]$. The temperature coefficient α is 0.0038 C^{-1} for copper and has a similar value for other metals. For a given amount of power to be delivered heat losses are reduced by increasing the voltage while reducing the intensity of the electrical current. The fact that alternating current allows to easily step up the voltage in order to reduce the transmission losses provides a distinctive advantage with respect to direct current.
Second, the passage of the alternating current across the conductor produces a magnetic field around it which induces an electromotive force in both the conductor itself and in any nearby conductors by mutual inductance making the transmission line inductive. Finally, due to their potential differences, the transmission lines exhibit capacitance with respect to each other.

Consumption

Electricity is consumed by a wide variety of loads, such as lights, heaters, motors, electronic equipment and domestic appliances. These loads are in general divided into residential, commercial and industrial, and are classified based on their impedance. Nowadays, in Europe, Asia, Africa and part of South America residential and some commercial premises use 220-240 V current transported from substations through distribution lines as it is shown in Fig. 1.6. These loads

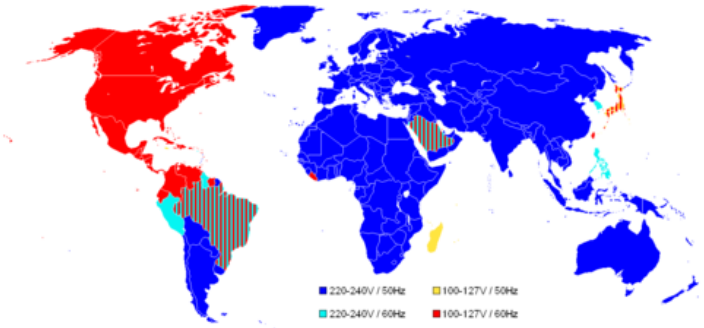

Figure 1.6: World map of mains voltages and frequencies. The countries are colored by the nominal voltage and frequency they use. Source:https:commons.wikimedia.org/wiki

consist mainly of lighting, cooling and heating. They are resistive loads. Consequently the power consumed by these loads is active or real power (reactive power is low) and they don't depend on frequency. Industrial loads mainly use high voltage current and are directly served from transmission lines. Industrial

loads are among others composed by inductive motors and composite loads which consume real and reactive power.

Power system protection and control

Apart from the above-mentioned elements, a power system includes methods to ensure protection, safety, control and satisfactory operation of the system. The protective devices also known as switchgear, include circuit breakers, electrical disconnect switches, fuses, and they are necessary to control, protect and isolate electrical equipment on the occurrence of faults in the system.
For a stable, reliable and economical operation, the power system has to be continuously controlled against disturbances. That is done through severals control stages going from automated devices to human actions by the energy center operators. Such controllers aim to ensure the following requirements or constraints [3, 9, 83]:

- The frequency must be equal to its target value or within the specified limits: ω=$50 \pm 0.2Hz$ (or $60 \pm 0.2Hz$).
- The active and reactive power must be balanced in the system.
- The voltages have to be bounded: $V_{min} < V < V_{max}$.
- The total power generation must be lower that is maximal generation capacity $P_{gen} < P_{gen}^{max}$.
- The power flowing through a line must be lower than the maximal capacity of the line: $F < F^{max}$
- The system should supply energy at minimum cost and with minimal ecological impact.

These requirements are grouped into *equality* and *inequality constraints*.
Indeed, *equality constraints* (composed by the two firsts requirements) are represented by the power balance constraints; meaning that the total power generation must be equal at any time to the total power demand and the power loss. While the *inequality constraints* (composed by the other requirements) reflect the limits on physical devices in power system as well as limits stated to ensure system security [3, 19, 42, 48, 83].
These constraints are ensured by controlling active and reactive power and by computing the optimal power flow (OPF) to determine economic dispatch which minimizes the electricity cost and the environmental impact of the electric production. In fact, changes in active or real power affect primarily the frequency, while reactive power which mainly dependents in voltage magnitude is on the

other hand less sensitive to frequency variations. Thus, the frequency and the voltage are controlled separately.

Frequency control

The figure 1.7 shows the hierarchical frequency control scheme in the traditional power plants and it is composed by the following steps:

Primary control is the automatic response of turbine governors against deviations in system frequency which occurs within few seconds. Once frequency changes are sensed, the governor modifies the mechanical power of the prime mover in order to balance the production and the load, hence to stabilize the frequency to a new steady value, which afterward has to be brought to its nominal value.

Secondary control secondary control is the combination of automatic generation control (AGC) and manual dispatch actions to maintain energy balance and nominal frequency. Secondary control is operating within tens of minutes and is provided by Spinning and Non-Spinning reserves. Spinning reserves are generating units with turbine spinning in synchronicity with the grid's frequency without supplying power, while non-spinning reserves are offline generating units, but can be synchronized with the grid [52]. AGC operates in synergy with the Supervisory Control and Data Acquisition (SCADA), which provides information about frequency, available reserves, generator output in order to schedule efficiently the generators enabling the economic dispatch.

Tertiary control Tertiary control is used to restore the reserves used and make them available to handle current and future contingencies.

The connection of renewable energy sources into the grid has brought new challenge on controlling the frequency of the grid. In fact this high and progressive integration of wind turbine and photovoltaics power plants into the grid reduces the global inertia of the system. It is well known that as higher is the total inertia of a system as higher it is stable against perturbations induced by power imbalance (frequency deviations). Thus, such RESs weaken system and lead it vulnerable against perturbations [11, 75]. From this issue has emerged new supplementary control concepts (Virtual Synchronous Machines (VSMs), phase locked loop, Voltage source converter, etc...) mainly applied to the electronic components responsible for the conversion of the dc power to ac power [6, 87]. The concept of VSMs presented as a flexible method for controlling power electronic converters in both grid-connected and stand alone modes [36] for frequency

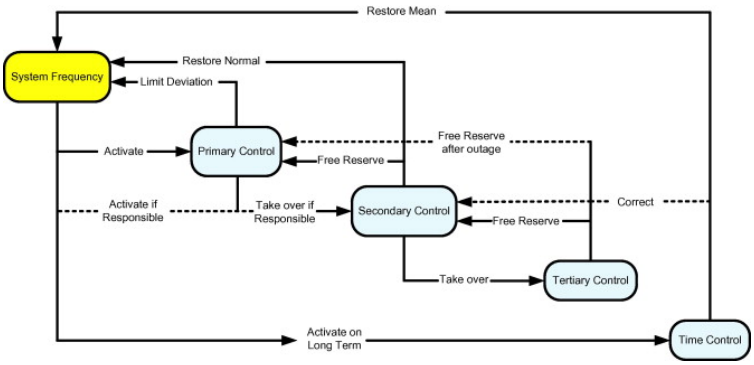

Figure 1.7: Schematic diagram of the frequency control [37].

stabilization. VSMs do so providing virtual inertia and damping to the system [112].

Voltage control

As it was mentioned above, in the stable operation active and reactive power must be balanced in the system, meaning that the reactive power produced by synchronous generators must be equal to the reactive power of the loads plus the reactive transmission losses. Thus, as the imbalance between active power and loads induce frequency variations, any imbalance in reactive power in the system results to fluctuations of the voltage from the desired value. Consequently, the voltage can be controlled by controlling the reactive power. As in the case of the frequency influence on the active power, increasing the reactive power production of the generators leads to a higher voltage at the generator. Conversely, increased consumption of reactive power leads to a lower voltage. The voltage is then controlled using the automatic voltage regulator (AVR) which operates in the exciter field by changing the exciter output voltage and the current field to follow any changes in the system. AVR is used to keep the voltage within designed limits, as well as to balance reactive power in the system.

Economic dispatch

Economic dispatch is the short-term determination of the optimal output of a number of electricity generation facilities to meet the system load at the lowest possible cost, subject to transmission and operational constraints. The objective of economic dispatch is to determine the optimal power flow (OPF) or generation for the units participating in supplying the load. The optimal power flow,

finds the optimal solution to an objective function subject to the power flow constraints and other operational constraints, such as generator minimum output constraints, transmission stability and voltage constraints, and limits on switching mechanical equipment. There exist in the literature severals optimal power flow algorithms differentiated from each other by the optimization method they use to compute the OPF. We can list: The Linear programming method, the Newtown-Raphson methods, the Quadratic programming method, the nonlinear programming methods, the interior point method and the artificial intelligence methods [90]. These controls applied on the supply side and managed by the electricity utility through the energy center operators, can face huge perturbations difficult to handle. That could lead then to an outage which can be an overload of a line, which may propagate across the network and eventually lead to a blackout. The system can therefore be found into the following five states [9, 90]: *normal, alert, emergency, in extremist and restorative state* as presented in Fig. 1.8.

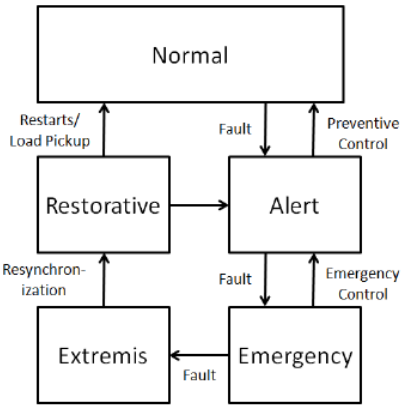

Figure 1.8: Power system operating states and control actions [13, 101]

Normal state: It is the desired state for the system. In this state, all the variables are within the normal range of operation. Equality and inequality constraints are satisfied and spinning and non spinning generator reserves are available. In this state the system can handle safely any small disturbances. Assuming that there is a sudden loss of generation or a sudden increase in demand or any fault causing frequency fluctuations, the system will provide its reserve to stabilize the frequency. The system has then moved to the *Alert state*.

Alert state: In this state, all the constraints are still satisfied but there is no or less spinning reserve available for any future disturbances. At this level the control operator has to monitor the system in order to bring it back to the

normal state through preventive control, otherwise it is susceptible to fall in the emergency state during the next outage or disturbance.

Emergency state: In the *Emergency state*, the equality constraints are not anymore satisfied, but the inequality constraints are still satisfied. The lines are closed to be overloaded and the emergency control has to be applied to bring the system back to the alert state or directly to the normal state. If nothing is done, the lines will be overloaded and will get out of use. That outage will be propagated and some generators or power grids will be disconnected from the rest of the network. The system is then said to be in an islanded mode or *In extremist state*.

In extremist state The equality and inequality constraints are not anymore satisfied. To bring back the system directly to the normal state, the operators have to restore the system.

restorative state In this state, the control operator restore the whole system through several steps restoring and improving the overloaded transmission lines, switching and improving generators, restoring the generators reserve and maintaining others defective electrical components.

Nowadays, due to the development of new technologies such as smart meters, internet, sensors, communication systems enabling bidirectional communication (utility-users and users-utility) a new control philosophy applied to the demand side, has emerged: it is known as demand side management (DSM) or energy side management (ESM). That philosophy encourages the consumers to participate to the stability of the grid through the electricity market where electric utilities propose to their consumers to reduce or to shift their consumption during time of peak demand in response to time-based rates or other forms of financial incentives. A grid using this new philosophy of management of electric network is known as wise or smart grid.

1.4

Demand-side management

A smart grid is basically an electricity supply network able to deliver electricity in a controlled and smart way using digital communications technology like smart meters and smart devices. The innovation of the new grid is the possibility for consumers to participate in the management of the grid through several programs: that is demand side management (DSM). DSM can be defined as the modification of consumer demand for energy through various methods such as

financial incentives and behavioral change through education. DSM through diverse programs and concepts, aims to encourage the consumers to participate in conservation of energy (turning off lights from unoccupied rooms, for example) and use energy efficiently (replace old devices by those consuming less energy and offering the same service). Smart grid enabling DSM programs is expected to overcome problems related to power fluctuations or environmental contamination via emission of CO_2 and greenhouse gases by some power plants [114]. These DSM programs consist of energy efficiency programs, demand response programs and dynamic demand control [43, 89, 94, 102].

Energy efficiency programs defined as programs proposed to consumers to replace their devices by new ones consuming less energy. Simply, energy efficiency is a way of saving energy but keeping the same level of services. As a concrete example a LED (light emitting diode) bulb uses less electrical energy than a traditional incandescent bulb to produce the same amount of light. A compact fluorescent is then said to be more efficient than the tradition bulb. Another example concerns house or building insulation. An insulated house consumes less heat than a normal house.

Demand response (DR) is defined as the changes in electricity usage by end-use customers from their normal consumption patterns in response to changes in the price of electricity overtime [2]. Customers willing to participate to DR can modify their electricity consumption by [103]:

- reducing their energy consumption through interruptible load programs;
- shifting their energy consumption to various time periods;
- reducing their level of consumed energy by utilizing modern, efficient devices, and without interruption in the consumption activity itself [28]

DR programs can be divided into two main classes: Incentive-Based Programs (IBP) and Price-Based Programs (PBP)[1, 2].

Incentive-Based Program are divided into four categories including:

- Direct Control programs: In this program, consumers make available devices such as fridges, air conditioners which can be remotely shut down on a short time by utilities.
- Interruptible programs: As in the case of Direct control programs, customers signing up for that program receive incentive payments or rate discounts to reduce their consumption to defined values otherwise they receive penalties related to the program terms and conditions [1].

- Buy Back programs: (also know as demand bidding programs) are programs which encourage large customers to change their energy consumption pattern and reduce their peak load in return for financial rewards [27, 91]. Customers face penalties in case of not responding to load reduction according to the terms and conditions of the program.
- Capacity market: in this program customers commit to providing pre specified load reductions when system contingencies arise, and are subject to penalties if they do not curtail when directed.

The Price-Based Programs (PBP) include the four following programs:

- Time of Use (TOU): It gives consumers possibilities to manage their electricity bill by shifting use from on-peak periods where the electricity price is higher to mid-peak and off-peak periods where the electricity price is lower.
- Critical Peak Pricing (CPP): During peak hours on critical days announced in advance, utility increases electricity price to punitive levels, such that the users are obliged to turn off their devices or to avoid to use electricity during that period [53].
- Extreme Day Pricing (EDP): This rate design is similar to CPP, except that the higher price is in effect for all 24 h for a maximum number of critical days, the timing of which is unknown until a day ahead [39].
- Real Time Pricing (RTP): This rate reflects the hourly variations in electricity costs due to changes in demand. So the customers can then turn off their devices when electricity prices is high and consume once it goes down.

Incentive-Based Programs (IBP) and Price-Based Programs (PBP) are conceived to lower system costs for utilities and reduce customer bills by raising prices during expensive hours and lowering them during inexpensive hours. They both use financial incentives.

Dynamic Demand Control (DDC) on the other hand, is a technology enabling devices such as heaters, boilers, dishwashers, washing machines, air conditioners, refrigerators, etc. to control their consumption by turning on or off depending on the electric frequency of the grid. DDC provides faster response to any power imbalance sensed by the frequency, and smart devices automatically adjust their consumption in order to restore the frequency to its target value allowed by the legislation. DDC is easily implementable in a fridge or any rechargeable devices such as cell phones or laptops [109]. In fact, there is in every refrigerator a thermostat which controls the temperature by keeping it within a certain threshold by turning on and off the

refrigerator awhen the temperature limits are crossed. As an example, in [100] authors propose to change the operation of that thermostat, designing it to modify the temperature thresholds by a quantity proportional to the frequency of the grid as it is showed in Fig. 6 of [100] (See also Fig. 1.9). Thus, dynamically controlled devices or frequency-responsive devices will

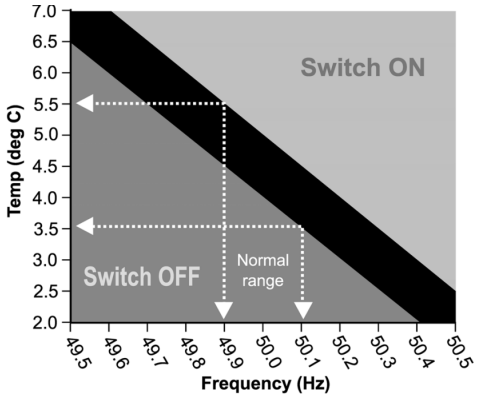

Figure 1.9: Operating strategy of dynamically controlled refrigerator [100]

be turned on/off depending on the grid frequency. It has been reported in [78, 100, 109], that such collective response could infer a synchronization of devices, that is emergence of frequency oscillations in the grid corresponding to a simultaneous switching of these controlled devices. A method proposed to solve that issue is the randomization of the device response to frequency variations [76, 78, 100].

Application of the PBP within households seems to pose a problem related to the presence of users to manage the smart appliances following the complex variation of electricity price. To cope with that problem, it has been proposed a device called home energy management system (HEMS) which using a two way communications, automatically manages the appliances within the house as a function of the information obtained either from the utility company or from smart meters [62, 63, 86, 119]. Basically, HEMS often creates optimal consumption and production schedules of smart appliances in a prioritized manner, considering several objectives such as energy costs, environmental concerns, load profiles, and consumer comfort [8].
Thus, the use of PBP and HEMS to the electric power grids could provide important financial savings for consumers, increasing system reliability, reducing the number of blackouts, reducing environmental degradation by the reduction of emission of greenhouse gases and saving spinning reserves.

1.5 Outline

The thesis is divided into the following chapters:

- Chapter 2 deals with the power plant modeling. In this chapter we review a complete model of a power plant considering the generator model as well as the different frequency regulators applied on the power plant. This model proposed is then used in [109] as power plant model powering stochastic demand and controlling the resulting frequency fluctuations.

- Chapter 3 deals with the demand model. We introduce a stochastic model for the electric consumption. The calibration of the model with respect to the frequency fluctuations is done comparing them to the real frequency recorded in the laboratory. Some The demand model and some results of this chapter are parts of results contained in [109].

- Chapter 4 of the thesis focuses on the application of the dynamic demand control on the system and its effects on the frequency stabilization. The improvement of the control via communication between devices is investigated. Most of the results from this chapter are contained in the articles entitled: *Effects of dynamic-demand-control appliances on the power grid frequency* [109] and *Reduction of power grid fluctuations by communication between smart devices* [107].

- Chapter 5 we extend the results of the previous chapter by considering an electric network made by severals nodes corresponding to the generations units. In this chapter the effects of DDC on the propagation of outages are studied.

- Chapter 6 we study the dynamical consequences of secondary control in a AC power grid model. We mainly investigate whether secondary control avoids or not Braess' paradox. Most of the results from this chapter are contained in the scientific article entitled: *Curing Braess' paradox by secondary control in power grids*, that we have published in New journal of Physics [108].

- Chapter 7 is dedicated to the effects of DDC on the computation of the optimal power flow, considering a specific model (the OPA model). This chapter is based of the blackout analysis model developed in [12, 15, 29, 30] combine to the DDC protocols established in [109].

Finally, we offer some concluding remarks and point out some possible future developments.

CHAPTER 2

Power plant modeling

2.1

Introduction

In this chapter we consider an ac synchronous generator supplying composite loads (motors and constant impedance or resistive loads). The generators are equipped with a frequency regulator and the voltage is assumed to be constant or ideally controlled. We describe a mathematical model governing the dynamics of the generator as well as its frequency regulator. Fig. 2.1 shows the schematic description of powers in a turbine-synchronous generator, where P_m and P_e denote respectively the aggregated mechanical power input (or prime mover) and the aggregated power demand. The aggregation of generators is done such that the ensemble of synchronous generator participating in the grid is viewed as a single generator with large inertia and fixed power P_m. Likewise, an aggregate of consumers include residential, industrial and commercial consumers such that the whole power consumed is viewed as a single power P_e [82, 100]. Further electric models can be found in [82], where the authors have done comparative analysis of existing model for power grids.
Throughout this thesis, the modeling of renewable energy sources and their appropriate control system are not considered. A more realistic electric network model would include synchronous machines (generators and consumers), distributed generations, energy storage systems modeling.

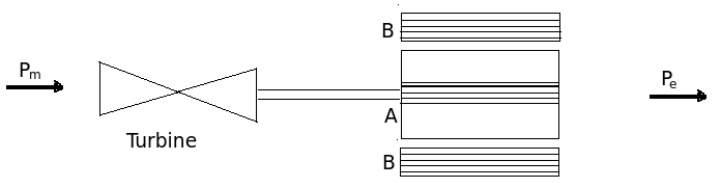

Figure 2.1: Schematic description of powers in synchronous generator.

2.2

Swing equation

A conventional power plant is, roughly speaking, constituted by a generator and a governor [90]. The generator is responsible to produce electricity from fossil fuel or renewable energy sources. The governor is the specific control method used to match the generation to the demand. The generator is typically composed of a mechanical part, often a turbine fixed to a ferromagnetic rotor which rotates in the stator winding, and an electrical part formed by coils wound around the stator. The rotor is a magnet or an electromagnet attached on the turbine shaft rotating at a constant speed. When the rotor moves relatively to the armature winding, an induced current flows in the wires constitutive of the stator and a voltage is developed at the generator output terminal. Thus, Eq. (2.1) describing the dynamics of the rotor, sets that the rate of change of the angular momentum of the rotor equals to the net torque acting on the rotor

$$J\frac{d^2\theta}{dt^2} = T_m - T_e, \tag{2.1}$$

where θ is the rotor angle with respect to a stationary reference, J is the moment of inertia of the rotor, T_m and T_e are the mechanical torque from the turbine and the electrical torque applied on the rotor respectively. Multiplying both sides of the Eq. (2.1) by ω and dividing by the rated power of the generator P_G we obtain

$$\frac{J\omega}{P_G}\frac{d^2\theta}{dt^2} = \frac{1}{P_G}(T_m\omega - T_e\omega). \tag{2.2}$$

We define by H the inertia constant of the generator (in seconds) which is the ratio of the kinetic energy over rated power P_{G}:

$$H = \frac{\frac{1}{2}J\omega^2}{P_G}. \tag{2.3}$$

By substituting Eq. (2.3) in Eq. (2.2), one obtains the equation describing the rate of change of the frequency with respect to the mechanical and electrical power, which is known as the *swing equation*

$$\frac{d\omega}{dt} = \frac{\omega}{2HP_G}(P_m - P_e). \tag{2.4}$$

The swing equation describes the dynamics of the generator [90]. $P_{\mathrm{m}} = T_m\omega$ is the mechanical power generated by the turbine (or prime mover), and $P_{\mathrm{e}} = T_e\omega$ is the total power of the electric current passing through the coils around the stator. The electric power P_e delivered by the generator is composed by the real or active power and the reactive power. The real power is the power absorbed by the resistive components of the load, while the reactive power accounts for power borrowed from the generator during a cycle and returned to it the next cycle by the inductive and capacitive components of the load such that it has an average null [9, 50, 58, 90].
Any change in real power affects the system frequency while the variation of the reactive power induces voltage changes [50, 90]. Then for a reliable and stable operation, the frequency has to be bounded into a narrow band, which is geographically dependent, meaning in the US this range is $[59.8, 60.2]Hz$ and in most of European and African countries it is $[49.8, 50.2]Hz$. The control of the frequency in the power plant is achieved by the turbine-governor, using the combination of the Load Frequency Control (LFC) and the Automatic Generation Control (AGC), which are going to be introduced in the next section.

2.3

Turbine-governor model

The turbine-governor is a device used to maintain the speed of the turbine in a power plant. It does so by sensing the turbine speed and adjusting the mechanical source of energy (or prime mover) driving the turbine. That control procedure composed by the load frequency control (LFC) and the automatic generation control (AGC) is well known as primary and secondary control acting in different time scales. Indeed, if at any time the

mechanical power P_m is lower (greater) than the demand P_e, the frequency drops (rises). The LFC acts in tens of seconds by adjusting the mechanical power to the demand load, which leads to the stabilization of the frequency to a value different from the nominal value of $50Hz$ (or 60 Hz). After the frequency is stabilized, the AGC acts in tens of minutes to restore the frequency to its nominal or target value by activating some spinning and non-spinning reserves, which increase or reduce the mechanical power appropriately. The spinning reserves are power reserves from on-line generators, while non-spinning reserves denote the power reserves available from generator which have to be started up [46]. We consider a mathematical model of the combined LFC and AGC controllers representing the primary and secondary control applied to the generator.

Once a frequency deviation $\Delta\omega$ is sensed by the turbine governor, it is

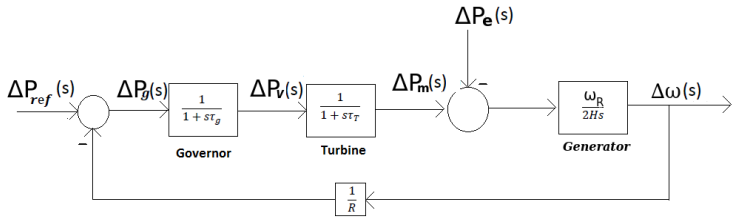

Figure 2.2: Load frequency control block diagram of an isolated power system

converted into a real power command signal ΔP_V, which is transfered to the turbine which produces a corresponding mechanical power input ΔP_m necessary to stabilize the deviation $\Delta\omega$ or to stabilize the frequency to its new steady state [90]. The speed governor mechanism acts as a comparator whose output is the difference between the reference set power ΔP_{ref} and the power $\frac{P_G}{R\omega_R}\Delta\omega$, where R is the governor speed regulation per unit. The action of the LFC which consists just to adjust the governor set point in order to compensate for the power imbalance is represented by the block diagram in figure 2.2 and the corresponding stages of control are modeled in the frequency domain by the equation

$$\begin{cases} (1+\tau_T s)\Delta P_m(s) = \Delta P_V(s) \\ (1+\tau_g s)\Delta P_V(s) = \Delta P_{ref}(s) - \frac{P_G}{R\omega_R}\Delta\omega(s) \\ (\frac{\omega_R}{2HP_G})s\Delta\omega(s) = \Delta P_m(s) - \Delta P_e(s), \end{cases} \tag{2.5}$$

where s is the frequency, τ_T and τ_g representing the turbine and governor time constant. Assuming that the change of frequency implies instantaneously the change in mechanical power ($\tau_T = 0$), equation (2.5) reduces to

Eq. (2.6) written in the time domain,

$$\begin{cases} \frac{d\Delta P_m}{dt} = \frac{1}{\tau_g}[\Delta P_{ref} - \Delta P_m - \frac{P_G}{R\omega_R}\Delta\omega] \\ \frac{d\Delta\omega}{dt} = \frac{\omega_R}{2HP_G}(\Delta P_m - \Delta P_e). \end{cases} \tag{2.6}$$

This set of equations describing the LFC can be re-written as:

$$\begin{cases} \frac{dP_m}{dt} = \frac{1}{\tau_g}[P_{ref} - P_m - \frac{P_G}{R\omega_R}(\omega - \omega_R)] \\ \frac{d\omega}{dt} = \frac{\omega_R}{2HP_G}(P_m - P_e), \end{cases} \tag{2.7}$$

where P_{ref} is the reset action or the reference mechanical power. Despite the LFC stabilizes the frequency deviation by the use of the governor, the system will not operate at the reference state regime. Thus, the automatic generation control, which acts slower than the LFC, reduces the frequency deviation to zero in tens of minutes, to restore the frequency to its nominal value. To achieve that frequency restoration, a reset or rest action has to be provided [90]. A way to achieve this objective is to add an integral controller on the LFC block diagram as it is showed in Fig. 2.3. The integral controller acts on the load reference setting to change the governor speed set point. Thus, using the same transformation as before going from the

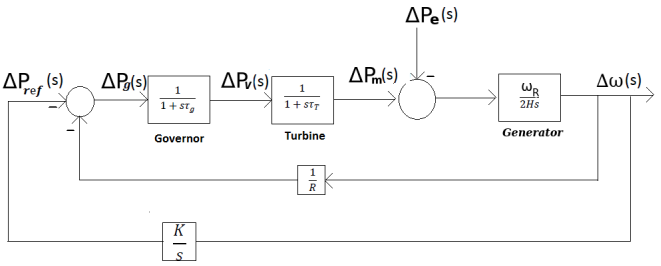

Figure 2.3: Automatic generator control block diagram of an isolated power system.

frequency domain to the time domain, the mathematical model describing the AGC is given by

$$\frac{dP_{ref}}{dt} = -\frac{K}{\omega_R}(\omega - \omega_R). \tag{2.8}$$

Thus, the frequency regulator applied to a generator or a power plant is described by the following set of equations:

$$\begin{cases} \frac{dP_m}{dt} = \frac{1}{\tau_g}[P_{ref} - P_m - \frac{P_{Gmax}}{R\omega_R}(\omega - \omega_R)] \\ \frac{dP_{ref}}{dt} = -\frac{K}{\omega_R}(\omega - \omega_R). \end{cases} \tag{2.9}$$

Equation (2.4) and the set of equations (2.9) govern the dynamics of a power grid where P_m and P_e represent respectively the aggregated generation power and aggregated demand power consumption. The considered model assumes that the whole system operates in a *synchronous* regime, namely the generators have the same frequency and the whole system is robust against small perturbations. Furthermore, the voltage is assumed to be controlled separately as said before, in such a way that the only task here will be the control of the frequency. Considering such assumptions, one can then model the aggregated load as a function of the frequency [77] as follows:

$$P_e(t,\omega) = (1 + \frac{D}{\omega_R}(\omega - \omega_R))P(t). \tag{2.10}$$

Where $P(t)$ is the total aggregated electrical time varying power and D is the frequency coefficient, which, when multiplied by the load represents the frequency sensitive load. D is null for resistive loads but non-zero for rotating machines. We assume $P(t)$ to be constant and we denote by P^{Load} the nominal load such that $P(t)= P^{Load}$. The power plant model is then described by the following set of equations:

$$\begin{cases} \frac{d\tilde{\omega}(t)}{dt} = \eta(P_m - P^{Load}) - \alpha\tilde{\omega} \\ \frac{dP_m}{dt} = \frac{1}{\tau_g}(P_{ref} - P_m - \beta\tilde{\omega}) \\ \frac{dP_{ref}}{dt} = -\gamma\tilde{\omega}, \end{cases} \tag{2.11}$$

with $\tilde{\omega} = (\omega - \omega_R)$ representing the frequency deviation, $\alpha = \frac{DP^{Load}}{2HP_G}$ is frequency sensitive load, $\beta = \frac{P_G}{R\omega_R}$ is the gain of the primary control, $\gamma = \frac{K}{\omega_R}$ is the gain of the secondary control and $\eta = \frac{\omega_R}{2HP_G}$. In order to observe the action of the controller stages, we compute for an arbitrary power system, the frequency in presence of only primary control and then with both primary and secondary control.

Without secondary control ($\gamma = 0, P_{\text{ref}} = P_{\text{m}}(0) = constant$), the role of the frequency regulator is to stop a frequency drop or rise to a steady state determined by the power imbalance in the system. So let assume that the system is subject to a power imbalance ΔP^{Load} due to a sudden increase in demand, then the frequency drops. The primary control adjusts the mechanical power through the governor in order to meet the new demand. Once it is done, the frequency is stabilized to a new steady state which is given by the relation

$$\omega_{st} = \omega_R - \frac{\eta\Delta P^{Load}}{\beta\eta + \alpha}, \tag{2.12}$$

where ω_{st} denotes the new steady state value for the frequency system.

From the expression of ω_{st}, one can easily notice that it depends on the parameter α which, for $\beta = 0$, plays a similar role as the primary control. Relation (2.12) reveals also that for big machines (machines with large inertia H), the frequency deviation is smaller. Fig. 2.4 illustrates the behavior

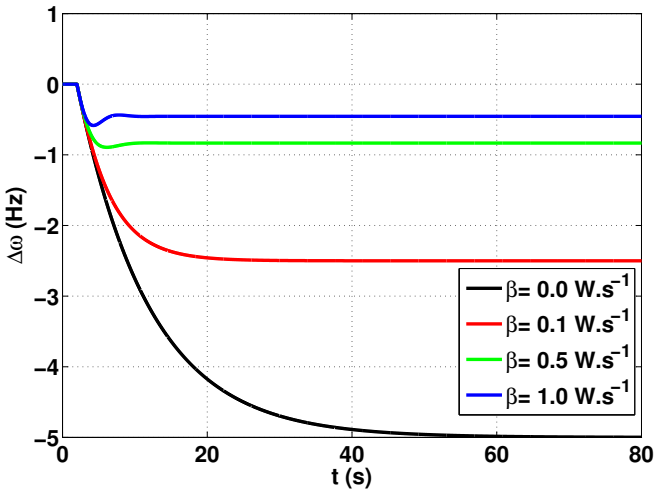

Figure 2.4: Frequency response after a sudden increase of the demand ΔP^{Load}= 0.5 P^{Load}, without secondary control and for different values of the primary control gain β. Other parameters $\eta = 1.0\ W^{-1}s^{-2}$, $\alpha = 1.0\ s^{-1}$, $\gamma = 0\ W$ τ_g= 1.0 s, $P_{ref} = P_m = P_e = 1.0\ W$.

of the system after a sudden increase in load for different value of β and for fixed value of the other parameters. Furthermore, as it is shown in Fig. 2.4, after the sudden increase of consumption ΔP^{Load}, we observe a large the frequency drop without primary control (β= 0 Ws^{-1}), which reaches its new steady state ω_{st}. While it is stabilized earlier in presence of primary control to a new steady state ω_{st}, whose value is closer to the nominal value ω_R when β is increased. The same is observed when the damping coefficient increases. From the mathematical expression of the new frequency steady state (2.12), it is possible to calibrate the primary control parameter β and have a tunable controller, such that for any power imbalance, the system reacts to stabilize the frequency to a predefined value. Let's denote by ϵ the predefined frequency deviation from its reference ω_R. In normal operation, the frequency deviation has to be kept within $[\omega_R - 0.2, \omega_R + 0.2]$ Hz, i.e $\epsilon = 0.2$ Hz. The primary control parameter is then given:

$$\beta = \frac{\eta \Delta P^{Load} - \epsilon\alpha}{\epsilon\eta}. \tag{2.13}$$

Figure 2.5 shows the frequency deviation as a function of time after a sudden increase in demand. Automatically the governor system computes the appropriate value of β necessary to stabilize the frequency to a predefined value $\omega_R \pm \epsilon$.

Once the frequency is stabilized, the secondary control is applied to bring

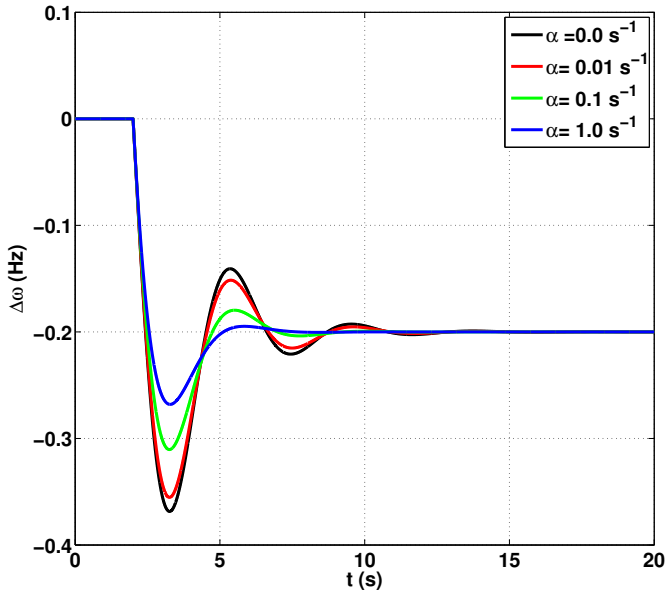

Figure 2.5: Frequency response after a sudden increase of the demand ΔP^{Load}=0.5P^{Load}, without secondary control and for different values of the parameter α. Other parameters $\eta = 1.0\ W^{-1}s^{-2}$, τ_g=1.0 s, $P_{ref} = P_m = P_e = 1.0\ W$.

the frequency back to its reference value ω_{R}. Fig. 2.6 illustrates the time evolution of the frequency for different value of the control gain γ. As it has been represented in figure 2.4 and figure 2.6, the primary and secondary controls act at different time scales. In real power system, the first acts in the order of tens of seconds, while the other in tens of minutes. Adjusting the parameter β, γ and τ_g are enough to calibrate the turbine governor control system.

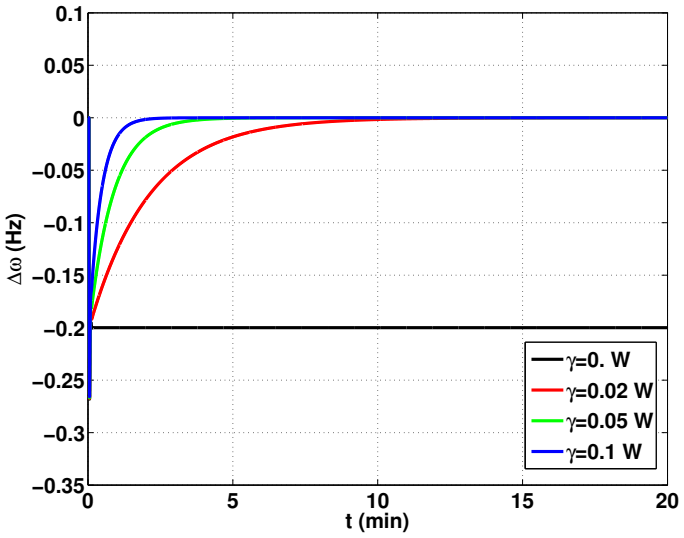

Figure 2.6: Frequency response after a sudden increase of the demand ΔP^{Load}=0.5P^{Load}. Other parameters $\eta = 1.0\ W^{-1}s^{-2}$, $\alpha = 1.0\ s^{-1}$, τ_g=1.0 s, $P_{ref} = P_m = P_e = 1.0\ W$.

2.4

Stability analysis of the model

The stable operation of the power system requires a constant balance between the power consumption and the power supply. Any imbalance leads to the deviation of the frequency system. Such power imbalance can be caused by either a sudden increase in demand, an outage of a line or a loss of generation. These disturbances, which could be accidental, natural or due to a lack of maintenances or the age of the materials, can induce instability in power system. Then a system will be referred to as stable if it is able to return to its origin state after any disturbances or perturbations. This section is dedicated to the determination of the conditions of stability of the system.

To derive the stability conditions of the synchronous state with respect to small perturbations, we linearize Eq. (2.11) around a steady state $(\tilde{\omega}^*, P^*_{\mathrm{m}}, P^*_{\mathrm{ref}}) = (0, P^{Load}, P^{Load})$. We define small perturbations around

the fixed point as:

$$\begin{cases} \tilde{\omega} = \tilde{\omega}^* + \delta\tilde{\omega} \\ P_m = P_m^* + \delta P_m \\ P_{ref} = P_{ref}^* + \delta P_{ref}. \end{cases} \tag{2.14}$$

Let's denote by $\nu = \begin{bmatrix} \delta\tilde{\omega} \\ \delta P_m \\ \delta P_{ref} \end{bmatrix}$ a small perturbation of the steady state. The equation of motion of these small perturbations is then given by:

$$\dot{\nu} = J\nu, \tag{2.15}$$

where the Jacobian matrix J is defined as $J = \begin{bmatrix} -\alpha & \eta & 0 \\ \frac{-\beta}{\tau} & \frac{-1}{\tau} & \frac{1}{\tau} \\ -\gamma & 0 & 0 \end{bmatrix}$.
The characteristic polynomial of J is given by

$$\lambda^3 + (\frac{1}{\tau} + \alpha)\lambda^2 + (\frac{\alpha}{\tau} + \frac{\eta\beta}{\tau})\lambda + \frac{\eta\gamma}{\tau} = 0. \tag{2.16}$$

According to Routh-Ruwitz criterion, the synchronous or steady state of the system is stable if the following conditions are fulfilled [124]:

$$\begin{cases} (\alpha + \frac{1}{\tau}) > 0 \\ \frac{\eta\gamma}{\tau} > 0 \\ (\alpha + \eta\beta)(\alpha + \frac{1}{\tau}) - \eta\gamma > 0. \end{cases} \tag{2.17}$$

The two first conditions are always satisfied since the parameters are all positive. Thus, the system is stable if the gain of the controller is lower than a critical value γ_c ($\gamma < \gamma_c$).

$$\gamma_c = \frac{(\alpha + \eta\beta)(\alpha + \frac{1}{\tau})}{\eta} \tag{2.18}$$

In figure 2.7 we plot the critical secondary control gain γ_c as a function of α, for different values of β keeping other parameters of the system fixed. It illustrates the increase of γ_c with α as well as with the parameter β. These results show that, controlling a system could destroy its stability if too much gain is applied to the controller. Basically there is a range of variation of the control parameter bounded by the critical gain γ_c, below which the control is effective and above which the application of the control leads to the instability of the grid. That range is increasing with the frequency sensitive loads present in the system, meaning that a system with purely resistive loads is more vulnerable in presence of control than systems with

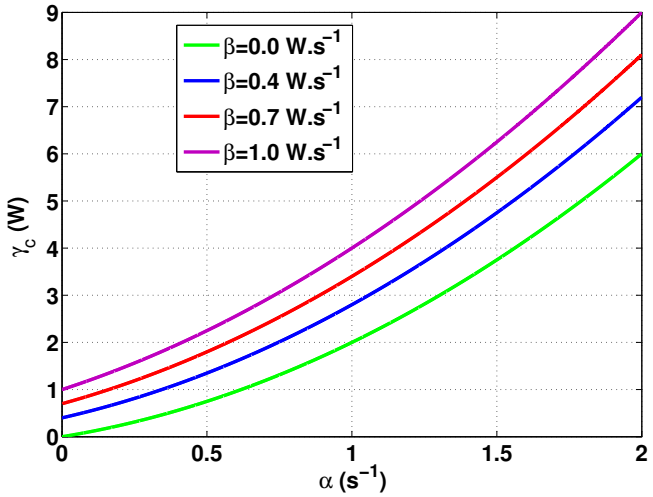

Figure 2.7: Illustration of the critical secondary control gain γ_c as a function of α, for different values of β. Other parameters $\eta = 1.0\ W^{-1}s^{-2}$, τ_g=1.0 s, $P_{ref} = P_m = P_e = 1.0\ W$.

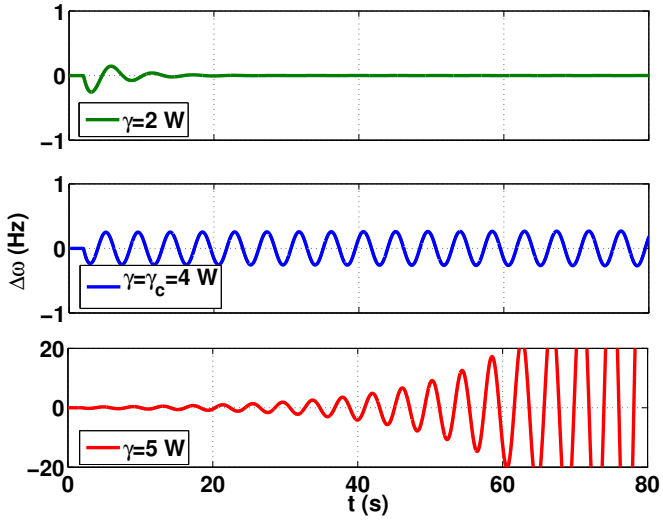

Figure 2.8: Frequency response after a sudden increase of the demand ΔP^{Load}=0.5P^{Load}. Other parameters $\eta = 1.0\ W^{-1}s^{-2}$, $\alpha = 1.0\ s^{-1}$, τ_g=1.0 s, $P_{ref} = P_m = P_e = 1.0\ W$.

rotative loads. Fig. 2.8 illustrates how the system becomes unstable if too strong control is applied. In fact, for the parameters chosen for that particular case $\gamma_c = 4\ W$. There we plot the time evolution of the frequency deviation ($\tilde{\omega} = \Delta\omega = (\omega - \omega_{\mathrm{R}})$) for three values of γ ($\gamma = 2W$, $\gamma = 4W$ and $\gamma = 5W$). As expected, after a small perturbation, the system regains its steady state for $\gamma = 2W$ and moves to an oscillatory state with for $\gamma = 4W$, $\gamma = 5W$. That oscillatory mode is a signature of an instability induced into the system by the secondary control.

2.5

Power grid subjected to fluctuations

In the previous section we have established the generator and governor model for aggregated producers, for constant load. We can determine through the proposed model the state of the system at any time for given parameter values: the system is said to be deterministic. On the other hand, if the evolution of the system is not predictable nor in the short and neither in long term, meaning that the system has many possible trajectories, then such system is said to be stochastic at difference to chaotic system which is predictable for a very short period. Thus, the existence of these trajectories in such stochastic system is due to the presence of parameters or variables whose value changes over a time in a random way. Such process is called stochastic process or random process, which is a mathematical object defined as a set of random variables. From the physics point of view, a stochastic process is often related to a trajectory in phase space which is random enough to demand a probabilistic description [111].
If the parameters of a dynamical and deterministic system vary in a random way, then the effects of these fluctuations could be studied by coupling the equation of motion of the dynamical system to a noise which mimics the global parameter variation or fluctuations in the system. We distinguish different type of noises:

- Parametric noise: the noise affects a parameter of the system.
- multiplicative noise: in such case the noise depends on the value of one or many state variables.
- Additive noise: the noise is totally independent of the state of the system.

So, dynamical systems subjected to such noises are called stochastic dynamical systems which is the topic of this section.

In electric power systems, such noise can be induced by either the generation side through renewable energy sources (wind power and solar power plants...) as mentioned in the introduction, or by the demand side. Fluctuations from mechanical power are, for instance, due to intermittent renewable energy power generation whose production depends on the weather [5, 60, 81, 92]. The variations of demand come from the randomness pattern of consumption of individual consumers. Such pattern corresponds to turning on and off of devices unpredictably [**?**].

We propose in this part a way for modeling that induced noise, which will be considered as additive noise. Thus we will provide a statistical characterization in terms of Gaussian random noise.

Electric power subjected to white noise

We assume that the noise acting at different times is uncorrelated (white noise) and that the statistics of the noise follows a Gaussian distribution, namely we consider a Gaussian white noise $\xi(t)$ which is statistically characterized by its mean and correlation:

$$\begin{cases} <\xi(t)>=\mu \\ <\xi(t),\xi(t^{'}))=\delta(t-t^{'}) \end{cases} \tag{2.19}$$

The Gaussian random noise used here is assumed to have a null mean ($\mu = 0$) and we consider that the noise acts additively on the system dynamics. The equation of motion governing the system is then given by

$$\begin{cases} \frac{d\tilde{\omega}(t)}{dt} = \eta(P_m - P^{Load}) - \alpha\tilde{\omega} + \epsilon\xi(t) \\ \frac{dP_m}{dt} = \frac{1}{\tau_g}(P_{ref} - P_m - \beta\tilde{\omega}) \\ \frac{dP_{ref}}{dt} = -\gamma\tilde{\omega}, \end{cases} \tag{2.20}$$

where ϵ is the strength of the noise. As in the case of the linear stability, the equation of motion of the system can be written for small perturbation around its steady state as

$$\dot{\nu} = J\nu + \epsilon\xi(t) \begin{bmatrix} 1 \\ 0 \\ 0 \end{bmatrix} \tag{2.21}$$

The stability analysis done in the previous section and the conditions of stability obtained are valid here.

Now let's define by λ_1, λ_2 and λ_3 the three eigenvalues associated to the

steady state of the system, with the corresponding eigenvectors v_1, v_2 and v_3 respectively, by P_{ij} the elements of the change basis matrix and by Q_{ij} the elements of its inverse with $i, j = 1, 3$. Let also define by $\mathbf{X} = (X_1, X_2, X_3)^T$ the vector in the canonical basis, and $\mathbf{V} = (V_1, V_2, V_3)^T$ its corresponding state vector in the eigenvector basis such that: $\mathbf{X} = \mathbf{PV}$ or $V = \mathbf{P}^{-1}\mathbf{X} = \mathbf{QX}$.
By applying the previous definitions and using some mathematical tools, the equation of motion describing the state $\mathbf{V}$ of the system is given by

$$\begin{cases} \dot{V_1}(t) = \lambda_1 V_1(t) + \epsilon Q_{11}\xi(t) \\ \dot{V_2}(t) = \lambda_2 V_2(t) + \epsilon Q_{21}\xi(t) \\ \dot{V_3}(t) = \lambda_3 V_3(t) + \epsilon Q_{31}\epsilon\xi(t), \end{cases} \tag{2.22}$$

where each equation represents the well known Ornstein-Uhlenbeck process, whose solutions are given by the following relations:

$$\begin{cases} V_1(t) = V_1(0)e^{\lambda_1 t} + \epsilon Q_{11} \int_0^t e^{\lambda_1(t-s)}\xi(s)ds' \\ V_2(t) = V_2(0)e^{\lambda_2 t} + \epsilon Q_{21} \int_0^t e^{\lambda_2(t-s)}\xi(s)ds' \\ V_3(t) = V_3(0)e^{\lambda_3 t} + \epsilon Q_{31} \int_0^t e^{\lambda_3(t-s)}\xi(s)ds'. \end{cases} \tag{2.23}$$

As a stochastic problem, we describe the state of the system in terms of mean and variance for the V_i variables for $i = 1, 3$:

$$\begin{cases} \langle V_1 \rangle = V_1(0)e^{\lambda_1 t} \\ \langle V_2 \rangle = V_2(0)e^{\lambda_2 t} \\ \langle V_3 \rangle = V_3(0)e^{\lambda_3 t} \end{cases} \tag{2.24}$$

$$\begin{cases} \langle V_1^2 \rangle = \frac{-\epsilon^2 Q_{11}^2}{2\lambda_1}(1 - e^{2\lambda_1 t}) + V_1^2(0)e^{2\lambda_1 t} \\ \langle V_2^2 \rangle = \frac{-\epsilon^2 Q_{21}^2}{2\lambda_2}(1 - e^{2\lambda_2 t}) + V_2^2(0)e^{2\lambda_2 t} \\ \langle V_3^2 \rangle = \frac{-\epsilon^2 Q_{31}^2}{2\lambda_3}(1 - e^{2\lambda_3 t}) + V_3^2(0)e^{2\lambda_3 t} \end{cases} \tag{2.25}$$

One notices that for a stable synchronous state ($\lambda_i < 0$) the mean of the variables of the system is null and the variance is constant, while for an unstable synchronous state, the mean and the variance are growing exponentially. The variance of the variables in the canonical basis is given by:

$$\begin{cases} \langle X_1^2 \rangle = P_{11}^2\langle V_1^2 \rangle + P_{12}^2\langle V_2^2 \rangle + P_{13}^2\langle V_3^2 \rangle + 2P_{11}P_{12}\langle V_1, V_2 \rangle + 2P_{11}P_{13}\langle V_1, V_3 \rangle \\ \langle X_2^2 \rangle = P_{21}^2\langle V_1^2 \rangle + P_{22}^2\langle V_2^2 \rangle + P_{23}^2\langle V_3^2 \rangle + 2P_{21}P_{22}\langle V_1, V_2 \rangle + 2P_{21}P_{23}\langle V_1, V_3 \rangle \\ \langle X_3^2 \rangle = P_{31}^2\langle V_1^2 \rangle + P_{32}^2\langle V_2^2 \rangle + P_{33}^2\langle V_3^2 \rangle + 2P_{31}P_{32}\langle V_1, V_2 \rangle + 2P_{31}P_{33}\langle V_1, V_3 \rangle, \end{cases} \tag{2.26}$$

with the elements of the vector $\mathbf{X}$ defined by:

$$\begin{cases} X_1 = P_{11}V_1 + P_{12}V_2 + P_{13}V_3 \\ X_2 = P_{21}V_1 + P_{22}V_2 + P_{23}V_3 \\ X_3 = P_{31}V_1 + P_{32}V_2 + P_{33}V_3 \end{cases} \tag{2.27}$$

.

$$\langle V_i, V_j \rangle = \frac{-\alpha^2 Q_{i1} Q_{j1}}{(\lambda_i + \lambda_j)}. \tag{2.28}$$

These solutions are valid only for real negative eigenvalues. For complex eigenvalues, $\langle V_2^2 \rangle = \langle V_3^2 \rangle = 0$, $\lambda_3 = \lambda_2^*$ and $V_3 = V_2^*$ because λ_2 and λ_3 are complex conjugate.

The basis transformation matrix P is given by:

$$P = \begin{bmatrix} 1 & 1 & 1 \\ \frac{\alpha+\lambda_1}{\eta} & \frac{\alpha+\lambda_2}{\eta} & \frac{\alpha+\lambda_3}{\eta} \\ \frac{-\gamma}{\lambda_1} & \frac{-\gamma}{\lambda_2} & \frac{-\gamma}{\lambda_3} \end{bmatrix} \tag{2.29}$$

Fig. 2.9 (a) shows the time evolution of the electrical (in blue) and mechanical (in green) power of the system subjected to an additional white noise. Fig. 2.9 (b) illustrates the time evolution of the electrical frequency resulting from introducing the noise. These results have been obtained integrating numerically the set of eqs. (2.20) using the Milshthein alghoritm [111] with a time step of 10^{-3}. The Gaussian random numbers have been generated using the Box-Muller-Wiener algorithm. The fluctuation of the system around its steady state value $(0, 1, 1)$, are observed. The parameters of the system have been chosen in such away that the synchronous state is stable. Furthermore, for these parameters, we show in figure 2.10, the frequency variance numerically calculated from Eq. (2.30) and analytically using the expression given in Eq. (2.26).

$$\sigma_V^2 = \langle V^2 \rangle - \langle V \rangle^2. \tag{2.30}$$

We get a perfect agreement between both methods, which is the increase of the variance σ_ϖ^2 with the amplitude of the noise. These simple study case shows the big challenge the traditional grid is facing with the integration of renewable energy sources which feed huge power fluctuations into the grid. That is somehow the objective of this work, which is to conceive some protocols able to handle the fluctuations while preserving the comfort of consumers.

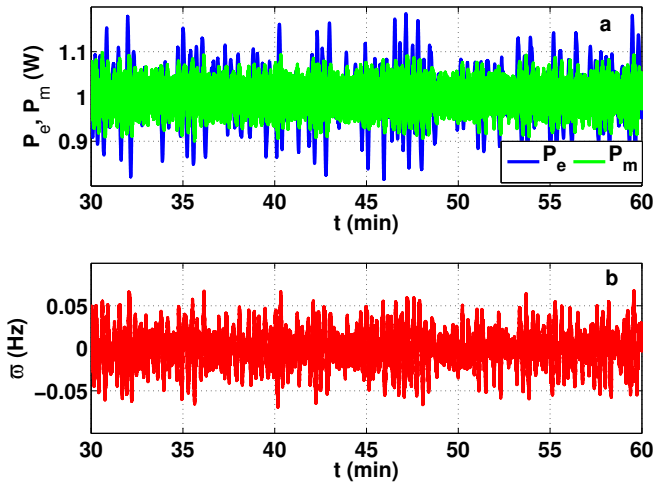

Figure 2.9: Time histories of the variables of the system for ϵ=0.01. Other parameters $\eta = 0.1\ W^{-1}s^{-2}$, $\alpha = 1.0\ s^{-1}$, τ_g=1.0 s, $P_{ref} = P_m = P_e = 1.0\ W$.

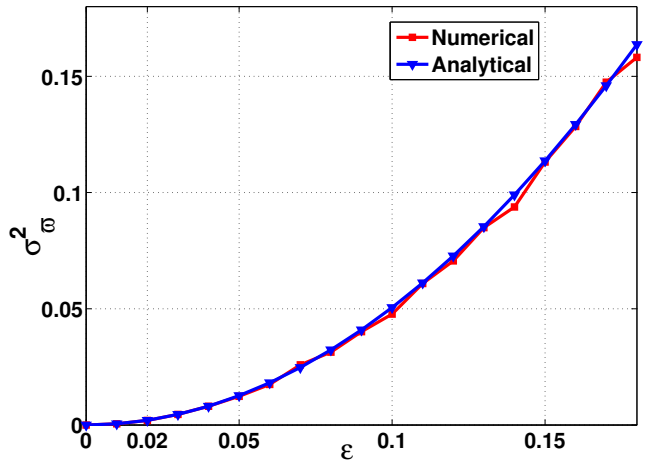

Figure 2.10: Frequency variance versus amplitude of the Gaussian white noise for the following parameters $\eta = 0.1\ W^{-1}s^{-2}$, $\alpha = 1.0\ s^{-1}$, τ_g=1.0 s, $P_{ref} = P_m = P_e = 1.0\ W$.

CHAPTER 3

Demand model

3.1

Introduction

In this chapter, it is assumed that fluctuations are brought by individual loads ($P_j(t)$) switching on and off randomly and we propose a very simple stochastic model able to reproduce the main statistical properties of real demand fluctuations [109]. To do so, we recorded at the IFISC the frequency fluctuations of the Balearic island grid. This data obtained is used for fitting a single parameter of our stochastic demand model.

3.2

Stochastic demand model

Residential loads are composed by generic domestic appliances such as: refrigerators, freezers, air conditioners, electric heaters, dishwashers, chargeable portable devices that can switch on and off at any time, such that each load P_j can be considered as time varying. Then for a population of N devices or bunches of aggregated devices the total load demand will be

$$P(t) = \sum_{j=1}^{N} P_j(t), \tag{3.1}$$

where $P_j(t)$ is the load of device (or group of devices) j at time t. For the sake of simplicity in this work we consider that $P_j(t)$ can only take the values 0 (off) or P_0 (on). We consider that appliances in the off state switch on with a rate p, while running devices switch off with rate q. This creates a fluctuating demand with statistical properties that depend on the parameters p, and q. Throughout this work we will consider that the rates are constant and identical, $p = q$, such that the average power remains constant. Furthermore, we take the load parameters $N = 1000$ and $p = q = 6.55 \times 10^{-4}$ and the power plant parameters $\omega_{\mathrm{R}} = 50$ Hz, $P_{\mathrm{G}} = 37320$ MW, $\tau_{\mathrm{g}} = 0.78$ s, $H = 4s$, $D = 0.026$, $R = 0.04$ and $K = 6600$ MW/s.

The simple model proposed here corresponds exactly to a Markov process for a system composed of N *particles* each one making transitions between two states (on, off) with rates p and q [111]. If there is no interaction among devices this problem can be solved exactly, and for the case $p = q$ the average power demand is $\langle P \rangle = NP_0/2$, and, in the stationary regime, the size of the fluctuations is proportional to $\sqrt{N}$, with variance $\sigma_P = \sqrt{N}P_0/2$. As a matter of fact the variance of the fluctuations at all times is given by

$$\sigma_P^2(t) = NP_0^2[\mu(t) - \mu(t)^2], \tag{3.2}$$

where the probability $\mu(t)$ of finding a device on is given by

$$\mu(t) = \frac{1}{2}(1 - e^{-2pt}) + \mu(0)e^{-2pt}. \tag{3.3}$$

Fig. 3.1 shows the evolution of the probability of finding a device on as obtained from Eq. (3.3) for different values of p to illustrate the difference in the characteristic time $\tau = \frac{1}{2p}$ to reach the stationary state. In blue the probability computed averaging over a large number of noise realizations is shown for $p = 6.55 \times 10^{-4}$ s^{-1}.

Time varying rates $p(t)$, $q(t)$ following daily demand patterns as the one shows in figure 3.2 (where fluctuations represent unexpected switchings of devices or aggregated of devices) will be considered elsewhere. In fact, figure 3.2 shows on the panel (a) the rate of switching on taken as $p(t) = q+\sigma\times f(t)$ and the rate of switching off is kept constant. $f(t)$ is a polynomial function fitting the real demand daily variation. On the panel (b) there is the corresponding number of devices on, among a sample of $N = 1000$ devices. One observes that, the number of device on follows $p(t)$.

We now focus on the fluctuations in the total load predicted by the model, in the case of constant p and q, with $p = q$. Time scales play a very important role here, as the features of the fluctuations in Fig. 3.3 are quite different depending on the observation time scale. For short time scales, the

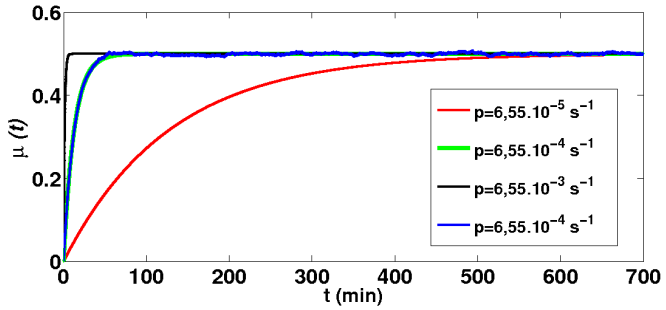

Figure 3.1: Probability $\mu(t)$ of finding a device on as obtained from Eq.(3.3) for different values of the switching on probability p. The corresponding characteristic times to reach the stationary states are $\tau = 125$ min (red line), 12.5 min (green line), and $\tau = 1.25$ min (black line). Here $\mu(0) = 0$.

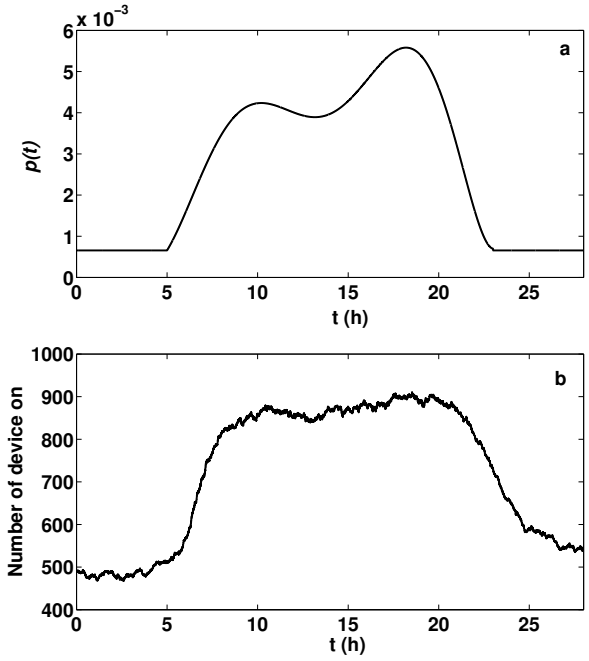

Figure 3.2: Demand consumption of a system of N=1000 devices with the rate of switching off $q = 6,55 \times 10^{-3}$ s^{-4}, the rate of switching on $p = q + \sigma \times f(t)$, with $\sigma = 1,0 \times 10^{-4}$

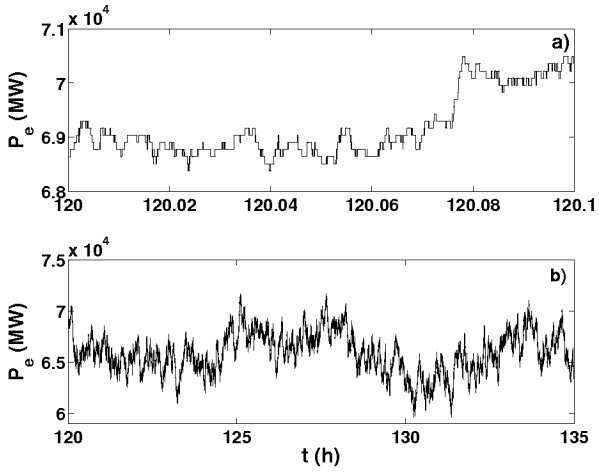

Figure 3.3: Demand fluctuations at different time scales for $N = 1000$ devices of power $P_0 = 132MW$. The switching probability is $p = 6,55 \times 10^{-4}\ s^{-1}$.

above stochastic process is essentially a random walk, the on/off switchings of a device at each time correspond to the characteristic step forward or backward of a random walk. As a matter of fact, from (3.2) one can show that for short times the variance of the fluctuations growths as $\sigma_P(t) \propto \sqrt{t}$, characteristic of a random walk. Fig. 3.3 a) shows a time series of the demand P for $N = 1000$ devices of power $P_0 = 132MW$ with a high time resolution, where the discrete jumps can be clearly appreciated.

However, as the number of devices is finite, the random walk is bounded, and fluctuations can not grow indefinitely. For long times ($t \gg \tau$) the variance saturates to $\sigma_P = \sqrt{N}P_0/2$. At these large time scales the fluctuations look more like white Gaussian noise with the latter standard deviation (Fig. 3.3 b). These features become clear looking at the Fourier transform of the total load $P_{\rm e}(\omega') = \int e^{i\omega' t} P_{\rm e}(t)dt$. In Fig. 3.4 we show the power spectrum $|P_{\rm e}(\omega')|^2$. For observations at very large time scales (low frequencies) the spectrum is flat, characteristic of white noise, while for short time scales (high frequencies) the spectrum displays a power-law shape with a slope of -2, characteristic of a random walk [111].

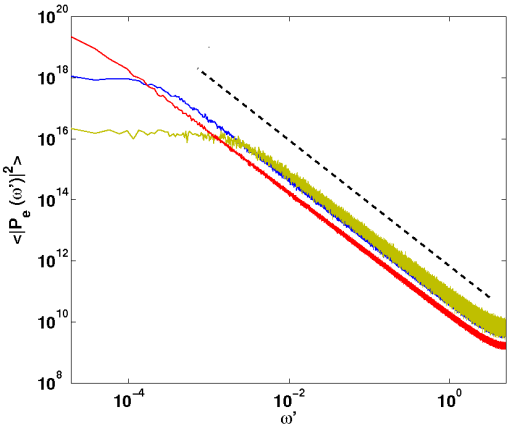

Figure 3.4: Power spectrum of the electric load produced by the demand model for $p = 6,55 \times 10^{-5}$ s^{-1} (red), $p = 6,55 \times 10^{-4}$ s^{-1} (blue), and $p = 6,55 \times 10^{-3}$ s^{-1} (green). Averages over 100 noise realizations are shown. Dashed line has slope -2 for comparison.

3.3

Comparison of the stochastic demand model with real measurements

We next compare the spectrum of the frequency fluctuations obtained from numerical simulations of the model with the spectrum of frequency fluctuations measured from a wall-plug outlet. This allows us to estimate a realistic value of the probability p.

Measurements were performed using basic custom electronics implemented on a Raspberry Pi 2. The Raspberry Pi 2 device is a small, single board and general purpose computer with a 900 MHz quad-core ARM compatible CPU. The electrical grid voltage signal was obtained from a standard wall-plug and was subsequently scaled to the voltage range of an analog digital converter IC (ADC, Texas Instruments ADC7816). The analog digital converter was connected to the Raspberry Pi via a serial bus link. The grid signal was sampled using one of the CPU´s cores with a resolution of 12 bits at a rate of 62.5 KSamples/s. The power grid waveform was recorded in real-time during temporal windows of 10 s which corresponds to ≈ 200 periods of the grid signal. Following completion of the 10 s sampling window, the sampling core passed the data to the CPU´s second core for data

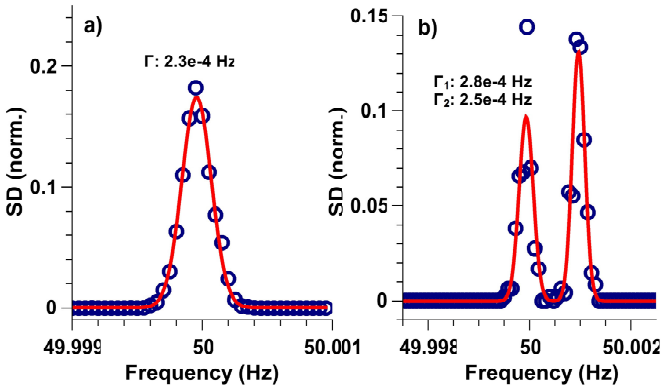

Figure 3.5: Calibration of the spectrum analyzer. Normalized Spectral Density (SD) for a constant frequency input during ∼10 h (a) and for a bi-modal spectrum with a frequency separation of 1 mHz.(b)

analysis. As such, the device was capable to continuously sample and process the input waveform without loss of data. By measuring the temporal positions of the grid signal's zero crossings, the second CPU core obtained an average frequency for each 10 s window.

Before its utilization as a grid frequency spectrum analyzer, we extensively calibrated the stability and resolution of our device, using a Keysight 33120A signal generator as calibration source. Figure 3.5 shows two example spectra obtained during calibration. Data shown in panel (a) corresponds to the spectral distribution during a $\sim$ 10 hour calibration test using a 50 Hz signal. The obtained stability was excellent, showing no indications of drifts while reaching a spectral resolution of $\sim 2.5 \times 10^{-4}$ Hz. In a second calibration, we use a signal which rapidly switches from 50 Hz to 50.001 Hz. Panel (b) shows the obtained spectra, demonstrating that the device is capable to clearly detect frequency changes below 1 mHz.
Fig. 3.6a) shows the experimental results for the frequency obtained measuring the output of a power outlet. One observes random fluctuations of the frequency within a range of ± 0.2 Hz around the 50 Hz reference value. Fig. 3.6c) shows the power spectrum of the frequency. At low frequencies the spectrum is basically flat while it shows a power law decay for large frequencies. For comparison Fig. 3.6b) and d) show the frequency time trace and power spectrum obtained from a simulation of Eqs. (2.11) with the stochastic demand model described in Section 3.2. Stochastic demand fluctuations as those shown in Fig. 3.3 translate to fluctuations of the frequency (Fig. 3.6b). The power spectrum of the frequency fluctuations displays a plateau

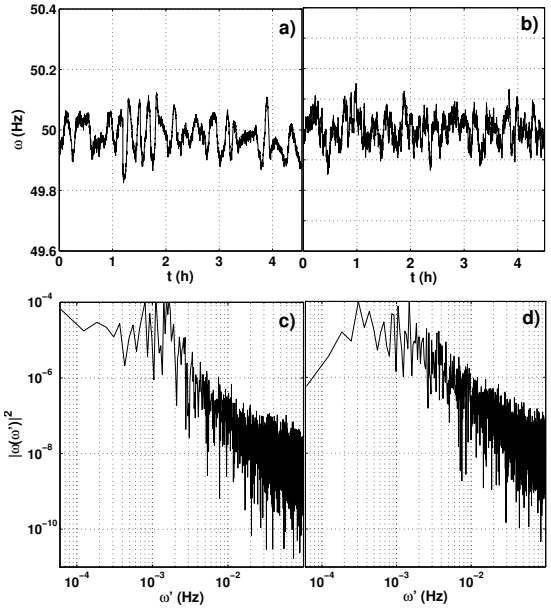

Figure 3.6: Time series (a) and power spectrum (c) of the frequency measured at an electrical outlet at IFISC. Panels (b,d) show the equivalent results from a numerical simulation with $p = 6.55 \times 10^{-4}$ s^{-1}, $N = 1000$, $P_0 = 132\ MW$ and power plant parameters are $\omega_{\mathrm{R}} = 50$ Hz, $P_{\mathrm{G}} = 37320\ MW$, $\tau_{\mathrm{g}} = 0.78$ s, $H = 4s$, $D = 0.026$, $R = 0.04$ and $K = 6600\ MW/s$.

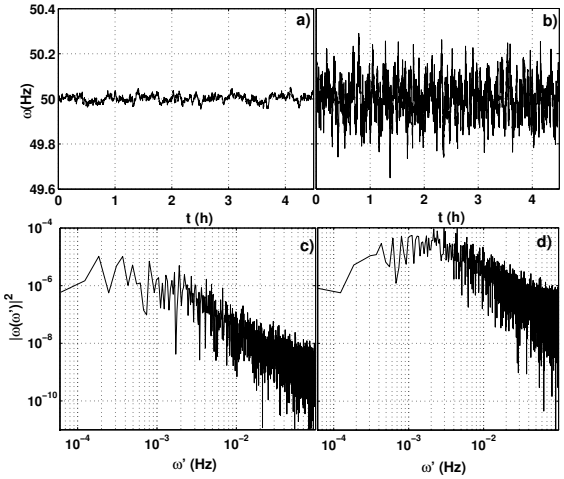

Figure 3.7: Frequency time series and power spectrum for a numerical simulation with $p = 6.55 \times 10^{-5}$ s^{-1} (a,c) and with $p = 6.55 \times 10^{-3}$ s^{-1} (b,d). Other parameters as in Fig. 3.6.

for low frequencies and decay as a power law for high frequencies (Fig. 3.6d), reproducing the characteristics of the power spectrum of the demand fluctuations (Fig. 3.4). Therefore, changing p in the stochastic model shifts the characteristic time scales of the frequency fluctuations as well, which allows us to adjust the value of p in order to fit the experimental data. Fig. 3.7 shows the result generated by the model for two very different values of p. A shift in the frequency where the power spectrum starts to decay can be clearly appreciated. We finally take $p = 6.55 \times 10^{-4}$ s^{-1} as a good value that reproduces the power spectrum of the frequency fluctuations measured experimentally (Fig. 3.6 a). For this probability of switching, in average, about six of the 1000 devices receive an order to switch on or off every 10 seconds.

We find that the adjusted probability p corresponds to a characteristic time for the saturation of the fluctuations around 12 min. Frequency fluctuations have a flat spectrum as white noise for time scales slower than this characteristic time. For faster time scales frequency variations behave as a random walk. The experimental data displays also a superimposed periodicity, as revealed by the peak in the power spectrum around 1×10^{-3} Hz, corresponding to oscillations with a period of approximately 15 min, clearly observable in the data, and which are not introduced in the model.

3.4

Conclusion

In conclusion, we proposed a demand model as combination of frequency and non frequency dependent loads [109]. This represents the ensemble of loads attached to the power system such as rotating machines, air conditioners, fridges, TVs, coffee machines, heaters and so on. We assumed that the global demand consumption follows the daily variation, meaning having two peaks of consumption in which the system is stressed. On the top of this demand we proposed a stochastic model, which consists of switchings on and off of devices randomly with a rate that we determined comparing the outcome of the model with empirical frequency fluctuations. This comparative study has been done measuring the frequency of the Balearic island grid using a basic custom electronics implemented on a Raspberry Pi 2. The fitting has allowed to find the rate of switchings for which the proposed demand model has the same statistical properties as the real electric power system (Balearic). This demand model including the stochastic fluctuations associated to the power plant model constitute the power system on which we are going to apply the dynamic demand control in the next chapter.

CHAPTER 4

Dynamic Demand Control protocol

4.1 Introduction

In the previous chapters, we introduced a model for the power plant and the demand. Fluctuations in individual loads have been introduced and the corresponding frequency variations have been compared with the real recorded data, in order to fit the parameters of the model. That process allowed us to generate frequency fluctuations similar to a realistic response of the power system against such fluctuations. The resulting frequency varies within the acceptable range $[49,8 - 50,2]\ Hz$. After having set these prerequisites, we propose in this chapter a generic Dynamic Demand Control (DDC) protocol that can be applied to any device susceptible to postpone energy consuming tasks [109]. As discussed in the introduction DDC is an example of demand side management. DDC is applied to the appliances in order to control their consumption with the objective of reducing the grid frequency fluctuations. This chapter is organized as follows: We first describe the DDC protocol in section.4.2. The calibration and application to a defined power system is done afterwards, and the effects of DDC on that system are discussed. The last section of this chapter is dedicated to the improvement of DDC using device-device communication. In that section, the implementation of the protocol of communication will be presented. Some cases will be analyzed afterward and a comparison with the cases without control and without interaction will conclude the section.

4.2

Dynamic Demand Control protocol

The idea behind the DDC algorithm is to delay the switching on or off of a device if the value of the electrical frequency is outside a given range. As discussed in the introduction, this is applicable to devices such as heaters, boilers, dishwashers, washing machines, air conditioners, refrigerators, etc. for which it is feasible to postpone a task for a while. The generic DDC algorithm we consider can be implemented on top of the demand model introduced in Chapter 3 and works as follows:
At every time step devices can randomly turn on, off or remain in the same state they were before. However for smart devices, before committing any change of state, the DDC controller measures the grid frequency ω and the change is only committed if ω is within a suitable range. Smart devices in the off state that randomly would switch on effectively do so only if the frequency is above a minimum level $\omega > \omega_{\mathrm{R}} - \epsilon$. When a switch-on is prevented by the DDC the missing consumed energy is accounted to be used at a latter time , frequency conditions permitting. Similarly smart devices in the on state that randomly would switch off effectively do so only if the frequency is below a maximum level $\omega < \omega_{\mathrm{R}} + \epsilon$, and when a switching-off is skipped, the extra consumed energy is accounted to be saved later. The objective is that, on the long run, every smart device has used the same total energy as if it were not smart. So, in the following we refer to the extra (saved) energy consumption generated by the DDC control as pending tasks. Energy consuming pending tasks, namely, pending tasks that require to switch on a device to recover from a previous instance in which the device could not turn on when it was required, are recovered only if frequency is above a threshold $\omega > \omega_{\mathrm{R}} + \epsilon_1$. Similarly pending tasks saving energy are recovered only if $\omega < \omega_{\mathrm{R}} - \epsilon_1$. To avoid the simultaneous switching of all devices with pending tasks when these thresholds are crossed, each device starts recovering pending tasks with probability γ. The randomization of the response of appliances is known to avoid oscillations created by the synchronizations of smart devices [57, 78, 90, 100]. Thus the overall DDC algorithm consists then of two distinct parts: decision on committing actions and recovery of pending tasks, and it has only three parameters, namely ϵ for the allowed range to commit actions, and ϵ_1 and γ for the recovery of pending tasks.

Calibration of DDC

We next analyze the role of the different DDC parameters. Typically it will be convenient to set ϵ below the statutory limit for frequency variations (± 0.2 Hz). Throughout this paper we take $\epsilon = 0.05$ Hz. In this section we consider that DDC is applied to all devices, while in section 4.2 we will address the effect of applying DDC only to a fraction of them.

We first consider a large value of ϵ_1 so that pending tasks are almost not recovered in practice. In this situation, as shown in Fig. 4.1 the control efficiency is very good and the frequency stays almost always within the tolerance range $\omega_R - \epsilon < \omega < \omega_R + \epsilon$. The counterpart is, however, that depending on the system conditions smart devices will consume more (or less) energy than what they were supposed to consume to perform whatever task they were designed to do, accumulating pending tasks indefinitely, which is unrealistic.

We define the pending tasks Q_i of smart device i as the absolute value of the energy that this device has consumed in excess or in shortage with respect to the reference case of not applying any DDC control. Total pending tasks on the whole grid are given by $Q = \sum_i Q_i$.

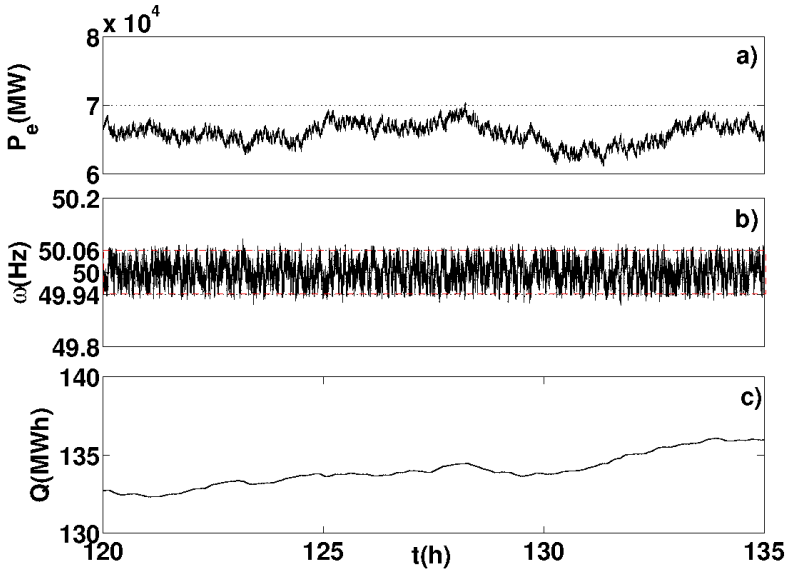

Figure 4.1: Time series of (a) the demand P_e, (b) frequency ω, and (c) pending tasks Q with DDC applied to all devices. We have considered $\epsilon = 0.05$ Hz, $\epsilon_1 = 0.1$ Hz and $\gamma = 1$. Other parameters as in Fig. 3.6

To effectively recover pending tasks we have to decrease ϵ_1. Decreasing the value of ϵ_1 and setting the recovery probability γ to 1 leads to an effective recovery of all pending task as soon as the frequency crosses the threshold. Although this avoids the accumulation of pending tasks, it leads to large frequency fluctuations (even larger than without DDC). All devices with energy demanding pending tasks turn on simultaneously when the frequency crosses $\omega_R + \epsilon_1$ from below. Similarly all devices with pending tasks saving energy will simultaneously turn off when the frequency crosses $\omega_R - \epsilon_1$ from above.

In order to avoid this synchronized switchings it is required that $0 < \gamma < 1$ such that pending tasks are recovered progressively, avoiding sudden demand peaks. To determine suitable values of ϵ_1 and γ we have explored this two-parameter space performing numerical simulations and computing the variance of the frequency fluctuations σ_ω^2 and the number of pending tasks averaged over noise realizations $\langle Q \rangle$. Fig. 4.2 shows the results for changing ϵ_1 for a fixed value of $\gamma = 1.2 \times 10^{-3}$. For $\epsilon_1 < -\epsilon$ pending tasks are recovered practically immediately, washing out the effect of DDC. As ϵ_1 is increased DDC starts acting, progressively reducing frequency fluctuations. We consider only positive values of ϵ_1 as recovering pending task under unfavorable frequency conditions is not recommendable. For ϵ_1 small the average number of pending tasks reaches a stationary value. This stationary value increases slowly with ϵ_1. A qualitative change in the number of pending tasks occurs at $\epsilon_1 \approx 0.06$ Hz, slightly above the value of the tolerance $\epsilon = 0.05$ Hz of the frequency control. At this value pending tasks increase very sharply. For ϵ_1 above this value the number of pending tasks does not reach an stationary value, it diverges for large times. The plateau shown in Fig. 4.2b corresponds to the value of the pending tasks after a finite time, $t = 135$ h, used for the numerical simulations. Physically, frequency fluctuations are quite reduced and very rarely reach this large values of ϵ_1, precluding the recovering of pending tasks. In this circumstances the recovery probability γ is practically irrelevant and the dynamics is similar to that shown in Fig. 4.1 for $\epsilon_1 = 0.1$ and $\gamma = 1$.

We note that, actually, for small values of γ and intermediate values of ϵ_1, the recovery of pending task helps in controlling frequency fluctuations, because additional devices switch on (off) only for high (low) frequencies, helping to reduce fluctuations even further. This is the reason why the variance of the frequency fluctuations can be even lower that in the case without recovery of pending tasks. As a matter of fact, the variance of the frequency fluctuations has a minimum around $\epsilon_1 = 0.037$ Hz.

Considering the variance of the frequency fluctuations σ_ω^2 and the number of pending tasks, from Fig. 4.2 one would conclude that the optimum value

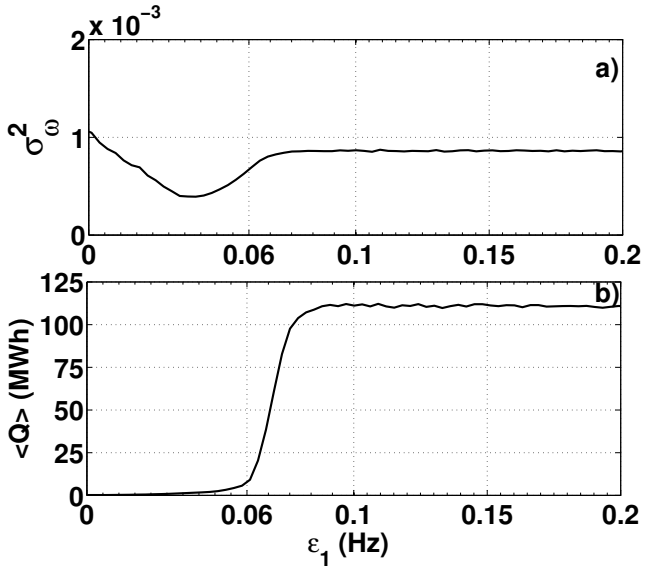

Figure 4.2: Frequency variance (a) and pending tasks at time $t = 135$ h averaged over 100 realizations of the noise (b). We have considered $\gamma = 1.2 \times 10^{-3}$. Other parameters as in Fig. 4.1.

for $\gamma = 1.2 \times 10^{-3}$ is $\epsilon_1 = 0.037$ Hz, but this is not the whole story. Looking in detail at trajectories of the frequency for $\epsilon_1 = 0.037$ Hz, one observes that, despite the variance is lower than for larger values of ϵ_1, there are extreme events in which the frequency takes very large or very small values, outside the statutory limits. These events are rare, but pose a great risk to the system since they could trigger a failure or blackout. Fig. 4.3 shows trajectories of the frequency in simulations with different values of ϵ_1. These extreme events are caused by the random synchronization of pending tasks recovery, and their probability increases with decreasing ϵ_1. Fig. 4.4 shows the estimated cumulative rank probability $R(\Delta\omega)$ of finding a fluctuation larger than $\Delta\omega = |\omega - \omega_R|$ calculated as

$$R(\Delta\omega) = 1 - \frac{i}{m-1}, \tag{4.1}$$

where i is the rank of the frequency fluctuation of size $\Delta\omega$ in a very long time series with m samples. The black dots shows the case of random switching on and off without DDC for comparison. For the parameters considered here, fluctuations above $\Delta\omega = 0.2$ Hz are practically inexistent. When applying DDC with a large ϵ_1, for instance $\epsilon_1 = 0.1$ Hz shown in yellow triangles in Fig. 4.4, the frequency fluctuations are largely reduced

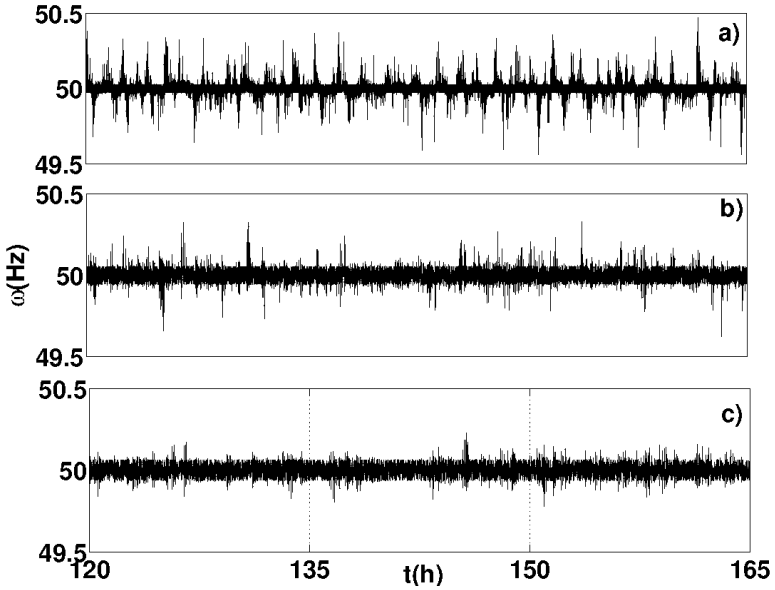

Figure 4.3: Time series of the frequency for different values of ϵ_1: a) $\epsilon_1 = 0.022$ Hz, b) $\epsilon_1 = 0.05$ Hz, and c) $\epsilon_1 = 0.06$ Hz. Other parameters as in Fig. 4.1.

as reflected in the narrowing of the width of the probability distribution. However, since the frequency variations rarely go above $\Delta\omega = 0.1$, pending task are very rarely recovered and they keep accumulating. For $\epsilon_1 = 0.037$ Hz, corresponding to the minimum of the variance of the frequency fluctuations, shown in green stars in Fig. 4.4, the average number of pending tasks is low and small/medium size fluctuations are largely suppressed, however we observe exponential tails in the probability distribution, indicating that large fluctuations have non negligible probabilities to occur.

A compromise is chosing $\epsilon_1 = 0.06$ Hz (gray circles in Fig. 4.4). For this value, we obtain a fairly low value for the variance of the fluctuations and average number of pending task, and a reasonably low probability of large events to occur, although the distribution still has exponential tails signaling that the problem of large fluctuations due to recovery of accumulated pending task does not disappear completely. This phenomenon is similar to what it is observed for the occurrence of large blackouts in power grids due to risk-adverse policies: strict control policies suppress small or mid-size blackouts but increases the probability of very large ones [12]. This is a signature of a system operating close to a critical condition [25]. As a matter of fact in Fig. 4.4 we observe a qualitative change in the shape of the

probability distributions for $\Delta\omega > \epsilon_1$, signaling the recovery of accumulated pending tasks as the cause for the long tail of the distribution.

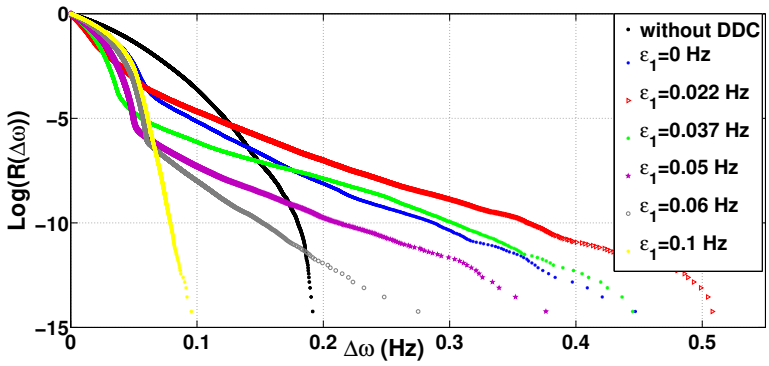

Figure 4.4: Cumulative rank probability distribution of finding a fluctuation larger than $\Delta\omega = |\omega - \omega_R|$. Parameters as in Fig. 4.1.

We now focus on the effect of varying the value of the recovery probability γ. Fig. 4.5 shows the variance of the frequency fluctuations and the pending tasks at time $t = 135$ h averaged over 100 realizations of the noise as as function of γ for a fixed value of $\epsilon_1 = 0.06$ Hz. For low values of γ the probability of recovering pending task is low, and therefore the control of the frequency fluctuations is very efficient at the expense of accumulating an increasing number of pending task. In fact for $\gamma = 0$, no task is recovered and $\langle Q \rangle$ diverges with increasing time. For γ not infinitesimally small the amount of pending tasks evolves in time to a stationary value. As γ is increased the stationary value for $\langle Q \rangle$ decreases rapidly without being detrimental for the frequency variance. If γ is too large (beyond the range of the figure) many devices start recovering pending task simultaneously causing synchronization peaks in the demand and increasing frequency fluctuations again. We find, then, that good values for the threshold and probability of recovering pending tasks are $\epsilon_1 = 0.06$ Hz and $\gamma = 1.2 \times 10^{-3}$ respectively. These values have been determined for a constant fixed grid load. As a matter of fact, the optimum value of ϵ_1 depends on the load of the grid. The smaller the load, the smaller the value of ϵ_1 in order to avoid the accumulation of pending task, otherwise, if the load is low and ϵ_1 too high, frequency fluctuations never reach this threshold and pending tasks can not be recovered. The precise dependence of ϵ_1 on the system load and the effect of time varying loads will be investigated elsewhere.

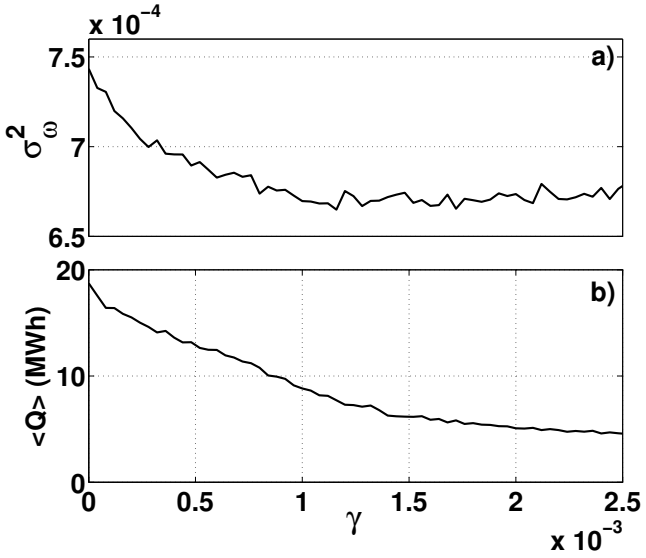

Figure 4.5: Frequency variance (a) and average pending tasks at time $t = 135$ h averaged over 100 realizations of the noise (b). We have considered $\epsilon_1 = 0.06$ Hz. Other parameters as in Fig. 4.1.

Fraction of smart devices on the grid

We now focus on the case in which only a fraction $\gamma_1 = n/N$ of devices are smart, n being the number of smart devices and N the total. So far we have considered the two extreme cases: no smart devices ($\gamma_1 = 0$) and all the loads smart ($\gamma_1 = 1$). A more realistic case would be a grid where only part of the load is smart, while the rest keeps switching on and off according to random demand. In order to study how the performance of the grid depends on the number of smart devices, we have performed a series of simulations with the same stochastic realization but varying the fraction of smart devices γ_1. Figs. 4.6, 4.7, and 4.8 show time traces of the demand P_e, frequency ω, and pending tasks per smart device Q/n for an increasing number of smart devices in the system. Fig. 4.9 shows the dependence of the frequency variance σ^2_ω and the number pending tasks per device at time $t = 135$ h averaged over 100 realizations of the noise $\langle Q \rangle / n$ on the fraction of smart devices γ_1. We observe that the frequency variance decreases very fast increasing the fraction of smart devices. The variance saturates at $\gamma_1 = 0.2$. Increasing the fraction of smart devices above this value does not significantly reduces the frequency variance. The number of

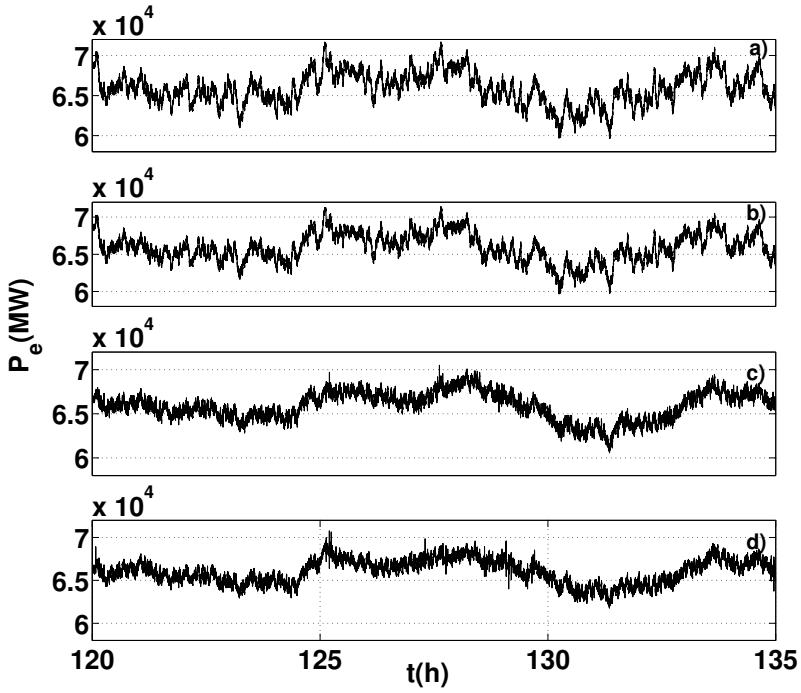

Figure 4.6: Time series of the demand P_e for an increasing fraction of smart devices: a) $\gamma_1 = 0$, b) $\gamma_1 = 0.01$, c) $\gamma_1 = 0.5$, and d) $\gamma_1 = 1$. We have consider $\gamma = 1.2 \times 10^{-3}$. Other parameters as in Fig. 4.5.

pending tasks per device decreases as well with the fraction of smart devices and saturates at a larger value $\gamma_1 \approx 0.5$. Thus for $0.2 < \gamma_1 < 0.5$ while increasing the number of smart devices only has a little effect on the overall frequency fluctuations it does reduce the average pending tasks.

Since the deployment of smart devices lead to additional costs and extra complexity for the appliances, and the global performance of the grid does not significantly increase for γ_1 above $0.2 - 0.4$, we conclude that aiming for a 30% of the total load being smart would be a reasonable objective in terms of cost-benefits for the society.

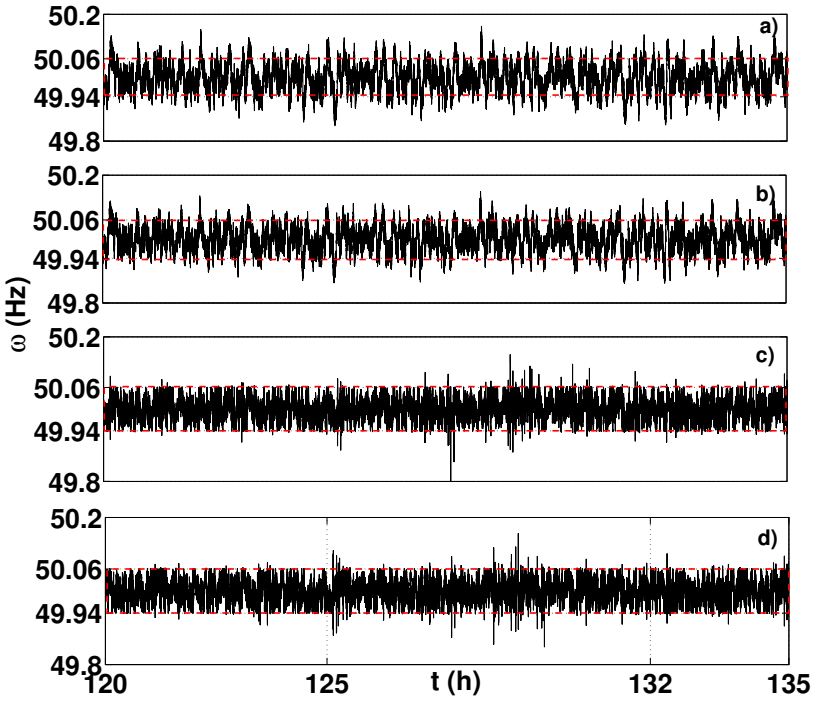

Figure 4.7: Time series of the frequency ω for an increasing fraction of smart devices: a) $\gamma_1 = 0$, b) $\gamma_1 = 0.01$, c) $\gamma_1 = 0.5$, and d) $\gamma_1 = 1$. Parameters as in Fig. 4.6.

4.3

DDC with communication

In section. 4.2 we determined proper values of the parameters ϵ_1 and γ to achieve efficient DDC operation. In particular, ϵ=0.05, $\epsilon_1 = 0.06$ and $\gamma = 1,2 \times 10^{-3}$ yielded a good reduction of frequency fluctuations without accumulating too many pending tasks. These values are to be used here. We analyzed the performance of the control considering the absolute value of the frequency fluctuations $\Delta\omega(t) = |\omega(t) - \omega_{\mathrm{R}}|$ and determining the complementary cumulative distribution $R(\Delta\omega)$ given in Eq. (4.1), which corresponds to the probability of having a frequency fluctuation with absolute value larger than $\Delta\omega$. Figure 4.10 shows the estimated values for $R(\Delta\omega)$ obtained from a numerical simulation with 1000 devices. As it has been described in the previous section, the black line corresponds to the

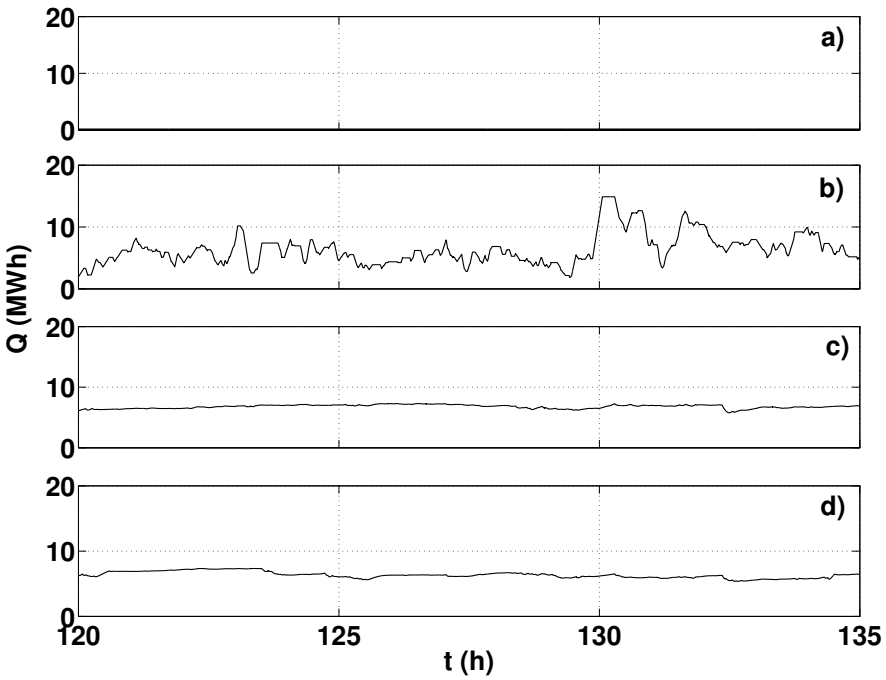

Figure 4.8: Time series of the pending tasks of a smart device Q/n for an increasing fraction of smart devices: a) $\gamma_1 = 0$, b) $\gamma_1 = 0.01$, c) $\gamma_1 = 0.5$, and d) $\gamma_1 = 1$. Parameters as in Fig. 4.6.

case in which no DDC is applied while the red line shows the results for the same system when all devices apply the basic DDC protocol described above. Small and medium size fluctuations are significantly reduced and the variance of the fluctuations decreases. However the shape of the distribution changes: there is now a crossover at $\Delta\omega \approx \epsilon_1$ beyond which the complementary cumulative distribution decays exponentially (linearly in the logarithmic scale of Fig. 4.10). As a consequence the probability of large-scale fluctuations is, in fact, larger than without DDC. The change in the shape of the complementary cumulative distribution comes from the constant necessity of recovering pending tasks in the basic DDC protocol, which triggers large demand peaks that translate in large frequency fluctuations, potentially harmful for real power grids. This effect can not be fully removed tweaking parameters.

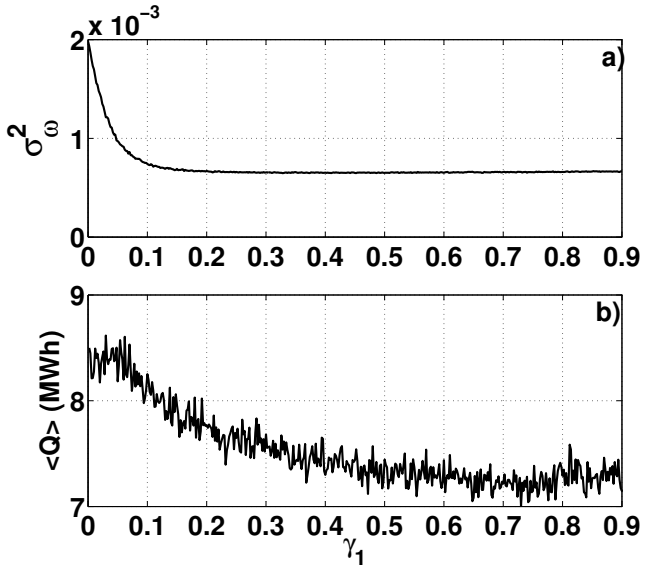

Figure 4.9: Frequency variance (a) and number of pending tasks per smart device at time $t = 135$ h averaged over 100 realizations of the noise (b). Parameters as in Fig. 4.6.

For this reason, in this section we propose introducing direct interactions among devices as a strategy to recover pending tasks without triggering large frequency fluctuations, enhancing the efficiency of DDC [107]. We consider that smart devices belonging to a given group or cluster can communicate among them. The group could be, for instance, composed by the smart devices belonging to the same household.

The interaction protocol proposed is as follows: when a device has to switch on or off, either due to a user action or to recover pending tasks, but the frequency conditions do not allow it, the device will check if another device in the same group has performed the opposite action during a past time window of duration T. If so, the device is allowed to switch on or off independently of the value of the frequency. As a consequence, this protocol allows more switchings of individual devices than without interaction, reducing the number of pending tasks, while the power consumption by each group has smaller variations. We note that this protocol does not intend to bring the frequency back to the reference value as soon as possible, but rather aims at reducing fluctuations at the group scale, giving time to the primary and secondary regulation to operate. We refer to this protocol as communication-enhanced DDC (CeDDC).

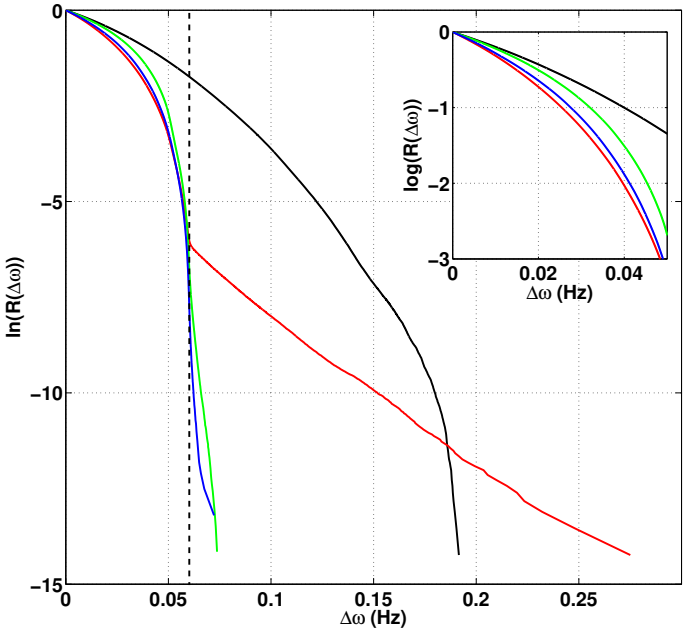

Figure 4.10: Estimated complementary cumulative distribution $R(\Delta\omega)$ which indicates the probability of having a frequency fluctuation whose absolute value is larger than $\Delta\omega{=}|\omega - \omega_{\mathrm{R}}|$. The black line corresponds to the case in which no DDC is used as obtained from a numerical simulation with $N = 1000$ devices. The red line shows $R(\Delta\omega)$ when applying the basic DDC protocol to the same system. Green and blue lines show the results when DDC devices communicate among them (CeDDC). The green line corresponds to the case of all-to-all communication while the blue line corresponds to the case where communication takes place within clusters of 250 devices. The vertical dashed lines indicates the threshold for the recovery of pending tasks ϵ_1. The inset shows in detail the initial part of the curves. Here we use $T = \Delta t$.

Smart devices can communicate through a hub, such as a household energy management system, in which case the hub has to keep an accounting of the devices that have switched on or off in the past time T. It is also possible to implement this protocol with direct communication among devices as follows: each smart device keeps a *power released* register $\mathcal{P}$ which can take three values: $+1$, 0 and -1. At switching on (off) the smart device sets $\mathcal{P} = -1$ ($\mathcal{P} = +1$). After a time window T the device resets $\mathcal{P} = 0$. The idea is that $\mathcal{P} = +1$ ($\mathcal{P} - 1$) potentially allows another device to be powered on (off) without changing the overall consumption of the cluster.

Let j be a smart device that has to turn on (resulting of a user action or to recover pending tasks) but the frequency is out of range to do so. Device j searches for other devices in his group (in a given order or randomly) until it finds one, say device k such that $\mathcal{P}_k = +1$. Then device j stops the search and powers on while device k resets $\mathcal{P}_k = 0$ since it is no longer capable to provide a slot for other devices to power on. j sets also $\mathcal{P}_j = 0$.

Although in here we only consider the case where all devices have the same rated power P_0, this protocol can be generalized to devices with different rated power or with a non-constant consumption by using a register $\mathcal{P}$ which instead of storing $+1$ or -1 at switching, it stores the actual value of the power released at the switching time. This value is positive if the device switches off and negative if it switches on. This is the amount of energy made available to other devices that intend to perform the opposite operation during a time slot T. A device j which has to switch but the frequency is out of range would search for other devices in his cluster until finding one, k, that covers its needs and $\mathcal{P}_k$ is adjusted to account for the power used by device j. It is also possible to consider more sophisticated procedures in which device j combines the power made available by several devices, although in this case an implementation is easier using a centralized hub.

Throughout this section we take the same load parameters as in the previous section and the power plant parameters $\omega_{\mathrm{R}} = 50\mathrm{Hz}$, $H = 2.26$ s, $\tau_g = 0.78$, $R = 0.07$, $P_{\mathrm{G}}/P_0 = N/2$ and $K/P_0 = 50\ \mathrm{s}^{-1}$. Results are independent of P_0.

Figure 4.10 displays the results for the complementary cumulative distribution $R(\Delta\omega)$ when communication among smart devices is included (CeDDC), for two cases, when all devices communicate with each other (green line) and when grouped in 4 clusters of size 250 (blue line). It can be clearly seen that, in addition to a large reduction of the frequency fluctuations variance, the long tails of the probability distribution are also largely suppressed.

The dynamical behavior is illustrated in Figures 4.11 for the total electric load, 4.12 for the frequency and 4.13 for the pending tasks.

Fig. 4.11a) shows a time trace for the total load including fluctuations in demand and without DDC, namely devices switch on and off when randomly schedule independently of the frequency conditions as described in the previous chapter. This is considered as the reference case. The corresponding time trace for the frequency is shown in Fig. 4.12a) and the time trace for the accumulated pending tasks in Fig. 4.13 a) (since DDC is not applied no pending tasks are accumulated).

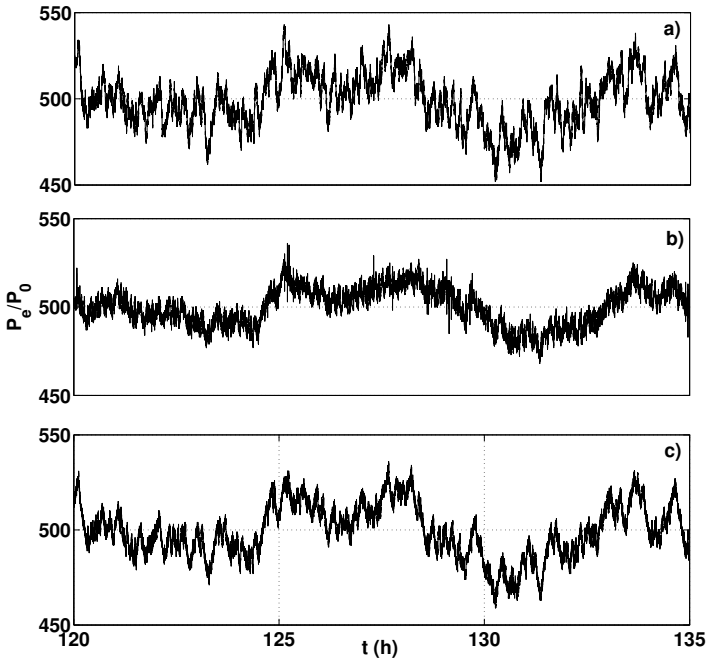

Figure 4.11: Time evolution of the scaled total electric load P_e/P_0: without DDC (a), with the basic DDC protocol (b) and with CeDDC when all devices communicate with each other (c).

Panels b) in Figs. 4.11-4.13 show the corresponding time traces when DDC is applied to the same stochastic realization, namely all devices intend to follow the same random schedule of switchings, but DDC postpones some tasks if frequency conditions are not suitable. There is a reduction of the fluctuations in the total load which translates in reducing the fluctuations in the frequency. As a direct consequence of DDC, now there is a relevant number of pending tasks. Despite the overall reduction in the frequency fluctuations, the presence of a few large peaks in the frequency in 4.12b) is noticeable. These rare events are triggered by the recovery of pending tasks. The effective rate of recovering pending tasks provided the frequency is in the right range is given by probability rate γ times the amount of pending tasks. This rate can be large if there are many tasks accumulated, and, as a consequence, there is a non negligible probability that the recovery of many pending tasks takes place simultaneously despite randomization. The

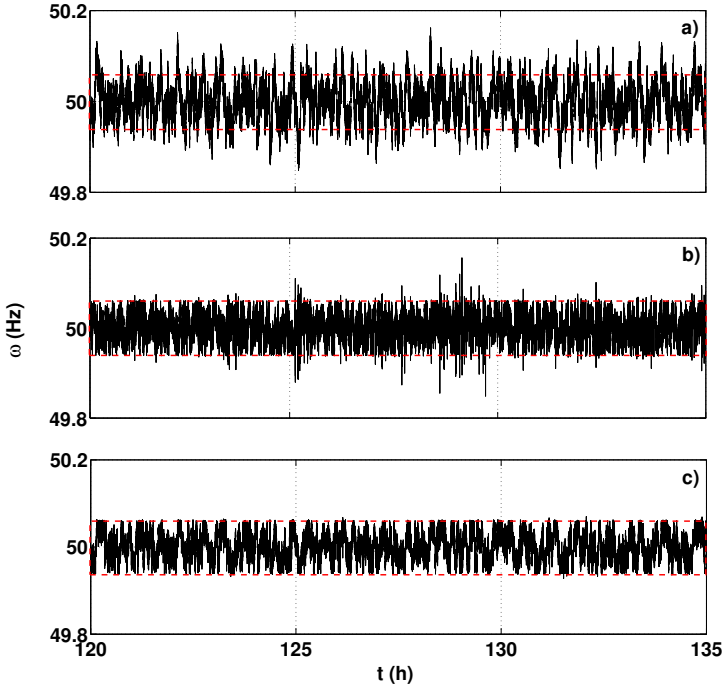

Figure 4.12: Time evolution of the electrical frequency: without DDC (a), with the basic DDC protocol (b) and with CeDDC when all devices communicate with each other (c). The red dashed line corresponds to $\omega_R \pm \epsilon_1$ which signals the boundaries in which pending tasks are recovered when DDC control is applied.

simultaneous switching of many devices induces a large variation of the load which leads to large frequency fluctuations.

Panels c) in Figs. 4.11-4.13 show the corresponding time traces when CeDDC is applied to the same stochastic realization as before. Here we consider the case in which all devices communicate with each other. In this situation the curve for the total load can be seen as an intermediate case between the total load without DDC and with DDC. Fluctuations are reduced with respect to the case without control, but the change in the global profile is smaller than with basic DDC. This reflects the fact that CeDDC is less intrusive than basic DDC. Since CeDDC generates less reschedulings than basic DDC the amount of pending tasks (Fig. 4.13) is almost 10 times smaller than with DDC. As a consequence the large peaks in the frequency difference are no longer present and fluctuations are now kept within the range $[\omega_R - \epsilon_1, \omega_R + \epsilon_1]$. Remarkably the variance of the

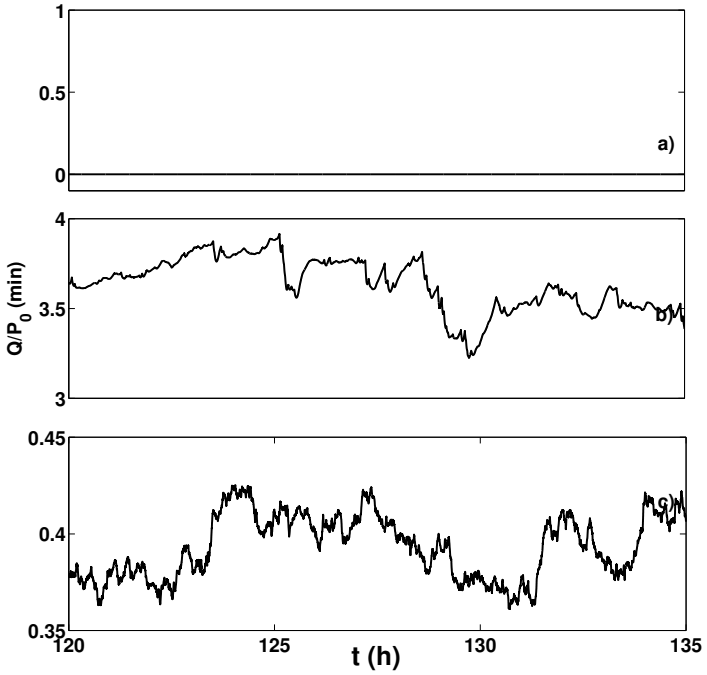

Figure 4.13: Time evolution of the average pending tasks per device scaled to P_0: without DDC (a), with the basic DDC protocol (b) and with CeDDC when all devices communicate with each other (c).

frequency fluctuations, it turns out to be $\sigma_\omega^2 \approx 6.7 \times 10^{-4}$ s^{-2} in the case of DDC and $\sigma_\omega^2 \approx 9.2 \times 10^{-4}$ s^{-2} in the case of CeDDC. The increase of the variance is a consequence of the changes in the frequency fluctuation pattern. For CeDDC there are periods of time in which the frequency fluctuates only in upper half of the range $[\omega_\mathrm{R}, \omega_\mathrm{R} + \epsilon_1]$ and periods of time in which the frequency fluctuates in the lower half range $[\omega_\mathrm{R} - \epsilon_1, \omega_\mathrm{R}]$. This sort of bimodal fluctuation pattern leads to a larger value for the variance than in the case of basic DDC. However since the fluctuations take place within the proper range the larger variance does not signal a deterioration of the performance in real situations.

The change in the pattern of fluctuations is also reflected in the shape of the complementary cumulative distribution function $R(\Delta\omega)$ shown in Fig. 4.10. For $\Delta\omega < \epsilon_1$, the green and blue lines corresponding to CeDDC are located above the red line corresponding to basic DDC without interaction and below the black line corresponding to the case without DDC (see

inset). Thus CeDDC leads to a larger amount of frequency fluctuations at small scale than basic DDC, although compared to no DDC the amount of fluctuations is always greatly reduced. The relevance of the communication comes into play for fluctuations larger than ϵ_1, for which the green and blue lines (CeDDC) are clearly below the red line (basic DDC).

We now address in more detail the effect of the size of the clusters in CeDDC. In particular we consider that interaction takes place within 4 clusters of size 250 or 2 clusters of size 500. Fig. 4.14 compares the results for the dependence of the variance of the frequency fluctuations [panel a)] and for the pending tasks [panel b)] with the case of basic DDC without interaction (cluster size 1) and with the case of all to all interaction (cluster size 1000). The variance of the frequency fluctuations increases with the group size due to the change in the dynamics discussed above. On the contrary, the average number of pending tasks decreases monotonously with the size of the group, as more opportunities for interchanging actions between devices are encountered. Very significant reductions of the number of pending tasks are already achieved for clusters of size 250. As shown in Fig. 4.10 for this cluster size, large frequency fluctuations are already fully avoided in practice.

Coexistence of DDC and CeDDC

In this section, we consider the coexistence of DDC and CeDDC, namely that out of the N devices, n_1 devices follow the basic DDC protocol while $n_2 = N - n_1$ interact among them. This can be viewed as having a interaction cluster of size n_2 and n_1 clusters integrated by a single device. In the following we identify each configuration by the pair of values (n_1, n_2). Two particular cases have already been studied, namely $(N, 0)$, which corresponds to basic DDC without interaction, and $(0, N)$ which corresponds to CeDDC with all-to-all interaction. For $n_1 \neq 0$ and $n_2 \neq 0$, interacting (CeDDC) and non-interacting (DDC) devices coexist in the system. We have performed several simulations with the same stochastic realization for the intended schedule of switchings, varying n_1. Fig. 4.15 a) shows the results for the variance of the frequency σ_ω^2. As expected from the previous results the variance increases slightly with the number of interacting devices. Fig. 4.15 b) shows the results for the average pending tasks per device for non-interacting devices (black line) and for interacting devices (red line). For the interacting devices the number of pending tasks decreases monotonously with the size of the cluster n_2 (red line). A side effect of the communication in the smart devices is the increase of pending tasks in the non communicating DDC devices. This comes from the fact that CeDDC

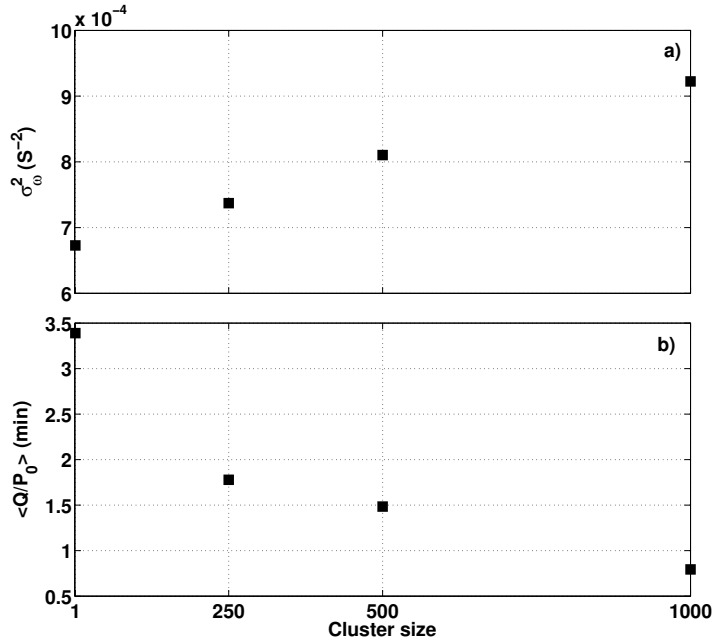

Figure 4.14: Dependence on the communication cluster size. (a) Variance of the frequency fluctuations and (b) average pending tasks per device scaled to P_0.

reduces the excursions of the frequency beyond the range $[\omega_R - \epsilon_1, \omega_R + \epsilon_1]$ and, thus, the opportunities for basic DDC devices to recover pending tasks. This side effect could be avoided by choosing a value for the recovery threshold ϵ_1 larger for communicating devices than for basic DDC devices without communications.

Figure 4.16 shows the time trace of the frequency for several values of $(n_1, n-2)$. As it can be seen already with a cluster of $n_2 = 200$ communicating devices the probability to observe large frequency fluctuations is greatly reduced. Increasing n_2 leads to a further reduction of this probability. Thus, including a fraction of devices which communicate each other can improve the overall stability of the power grid with a significant reduction of the probability to have large frequency fluctuations, despite the fact that non-communicating devices are now accumulating more pending tasks than before. This illustrative results of the dynamics can be quantified by looking at the the probability to have a frequency fluctuation of size larger than $\Delta\omega$, $R(\Delta\omega)$, which is plotted in Fig. 4.17. As in Fig. 4.10 the red line

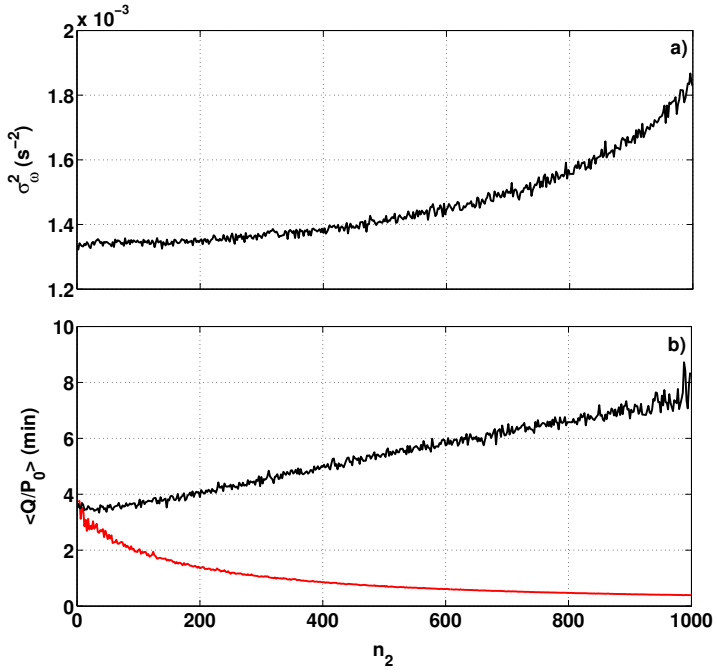

Figure 4.15: Coexistence of DDC and CeDDC devices. (a) Variance of the frequency fluctuations σ_ω^2 and (b) average pending tasks scaled to P_0 per basic DDC device (black line) and per CeDDC device (red line) as a function of the size of the CeDDC cluster n_2

corresponds to the case of basic DDC without control while the green line corresponds to the case of CeDDC with all-to-all interaction. Other lines correspond to the coexistence of non-communicating and communicating devices in the same ratios as in Fig. 4.16. As the number of devices with communication, n_2, increases the tails of the distribution are shortened. In fact even with only 20% of devices communicating among them there is a significant impact in the probability to have large size frequency fluctuations. As an example the probability of fluctuations larger than 0.1 is reduced by a factor 3.

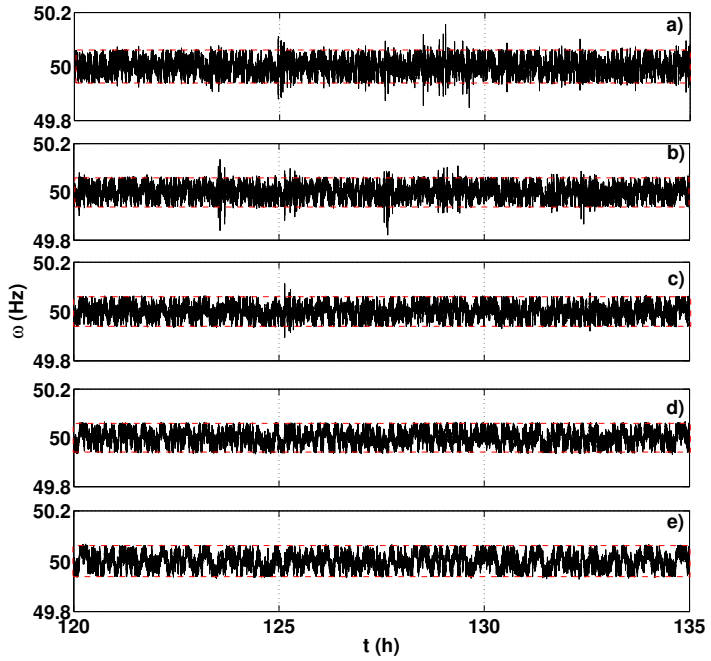

Figure 4.16: Time evolution of the electrical frequency for coexisting DDC and CeDDC. We consider different amounts of non-connected and connected DDC devices (n_1, n_2): $(1000, 0)$ (a); $(800, 200)$ (b); $(500, 500)$ (c); $(200, 800)$ (d) and $(0, 1000)$ (e). Red dashed lines correspond to $\omega_R \pm \epsilon_1$ which signals the boundaries in which pending tasks are recovered when DDC control is applied.

4.4

Conclusion

In the first part of this chapter, we have proposed a simple model to study the effects of dynamic demand control on the frequency of the power grid [109]. The model of the power plant with primary and secondary regulation introduced in chapter 2 and the simple stochastic model for the power demand described in chapter 3 have been used to define our system. The demand model has been shown to be able to reproduce the statistical properties of real measurements of the frequency fluctuations adjusting a single parameter, namely the switching probability of the devices (see chapter 3). To this model, we apply a generic DDC protocol to a fraction of devices

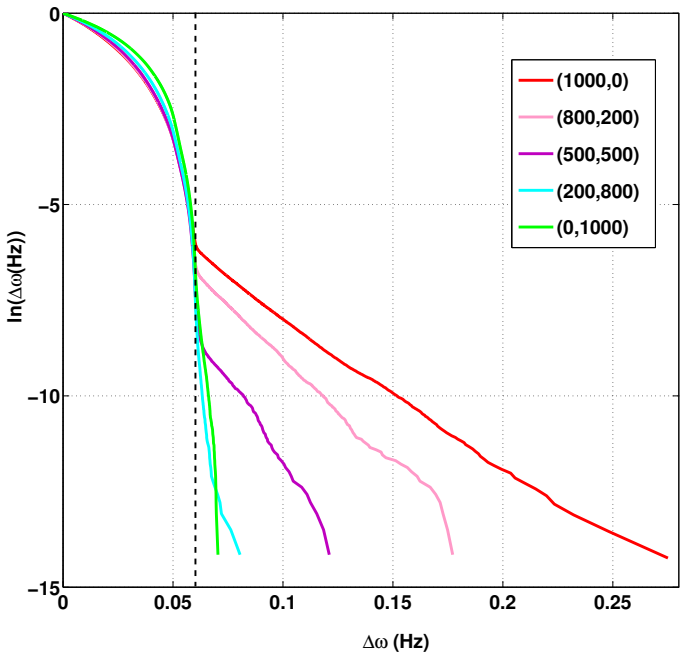

Figure 4.17: Estimated cumulative probability of having a frequency fluctuation of size larger than $\Delta\omega$, $R(\Delta\omega)$. Colors correspond to different amounts of non-connected and connected devices (n_1, n_2) as specified in the legend.

in order to study its effect on the dynamics [109]. The generic DDC protocol consist of two parts: control, by which on or off orders on devices are actually committed only if the frequency is within a suitable range, and recovery of pending tasks only when the frequency value is appropriate and performed randomly to avoid instabilities generated by simultaneous switching of all devices with accumulated pending tasks.

We have found that DDC can significantly reduce the variance of the fluctuations by delaying the switching of smart devices and recovering the pending tasks later. Furthermore we have found that there is no need to apply DDC to all devices in order to achieve significant effects. Frequency fluctuations can be effectively reduced already with 20% of devices being smart and a ratio of 30%– 40% allows to reduce the fluctuations while keeping the pending tasks per device low.

However, the recovery of pending tasks modifies qualitatively the probability distribution of the frequency fluctuations, introducing large exponential tails. Therefore, depending on parameters, while DDC can reduce small or medium size fluctuations, it can also increase the probability of observing large frequency fluctuations with respect to the case without control. This rare events can potentially trigger a failure of the system. Device-device communication is found to be a good strategy to avoid this rare events.

We have introduced in the second part of this chapter a DDC algorithm which allows for communication between devices which are part of a given cluster, in such a way that devices can switch on (off) even if the frequency is outside the suitable range provided another device within the cluster has switched off (on) [107]. This communication-enhanced DDC protocol is less intrusive than basic DDC, allowing more switches and reducing in a very significant way (up to 90%) the accumulated pending tasks. One of the major advantages of the protocol introduced here is that the probability of large scale fluctuations in the electrical frequency is strongly reduced and can even be practically suppressed. Having a non-negligible probability for large size fluctuations is one of the drawbacks of simple DDC algorithm that can no be avoided by tweaking parameters and which is relevant for practical implementations since large frequency fluctuations can trigger a failure of the power grid at large scale.

Large scale frequency fluctuations are fully avoided for all-to-all interaction. However an ideal all-to-all communication would require nation-wide internet communication and probably would not be practical. Nevertheless technologies as power line communication (PLC) could allow devices to interchange information over a certain range of distances. Thus an scenario of clusters of devices seems more plausible while still providing a very significant reduction of the probability of large size frequency fluctuations. Communication can be implemented through a hub such as a household energy management system or by direct communication among the devices of a cluster.

CHAPTER 5

Effects of Dynamic Demand Control on an electric network

In the previous chapters, we built up a resilient system incorporating dynamically controlled loads making it smart. To extend the previous work, we consider these systems interconnected forming what we call a smart network. Thus, this chapter analyses two important features, first the effects of secondary control in a network, and second those of dynamically controlled appliances in the network, in terms of frequency and phase synchronization. We structure this part as follows: the next section will deal with the modeling of the network as coupled oscillators, including secondary control. A brief introduction about the synchronization in oscillators network will be presented hereafter. The stability analysis of the network model will be done, first with an elementary example. That stability analysis will be done by the linearization method, which will allow the derivation of a stability condition using the Lyapunov exponents. That method will be completed with the Routh Hurwitz criterion of stability in the case where the Lyapunov exponents are not easy to determine. The last section before the conclusion will be dedicated to a case study of a network, in which the effects of DDC on the network synchronization will be investigated.

5.1

Synchronization, stability and control in an electric network

Synchronization constitutes one of the most dominant collective dynamics in complex systems such as communication networks [97], population dynamics [23, 54, 97], or power grids [54]. The synchronization of a network deeply depends on the dynamics of the nodes as well as on the topology of the network and the properties of the links, such as the strength of the coupling of a node with the rest of the network. Synchronization is very important tasks to be achieved in electric network to ensure quality, reliability of the whole system. In electric networks frequency and phase synchronization can be defined. The network is said frequency synchronized if and only if all frequencies $\dot{\theta}_i$ tend to a common constant frequency ω_{syn} as $t \to \infty$, θ_i, ω_{syn} being the phase at the node i and the synchronous frequency respectively. The network achieves full synchronization if it is phase synchronized, meaning the phase of each node tends to the same constant value (full or perfect synchronization) or the phase differences of connected nodes verify the inequality $|\tilde{\theta}_i - \tilde{\theta}_j| < \sigma$ (phase-cohesiveness). As it is going to be proved in the following sections, the stability of the network requires that the difference of phases between two connected nodes to be less $\frac{\pi}{2}$ ($|\tilde{\theta}_i - \tilde{\theta}_j| \leq \pi/2$). This stability criterion limits the electric power flowing through the power line, which can not exceed the maximal capacity of the line[26, 35, 67, 68]. In fact to reasonably maintain in practice the two connected nodes synchronized, $|\tilde{\theta}_i - \tilde{\theta}_j|$ should be comprise between 40 °C and 50 °C [9]. One could deduce that to ensure synchronism between two connected nodes $|\tilde{\theta}_i - \tilde{\theta}_j| \leq \pi/4$.

The stability and robustness of a network is determined by its capacity to remain synchronized against perturbations. In power systems such perturbations can be due to local failures, a voltage collapse, overloads or line breaks, bad weather, short-circuits, etc. [17, 23, 79, 80, 100]. Perturbations may cause a desynchronization of a node, which favors the emergence of destructive power oscillations [72] and somehow may lead to a cascading failures or/and blackouts if the affected node is not promptly disconnected from the rest of the network. The electric power network is designed to operate in the synchronous state [97], therefore the control of the power grid such that it is resilient against failures and local instabilities is an imperative for avoiding cascading breakdowns in the network [44, 72, 80]. A

large number of works have been dedicated to the study of the stability of electric grids against small and large perturbations.

Power system stability is divided into voltage stability and rotor and angle stability. Voltage stability in the power system defines the ability of the power system to maintain acceptable voltage in all bus bars in the system under normal condition and after being subjected to a disturbance. As it has already been mentioned in the previous chapter, the voltage is assumed to be constant at any time, such that the voltage dynamics is not considered in this chapter. Rotor stability on the other hand classified as transient stability and frequency stability, is defined as the ability of the network to remain in synchrony when subjected to disturbances. Synchrony can be lost when all the nodes do not oscillate with the same frequency and with acceptable phase differences between connected nodes. Thus, to ensure the stability of the electric network a control of its sychronization is required.

The study of the control of the synchronization of a complex network is an important research area in network science [23, 33, 34, 79, 80]. Several control strategies and methods, such as distributed, pinning, impulsive, or feed-back controls have been used to stabilize chaotic systems, neurons, cells, opinion networks in communication, and opto-electromechanical systems [23, 61, 105]. Indeed, based on Lyapunov theory and the impulsive control, Yang Li Xin and Liu Xiao Jun realized the synchronization of two coupled chaotic systems [61], while in the case of networks with huge numbers of nodes, pinning control is proved to achieve the synchronization of the network. In electric power networks, Sean P. Cornelius *et al.* proposed a realistic control strategy based on compensatory perturbations for stabilizing the network [23]. Per Sebastian Skardal and Alex Arenas developed a feedback method to stabilize the synchronized state of coupled oscillators [105]. On the other side Bing Wang *et al.* applied several feed-back controls to enhance the synchronization stability of a power grid; they then improved the network synchronization by changing the interlinks of the network [117]. Furthermore they showed how communication among clusters could improve the network stability. Aldison *et al.* proposed a new way to improve the local stability by tuning individual node parameters in the grid [80].
In this chapter we will analyze how DDC can help to improve the stability of the synchronized state.

5.2

Mathematical Model

The electric network can be viewed as an interconnection of power systems representing areas or cities. These areas (nodes) are connected to each other through the power transmission lines (links), such that a loaded area will see its frequency decrease, meaning that the difference between the local generation and local consumption is negative (see swing equation 5.1). Reversely an area with more mechanical power has its frequency increase, thus the power difference is positive. Such areas operate therefore under non synchronous frequency and there is a power flow from or to other nodes in order to balance the network. Thus, one can see the power grid as a network composed by synchronous generators (positive power differences) connected through transmission lines to consumers (negative power differences). We then consider a network composed by n nodes and l lines. Each line (j,k) is defined by its complex admittance Y_{jk}=G_{jk}+iB_{jk}, where G_{jk} and B_{jk} are respectively the conductance and the susceptance of the line, i is the imaginary unit. The generator at the node i is described by the following swing equation [90]:

$$\begin{cases} \dot{\theta}_i = (\omega_i - \omega_R) \\ \dot{\omega}_i = \frac{\omega_R}{2HP_{G_i}}(P_{m_i}(\omega_i) - P_{e_i}(\theta_i, \omega_i)), \end{cases} \tag{5.1}$$

where θ_i and ω_i denote the voltage phase angle and the frequency deviation of the *i-th* generator respectively. P_{m_i} is the net mechanical power input to the rotor while P_{e_i} represents the total power consumed at node i. Finally, ω_R=$2\pi \times 50$ or 60 Hz is the reference angular velocity of the grid and H is the inertia constant of the generator with a rated power P_{G_i}. The power consumption is given by:

$$P_{e_i}(\theta_i, \omega_i) = P_i^{load} + P_i^{diss} + P_i^{trans}, \tag{5.2}$$

where P_i^{diss}=$\frac{D_i P_i^{load}}{\omega_R}$$(\omega_i - \omega_R)$ is the frequency dependent load at the node i, θ_i and P_i^{load} denote respectively the phase of the *i-th* synchronous machine and the active loads attached to the *i-th* synchronous machine and

$$P_i^{trans} = Re[S_i] = Re[V_i I_i^*] = \sum_{j=1}^{n} |U_i||U_j|[G_{ij}\cos(\theta_i - \theta_j) + B_{ij}\sin(\theta_i - \theta_j)], \tag{5.3}$$

is the transmitted power from the node i to the rest of the network. Where V_i=$|U_i|e^{j\theta_i}$ is the voltage source of the machine i, U_i represents the voltage

magnitude and $I_i = \sum_{j=1}^{n} Y_{ij}V_j$ represents the current at the node i. In this chapter, we assume that the network is lossless (G_{ij}=0 $\forall$ i, j), and that the voltage source has a constant amplitude U_0 at all nodes. The power transmitted then reads: P_i^{trans}=$\sum_{j=1}^{n} U_0^2 B_{ij} \sin(\theta_i - \theta_j)$
Given the implementation of secondary control modeled in chapter 2, each machine i is governed by the following equations of motion:

$$\begin{cases} \dot{\tilde{\theta}}_i = (\omega_i - \omega_R) = \tilde{\omega} \\ \dot{\tilde{\omega}}_i = -\alpha_i \dot{\tilde{\theta}}_i + P_i^* - \sum_{j=1}^{n} K_{ij} \sin(\tilde{\theta}_i - \tilde{\theta}_j) + P_{c_i} \\ \tau_{g_i} \dot{P}_{ci} = -P_{c_i} - \gamma_i \tilde{\theta}_i - \beta_i \tilde{\omega}_i, \end{cases} \tag{5.4}$$

where $\tilde{\theta}_i$=$(\theta_i - \theta_i(0))$, P_i^* is the effective power fed into the grid or consumed at node i, α is a damping and K_{ij}=$\eta_i U_0^2 B_{ij}$ is proportional to the susceptance B_{ij} of line the (i, j) and gives the capacity of a line. Finally, P_{c_i} is the control power with time constant τ_{g_i} and β_i and γ_i are the primary and the secondary control gains respectively. These parameters are expressed as follows: P_i^*=$\eta_i(P_{ref_i}(0) - P_i^{load})$, P_{c_i}= $\eta_i(P_{m_i} - P_{ref_i}(0))$ α_i=$\frac{D_i P_i^{load}}{2H_i P_G}$, η_i= $\frac{\omega_R}{2H_i P_G}$, β_i=$\frac{1}{2H_i R}$, γ_i=$\frac{K}{2H_i P_G}$.
Then, the two first equations of the system form the well-known 2nd-order Kuramoto model used in [40, 44] to describe the phase dynamics of synchronous machines, and therefore is relevant to understand the synchronization problems emerging in such oscillator network [69], as well as the impacts of the secondary control in the global dynamics of the network.

Thus, we consider in this work that the electric network model is stable if it is frequency synchronized and phase cohesive. In the following we will explicitly study the dynamics of the network considering the uncontrolled and controlled electric network.

Uncontrolled two node system

We first study the dynamics of the simplest network motif composed by two coupled generators powering different loads (or aggregated loads). The mentioned system can be seen as a two connected power systems such that the generators, or aggregation of generators, are governed by Eqs. (5.4). The equations for this system can be simplified in such a way that only the phase of variables of the coupled system(ϕ=$\tilde{\theta}_1 - \tilde{\theta}_2$, $\dot{\phi}$= $\omega_1 - \omega_2$=χ, ΔP=$P_1 - P_2$, ΔP_m=$P_{m_1} - P_{m_2}$ and ΔP_{ref}=$(P_{ref_1} - P_{ref_2})$ matter. We

assume also that the two power plants have the same generator and controller parameters. Namely, $\alpha_i = \alpha$, $M_i{=}M$ and the coupling parameters are symmetric $K_{ij} = K_{ji}{=}K$. The two nodes system is thus described by the following set of equations:

$$\begin{cases} \dot{\phi} = \chi \\ \dot{\chi} = -\alpha\chi + \Delta P - 2K\sin(\phi) \\ \Delta\dot{P}_m = \frac{1}{\tau_g}(\Delta P_{ref} - \Delta P_m - \beta\chi) \\ \Delta\dot{P}_{ref} = -\gamma\chi. \end{cases} \tag{5.5}$$

The stability analysis of the two coupled sub-grids is first done by neglecting control. Doing so, the previous set of equations (5.5) is reduced to the 2^{nd} order Kuramoto model:

$$\begin{cases} \dot{\phi} = \chi \\ \dot{\chi} = -\alpha\chi + \Delta P - 2K\sin(\phi). \end{cases} \tag{5.6}$$

The steady state (synchronized) solutions ($\dot{\phi}{=}\dot{\chi}{=}0$) of the system are given by: $\begin{cases} \chi^* = 0 \\ \Delta P - 2K\sin(\phi^*) = 0. \end{cases}$

The existence of fixed points is conditioned by the constraint $\Delta P < 2K$, which basically means that the power flow through the line can not be bigger than its maximum capacity K. Thus the minimal value of K for which there is stable operation is $K_c{=}\frac{\Delta P}{2}$. For $\Delta P = 2K$ the two fixed points collide in a saddle-node on invariant circle (SNIC) bifurcation and no stable steady state is possible. The system shows then a limit cycle and the variables oscillate as shown in Fig. 5.1. This last case would corresponds to an outage in the power system. For $\Delta P < 2K$ the two fixed points S_1 and S_2 and their corresponding eigenvalues obtained from the Jacobian matrix are given by:

$$S_1 = \begin{pmatrix} \phi^* \\ \chi^* \end{pmatrix} = \begin{pmatrix} \arcsin(\frac{\Delta P}{2K}) \\ 0 \end{pmatrix}$$

$$\lambda_{\pm}(S_1) = -\left(\frac{\alpha}{2}\right) \pm \sqrt{\left(\frac{\alpha}{2}\right)^2 - 2K\sqrt{1 - \left(\frac{\Delta P}{2K}\right)^2}} \tag{5.7}$$

$$S_2 = \begin{pmatrix} \phi^* \\ \chi^* \end{pmatrix} = \begin{pmatrix} \pi - \arcsin(\frac{\Delta P}{2K}) \\ 0 \end{pmatrix}$$

$$\lambda_{\pm}(S_2) = -\left(\frac{\alpha}{2}\right) \pm \sqrt{\left(\frac{\alpha}{2}\right)^2 + 2K\sqrt{1 - \left(\frac{\Delta P}{2K}\right)^2}}. \tag{5.8}$$

S_1 is a stable fixed point since the eigenvalues are either both real and negative or complex with negative real part depending on the value of the damping coefficient α. S_2 is however always a saddle, as the eigenvalues are always real and have opposite signs. In addition, as reported in [69], for weak damping there exists a stable limit cycle which coexists with the stable fixed point. Depending on the initial condition, the system will converge to either the stable fixed point or to the non-synchronous limit cycle [72] whose amplitude is given by:

$$\chi_{ns} \approx \frac{\Delta P}{\alpha} + \frac{\alpha K}{\Delta P}\cos(\frac{\Delta P}{\alpha}t). \tag{5.9}$$

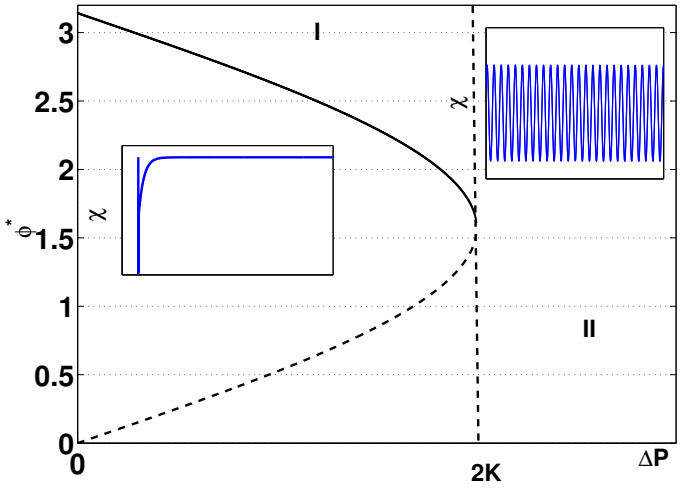

Figure 5.1: Bifurcation diagram of Eq. 5.6. Here we use the line capacity K as the main control parameter. Other parameter values: $\alpha = 3,25.10^{-3}$; ΔP=0,25;

The border between the region of global stability and coexistence can be determined by applying the Lyapunov criterion [9] in the low-friction limit (see [69] for more details). By defining the energy of the system

$$E(\phi) = \frac{1}{2}(\frac{d\phi}{dt})^2 - 2K\cos(\phi), \tag{5.10}$$

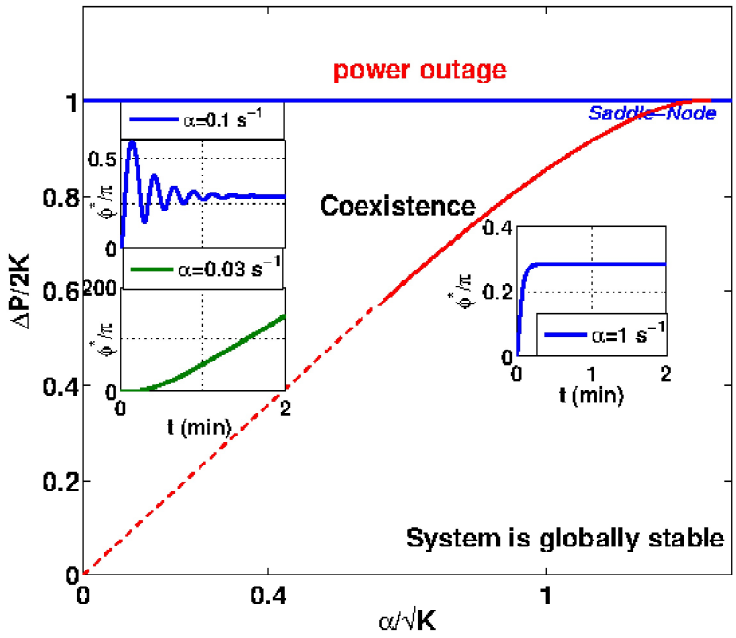

Figure 5.2: Phase diagram in the parameter space (α, ΔP). Here $K = 0, 16$. The dashed red line is the border between the region of coexistence and global stability in low-friction limit given by Eq. (5.12). The insets show the time evolution of the phase for the limit cycle in the region of coexistence and for a perturbation of the stable steady state in the globally stable regime.

the globally stable regime is found if the average energy E is decreasing over a full period. So the border between the coexistence and the globally stable regimes is described by:

$$\overline{\frac{dE(\phi)}{dt}} = 0. \tag{5.11}$$

Solving equation Eq. (5.11) in the low-friction approximation (neglecting energy dissipation), the following criterion is obtained:

$$\Delta P = \frac{4\sqrt{2}}{\pi}\alpha\sqrt{K}. \tag{5.12}$$

Fig. 5.2 shows the phase diagram of the system in the two parameter space (δP,α). It presents the different states to which the system evolves in each parameter region. For $\frac{\Delta P}{2K} > 1$ the system leads to a limit cycle, which implies a systems failure. For $\frac{\Delta P}{2K} < 1$, the dynamics of the system depends

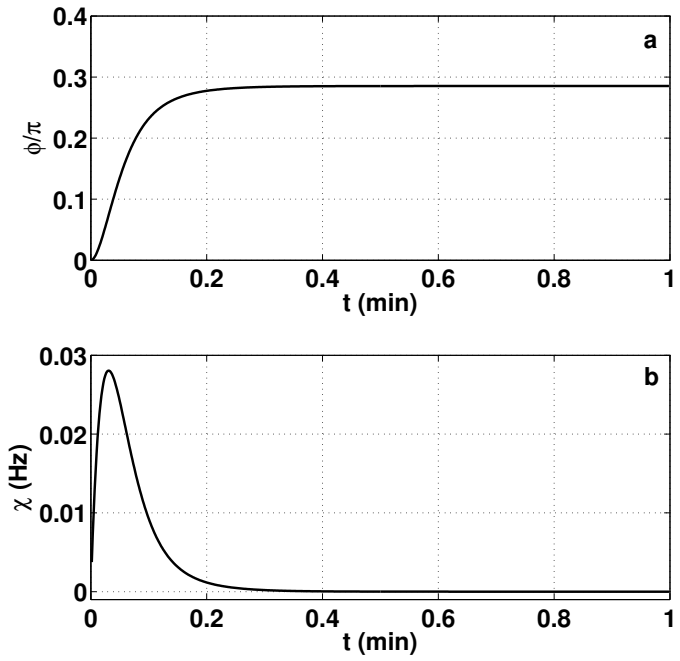

Figure 5.3: Time evolution of the phase a) and the frequency b) differences without controller for $\Delta P < 2K$, $\alpha = 1$, $\Delta P = 0.25$, and $K = 0.16$.

on the damping coefficient α. For small values of α there are two attractors in the system: a limit cycle and a stable fixed point as illustrated by the time evolution in the insets (green line for the limit cycle and blue line for the stable fixed point). The dashed red line separates that region of coexistence of attractors from the region of global stability, with a single fixed point and which it is reached for larger values of α. The time evolution in this case is also shown in the inset.

Fig. 5.3 and Fig. 5.4 show the time evolution of the phase and frequency differences for the different regimes discussed above. One observes that the variables tend asymptotically to the steady state for $\Delta P < 2K$, while for $\Delta P > 2K$ a phase drift is observed as well as the emergence of oscillations, which indicate the instability of the system. Basically, the non-synchronous state is characterized by a phase drift and frequency oscillations, while the synchronous state, the nodes are oscillating with the same frequency and the phase differences between the nodes are constant.

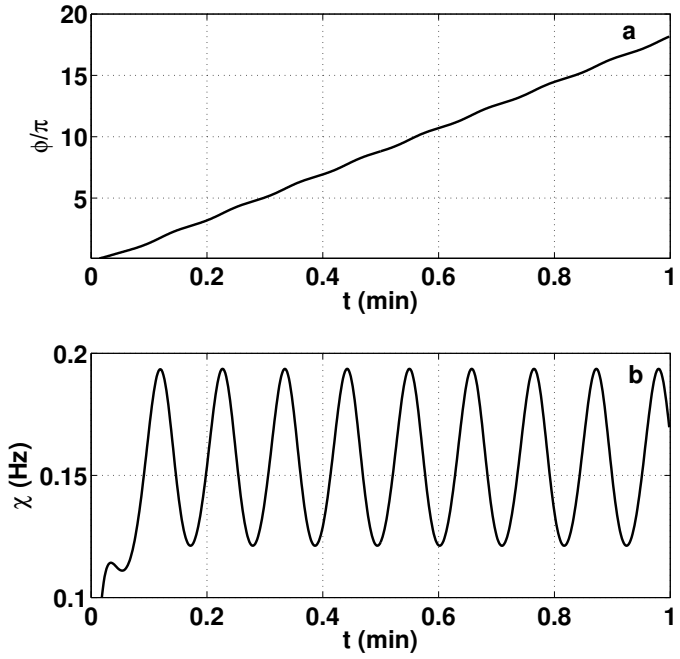

Figure 5.4: Time evolution of the phase a) and the frequency b) differences without controller for $\Delta P > 2K$ without control. Here $\alpha = 1\ s^{-1}$, $\Delta P = 0.5$, and $K = 0.16$

Controlled two nodes system

We now introduce the control such that the system is described by Eqs. (5.5). The fixed points exist if and only if the following equations are verified:

$$\begin{cases} \Delta P_{ref}(0) - \gamma(\tilde{\theta}_1^* - \tilde{\theta}_2^*) - \Delta P^{load} - 2K\sin((\tilde{\theta}_1^* - \tilde{\theta}_2^*)) = 0 \\ \gamma(\tilde{\theta}_1^* + \tilde{\theta}_2^*) + (P_1^{load} + P_2^{load}) - (P_{ref_1}(0) + P_{ref_2}(0)) = 0, \end{cases} \tag{5.13}$$

where $\Delta P_{ref}(0) = P_{ref_1}(0) - P_{ref_2}(0)$ and $\Delta P^{load} = P_1^{load} - P_2^{load}$. The first equation in (5.13) is transcendental and its solutions can only be found numerically. Nevertheless, it can be proved analytically that this equation has a least one root in a given interval by applying the intermediate value theorem[1] Let's consider the function $f(\phi) = -\gamma\phi - 2K\sin(\phi) + (\Delta P_{ref}(0) - \Delta P^{load})$ which is continuous in ϕ as it is a sum of continuous functions

[1]The intermediate value theorem states that, if a function $f(x)$ is continuous on the closed interval $[a, b]$, and if d is between $f(a)$ and $f(b)$, then there is a number $c \in [a, b]$ with $f(c) = d$.

(polynomial and sine). Since the maximum power transmitted between the two nodes is $\pm K$ for $\phi = \pm\frac{\pi}{2}$, the equation $f(\phi) = 0$ has at least one root $f(\phi^*) = 0$ in $[-\frac{\pi}{2}, \frac{\pi}{2}]$ if $f(-\frac{\pi}{2}) \cdot f(\frac{\pi}{2}) < 0$, where $f(\pm\frac{\pi}{2}) = [\Delta P_{ref}(0) - \Delta P^{load}] \pm [\frac{\gamma\pi}{2} + 2K]$. Then the necessary condition for the existence of a fixed point ϕ^* in the interval $[-\frac{\pi}{2}, \frac{\pi}{2}]$ is

$$|\frac{\Delta P_0}{2K}| < 1 + \frac{\gamma\pi}{4K} \tag{5.14}$$

where we define $\Delta P_0 = [\Delta P_{ref}(0) - \Delta P^{load}]$.

In absence of a controller ($\gamma = 0$), we clearly recover the condition of existence of a fixed point ($\Delta P_0 < 2K$) which has been discussed previously. We can then conclude that, verifying the condition given in (5.14), the system admits at least one stable steady state:

$$S_1 := \begin{pmatrix} \phi^* \\ \chi^* \\ \Delta P_m^* \\ \Delta P_{ref}^* \end{pmatrix} = \begin{pmatrix} \phi^* \\ 0 \\ \Delta P_{ref}(0) - \gamma\phi^* \\ \Delta P_{ref}(0) - \gamma\phi^* \end{pmatrix}. \tag{5.15}$$

We next perform the stability analysis of the fixed point. Let

$$\mathbf{X} = (\delta\phi, \delta\chi, \delta\Delta P_{\mathrm{m}}, \delta\Delta P_{\mathrm{ref}}) \tag{5.16}$$

be a small perturbation of the fixed point. The equation of motion of these small perturbations is given by

$$\dot{\mathbf{X}}(t) = J \cdot \mathbf{X}(t) + n, \tag{5.17}$$

where the Jacobian matrix J is defined as

$$J = \begin{bmatrix} 0 & 1 & 0 & 0 \\ -2K\cos(\phi^*) & -\alpha & 1 & 0 \\ 0 & -\frac{\beta}{\tau} & -\frac{1}{\tau} & \frac{1}{\tau} \\ -\gamma & 0 & 0 & 0 \end{bmatrix} \tag{5.18}$$

and

$$n = \begin{bmatrix} 0 \\ P_1 - P_2 \\ 0 \\ 0 \end{bmatrix}. \tag{5.19}$$

The characteristic polynomial of the Jacobian is given by

$$\lambda^4 + a_1\lambda^3 + a_2\lambda^2 + a_3\lambda + a_4 = 0, \tag{5.20}$$

where the parameters a_1, a_2, a_3 and a_4 are

$$\begin{cases} a_1 = \frac{1+\alpha\tau}{\tau}, \\ a_2 = \frac{\beta+\alpha+2K\tau\cos(\phi^*)}{\tau}, \\ a_3 = \frac{2K\cos(\phi^*)}{\tau}, \\ a_4 = \frac{\gamma}{\tau}. \end{cases} \tag{5.21}$$

Due to the difficulty to derive a simple expression for the roots of the characteristic polynomial to study the stability of the synchronous state, we use the Routh-Hurwitz (RH) criterion. RH criterion is a method which contains the necessary and sufficient conditions for the stability of the system. Given a polynomial $P(\lambda) = \lambda^n + a_1\lambda^{n-1} + ... + a_{n-1}\lambda + a_n$, where the coefficients a_i are real constants $(i = 1, 2, .., n)$, the n-Hurwitz matrices are defined using the coefficients a_i of the characteristic polynomial as:

$B_1 = (a_1)$, $B_2 = \begin{pmatrix} a_1 & 1 \\ a_3 & a_2 \end{pmatrix}$, ...,

$$B_n = \begin{pmatrix} a_1 & 1 & 0 & 0 & \ddots & 0 \\ a_3 & a_2 & a_1 & 1 & \ddots & 0 \\ a_5 & a_4 & a_3 & a_2 & \ddots & 0 \\ \vdots & \vdots & \vdots & \vdots & \ddots & \vdots \\ 0 & 0 & 0 & 0 & \ddots & a_n \end{pmatrix}.$$

The RH criterion states then that all of the roots of the polynomial $P(\lambda)$ are negative or have negative real part if the determinant of all Hurwitz matrices are positive: $\det(B_i) > 0, i = 1, 2, ..., n$. According to the Routh-Hurwitz criterion the steady state is stable if the following conditions are fulfilled:

$$\begin{cases} a_1 > 0, \\ a_2 > 0, \\ a_3 > 0, \\ a_4 > 0, \\ a_1a_2a_3 - a_3^2 - a_1^2a_4 = d > 0. \end{cases} \tag{5.22}$$

For the parameters used in this study, the four first conditions are always fulfilled since α, γ, $a > 0$. Hence, the steady state is stable if and only if $d > 0$. In terms of the control parameter γ, we obtain the following inequality:

$$\frac{2(1+\alpha\tau)(\beta+\alpha+2K\tau\cos(\phi^*))K\cos(\phi^*)}{\tau^3} - \frac{4K^2\cos(\phi^*)^2}{\tau^2} - \frac{(1+\alpha\tau)^2\gamma}{\tau^2} > 0. \tag{5.23}$$

Then the steady state is stable only if the control gain parameter takes a value within the following interval

$$0 < \gamma < \gamma_c = \frac{2K\cos(\phi^*)}{(1+\alpha\tau)}[\beta + \alpha + 2K\tau\cos(\phi^*) - \frac{2K\tau}{(1+\alpha\tau)}]. \qquad (5.24)$$

One notices that for weak damping ($\alpha, \beta \to 0$) γ_c is very small or can even take negative values, so the synchronous state can become easily unstable. The instability is explicitly observed in Fig. 5.5 where we show the time evolution of the phase and frequency differences for the parameter values reported in the caption. One observes the exponential growth of the oscillations of these variables, which characterizes the instability of the fixed point. This counterintuitive instability induced by the controller for small damping can cause a failure of the system.

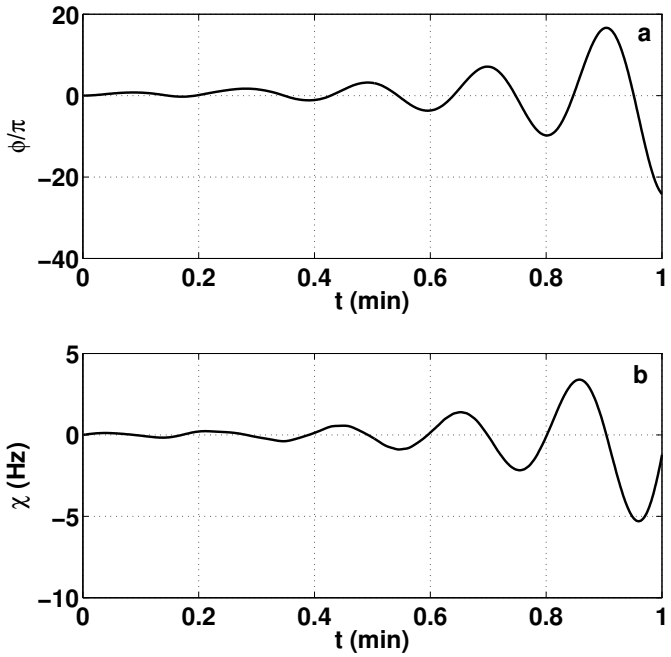

Figure 5.5: Instability: $\Delta P < 2K$ and $\Delta P = 0.25$; $K = 0,16$, $\gamma = 0.1$, $\theta_1(0) = \theta_2(0) = 0$, $\alpha = 0.03$.

From the condition of existence of a fixed point presented in Eq. (5.14), one observes that the control has reduced the critical coupling which is

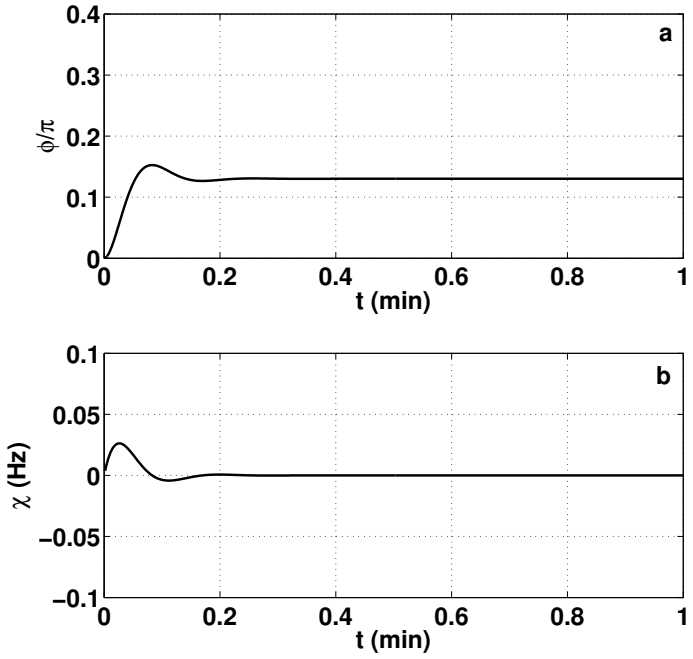

Figure 5.6: Time evolution of the phase a) and the frequency b) differences with controller for $\Delta P < 2K$ and $\alpha = 1$; $\Delta P = 0.25$; $K = 0,16$, $\gamma = 0.3$, $\theta_1(0) = \theta_2(0) = 0$, $\alpha = 1$.

now expressed by

$$K_c^{New} = \frac{\Delta P_0}{2} - \frac{\gamma\pi}{4} \tag{5.25}$$

.

It is known that the primary and secondary controls act to stop the frequency drop and to restore its reference value respectively. In fact, Figures 5.6 and 5.7, which show the time evolution of the phase and frequency difference for $\Delta P < 2K$ and $\Delta P > 2K$ after a perturbation has been applied, indicate that the system remains always stable, at difference with the corresponding figures in absence of primary and secondary control (see Figures 5.3 and 5.4). The controller in each subsystem tends to balance the mechanical and the electrical power in such a way that ΔP is always reduced and pushed into the domain of existence of stable fixed points. The frequency difference remains always null while the system is stabilized to

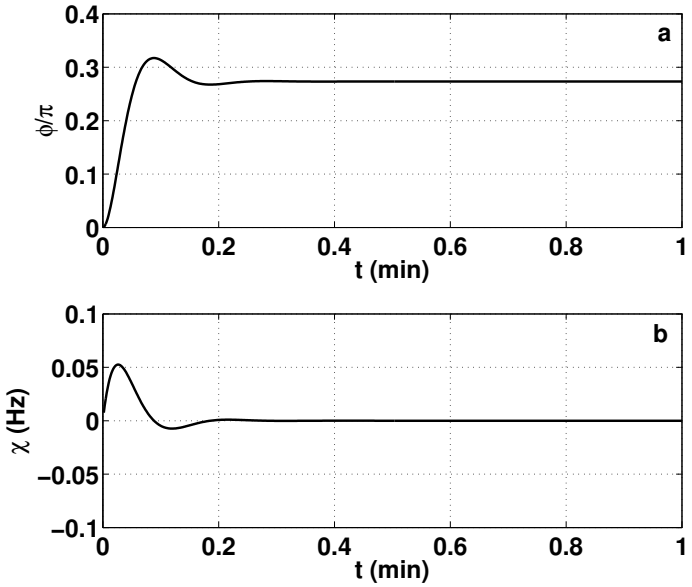

Figure 5.7: Time evolution of the phase a) and the frequency b) differences with controller for $\Delta P > 2K$, $\Delta P = 0.5$, $K = 0.16$, $\gamma = 0.3$, $\theta_1(0) = \theta_2(0) = 0$, $\alpha = 1\ s^{-1}$

a new phase difference, which is small (order of 10^{-1}) for $\Delta\ P < 2K$ and $\frac{\phi^*}{\pi} = 0.27$ for $\Delta P > 2K$. In fact once the primary control acts to stop the decline of the frequency, the phase deviates but the restoration of the frequency to its nominal value tends to stabilize the phase difference. These results show that the system with frequency regulation is reliable and robust against perturbations. The open question is still how will the system reacts against large perturbations?

Once a large perturbation hits the system, one can not infer its new operation state from a linear stability analysis. Several authors such as Paul Schultz *et al.* in [98], Peng and Kurths in [64], and J. Menck *et al.* in [73] propose to focus on the basin of attraction and the basin stability of the system, which are the fundamental system characteristics that determine the grid response to whatever large perturbations, to asses the stability of a system. In fact, the basin of attraction is defined as an ensemble of states in the phase space of system such that initial conditions chosen in that ensemble lead to a particular attractor. The basin stability, which is the volume of the basin of attraction, quantifies the ability of the system to regain an equilibrium state (synchronous state) after a perturbation [73].

Figure 5.8 shows the basin of attraction of the system with and without frequency regulation for different values of the damping coefficient α. The blue area corresponds to the stable attractor of the system without control, while the red the one for the system with frequency control, and the gray color corresponds to the limit cycle basin of attraction. One can first observe that the basin of attraction of the stable fixed point with frequency control does not depend on α, while it does so without control. The size of the region increases when the damping is increased. This result was already clear in Fig. 5.2 where the coexistence of the stable fixed point and limit cycle is reported. Then to quantify how stable the synchronous state is against large perturbations, we compute the basin stability S as defined in [98, 99] by:

$$S(\boldsymbol{B}) = \int \xi_{\boldsymbol{B}}(\phi, \chi)\rho(\phi, \chi)d\phi d\chi, \tag{5.26}$$

where $\xi_{\boldsymbol{B}}(\phi, \chi)= \begin{cases} 1 & \text{if}(\phi, \chi) \in \boldsymbol{B} \\ 0 & \text{otherwise} \end{cases}$ is a function which indicates if a point in phase space belongs to the synchronous state's basin of attraction $\boldsymbol{B}$, and ρ is the density of states [64]. So the number S is the ratio of the number of times the system converges to a synchronous state to the total number of random initial conditions uniformly distributed in phase space. Hence $0 \leq S \leq 1$. For $S = 0$ the system is unstable and $S > 0$ refers to a stable synchronous state. The larger S the more robust the system is. Fig. 5.9 shows the basin stability for a fixed value of damping coefficient as a function of the capacity of the line with (purple) and without frequency controller. Clearly with control the system remains always in the synchronous state, hence the system is reliable against large perturbation while the basin stability increases with the capacity of the line in absence of controller.

5.3

Effects of DDC on the grid synchronization

The previous elementary network constituted by two sub-grids has been proved to be stable, robust and reliable against small and large perturbations when frequency control is included. The electric grid is continuously operating under stress and it is often subjected to huge fluctuations due to distributed generation like wind or solar power which inject power intermittently to the grid. Other fluctuations can be caused by electrical vehicles starting to charge simultaneously, singular events, etc. These fluctuations

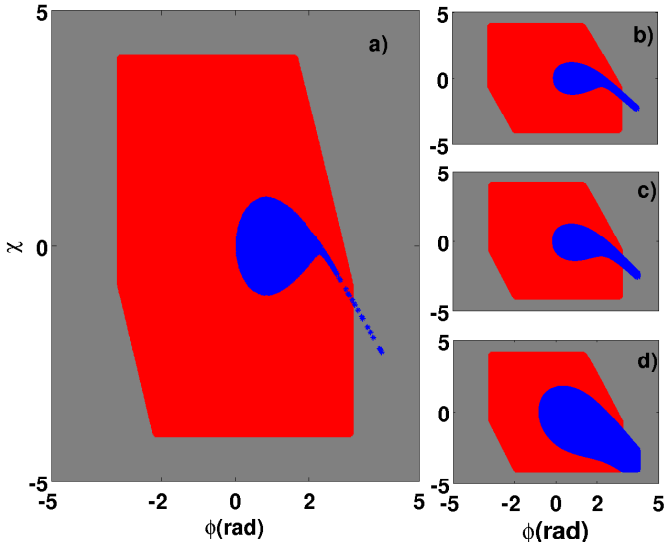

Figure 5.8: Basin of attraction of the steady state without (blue) and with (red) frequency control. The basin of attraction of the limit cycle is indicate in in gray. Here $\frac{\Delta P}{2K} = 0,75$ and $\alpha = 3,25.10^{-3}$ in the coexistence region. 500 random initial conditions homogeneously distributed within the range $\chi \in [-5;5]$, $\phi \in [-\pi;\pi]$ have been taken.

can cause a local instability in the network by affecting the frequency of a sub-grid, which will then be desynchronized with respect to the rest of the network. To control such instability several algorithms, such as F.A.P.E.R, Direct Load Control, and Demand response programs, have been proposed. Here we consider the use of DDC to improve the stability of the synchronization of the network. The effects of DDC on a power grid have been studied in detail in [107, 109] where the power grid was assumed to be perfectly synchronized. The power fluctuations are modeled as a Markovian process, where we suppose to have $N = 1000$ identical devices or group of devices of the same nominal power P_0 switching on and off with the same rate p. In [107, 109] we focused on the application of DDC for reducing the frequency fluctuations within a defined range. In this section the effects of DDC in a 2 node system representing to interconnected grid will be studied.

Effects of DDC on a 2 node system

For the parameter values defined in chapter 4, we compute the frequencies ω_1, ω_2 of the two sub-grids and their phase difference ϕ (see Fig.5.10).

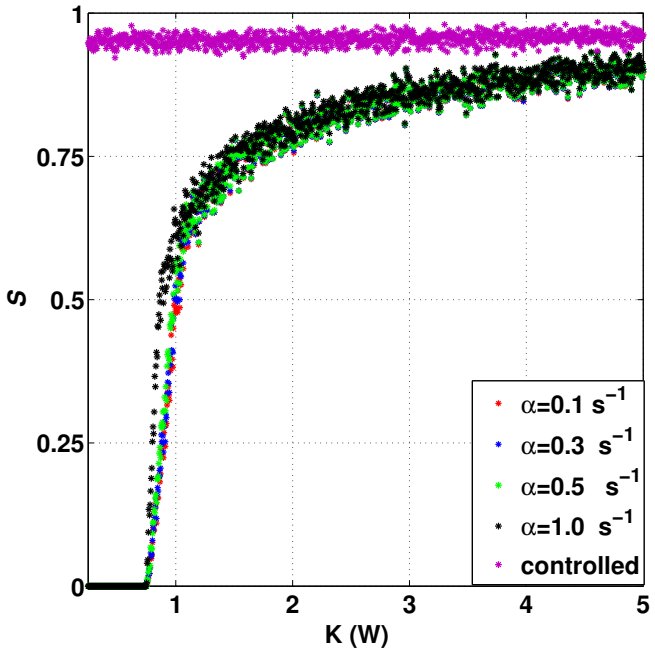

Figure 5.9: Basin stability S as a function of the line capacity K for the following parameter values:ΔP=1.5, $\chi \in [-5;5]; \phi \in [-\pi;\pi]$.

We observe that the frequency fluctuations in all the nodes are reduced with DDC (red line) with respect to the case without control (blue line) despite the presence of peaks due to the simultaneous recovering of pending tasks. These peaks can be suppressed by introducing device-device interactions as explained in the chapter 4. By increasing the line capacity, the reduction of the fluctuations is enhanced in both cases. The two sub-grids are fluctuating with the same frequency, then the system can be said to be partially synchronized. A full synchronization will be achieved if they are rotating with the same rotation angle, namely with a null phase difference. In general if the phase difference between nodes i and j satisfies the following condition: $|\theta_i - \theta_j| = |\phi_{i,j}| \leq \gamma_{ij} < \frac{\pi}{2}$ [34], where i and j indicate the node indexes, we speak of γ_{ij}-phase cohesiveness [22, 34]. Bergen reported in [9] that for a safe operation $\gamma_{ij} < \frac{\pi}{4}$. Figure 5.10 (c,f and i) shows the absolute value over π of the phase difference with (red line) and without DDC (blue line). Without control the system more often looses synchrony ($|\phi_{i,j}| > \frac{\pi}{2}$) while the control suppresses these huge peaks as well

as the fast fluctuations. Increasing the capacity of the line K reduces also

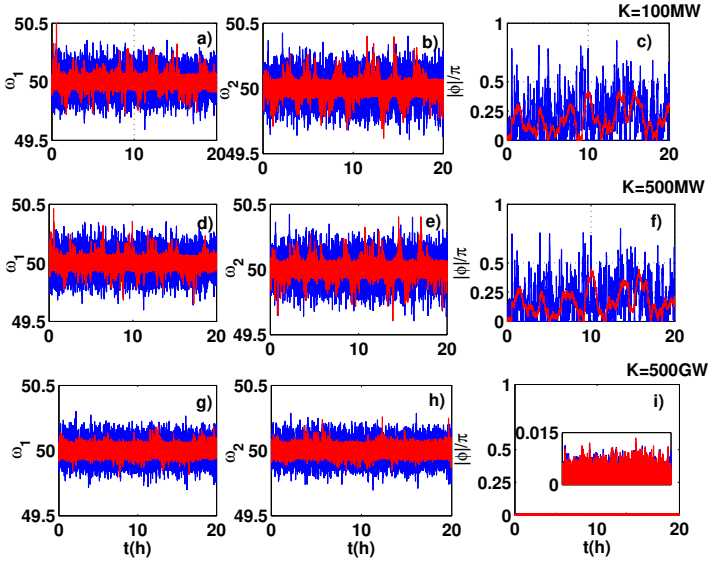

Figure 5.10: Illustration of the frequencies ω_1 and ω_2 of the two nodes , and the phase differences between these nodes as a function of time for different values of K, without (in blue) and with (in red) DDC. For the parameter values used in [109] these values will be used for the rest of the study.

the phase differences, both with and without DDC. Furthermore the DDC case (red curve) is smooth as compared to the fast fluctuations of the case without control, which can be seen as a consequence of the reduction of the frequency fluctuations. From these results one can remark that in the case of an elementary network, DDC helps to improve the stability of the synchronized state. What would happen in the case of larger networks? Is DDC able to avoid a cascading failures?

Effects of DDC on a 10 node system

In this section the effects of DDC in the case of an interconnected power grid will be investigated as well as its effects on the network synchronization of a network composed by 10 nodes. We consider next an undirected network with $V = 10$ vertices and $E = 12$ edges. The average degree is then $< k >= \frac{2|E|}{|V|} = 2.5$, close to that of real electric power grids. The large

model of the US Eastern Interconnect without isolate and parallel branches has, for instance, 49537 nodes and 62985 links, with an average degree $< k >$=2.54. The IEEE 300 bus system of 300 nodes and 409 edges has also an average degree $< k >$=2.74 [47].

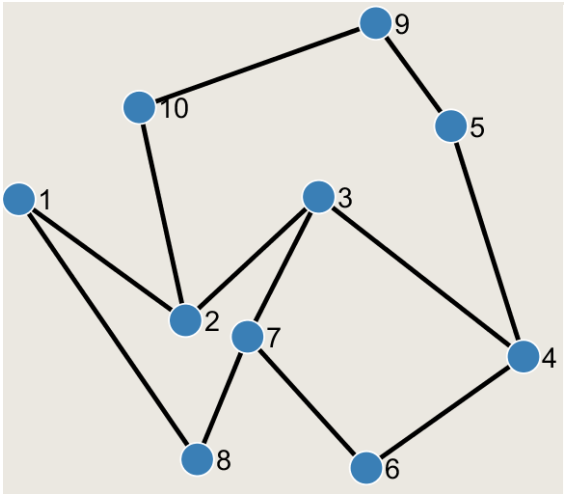

Figure 5.11: Network topology

A large perturbations can hit a defined power grid (or node) of the network making it malfunction, and the failure can propagate across the rest of the network. The failure propagation can be due to the structure of the network, then we speak of structural dependencies, or due to the overloading of the connected lines. In all cases a cascading failure can lead to a total blackout if the affected nodes are not isolated. This phenomenon has occurred several times during the last 20 years, as for instance in the September 2003 Italy blackout caused by the propagation of failures due to the overloading of two Swiss internal lines close to the Italian border. This led to the overloading of the interconnection line between Italy and Switzerland, and the coordination of the two power system operators was not enough to deal with the problem. It ended with the outage on the line which propagated across the Italian Grid and caused the blackout [10]. At least 56 million people across Italy and areas of Switzerland [51] were affected. Another example of a cascading blackout is the August 2003 Blackout in a large part of the north eastern US and eastern Canada which affected about 50 million of people and it costs likely 10 billion dollars [29]. Here we address how DDC can affect the propagation or can avoid cascading blackouts.

Figure 5.11 shows the network considered here, where nodes and lines have been assumed all to be identical. Every node represents a subgrid, namely a power plant in which a number of consumers with constant impedances are attached. Each power grid has a fluctuating load as described in previous paragraphs. In Figs. 5.12 and 5.13 we show the frequency and phase variations of individual nodes of the network without and with DDC. The frequency fluctuations are reduced despite the presence of high frequency peaks observed when the control is applied. Concerning the phases we observe that they have been reduced and are varying continuously between $[-\frac{\pi}{2}; \frac{\pi}{2}]$. Figs. 5.14 and 5.15 show the absolute value of the frequency and phase differences between connected nodes without and with DDC respectively. In the first case the phase differences are always within the $[0; 0.5]$ range. According to R. Berger in [9], to maintain the synchronization or the stability in real power networks, the phase differences θ_{ij} between two connected nodes should be strictly limited to maximum values in the neighborhood of 40° to 50°. Here we choose $\frac{\pi}{4}$ (45°) as the phase angle below which the system should operate. Fig. 5.14 shows clearly that, for the chosen fluctuating load and capacity, the phase differences without DDC (blue line) are often above this limit. This situation implies instability of the system due to large phase differences in all transmission lines. The more extreme case corresponds in this case to nodes 9 and 10. The size of these fluctuations can be reduced by either decreasing the power consumption of every node or by increasing the maximum capacity of the line. Nevertheless the control has the effects to stabilize the fluctuations by refining them (see red line) and to reduce the size of the fluctuations which are too close to its strict maximum value corresponding to the maximal power transmitted (at $\theta_{ij}=\frac{\pi}{2}$) between two connected nodes.

Next we increase the capacity of each line with the aim to reduce the fluctuations in the system and to reproduce a real grid case to simulate the fault of a line and see if the failure propagates or not according to the size of the phase and frequency differences. We simulate a fault on a network by breaking at a given time $t = 10h$ the line connecting the nodes 2 and 3. Figs. 5.16 and 5.17 show the phase and frequency differences of connected nodes without DDC comparing the case with failure (green) to the one without failure (blue). This case corresponds to K=10 GW which means that the maximum power which can flow across connected lines is about $\frac{1}{6}$ of the total demand in each node. One can appreciate that the increase in the difference of phases compared with the difference of phases without failure. The highest phase difference deviation is observed between the two disconnected nodes (nodes 2 and 3), and it is decreasing when we go far away from the affected nodes. That deviation is not significant already for the second nearest-neighbors of the affected nodes. That is the case

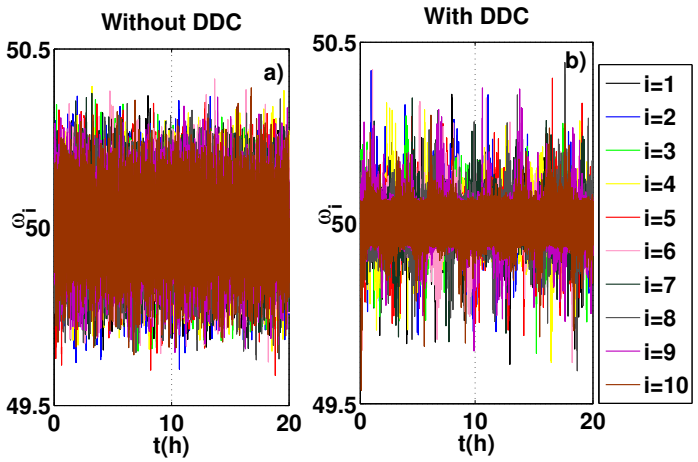

Figure 5.12: Time evolution of the frequency at different nodes without (a) and with (b) DDC.

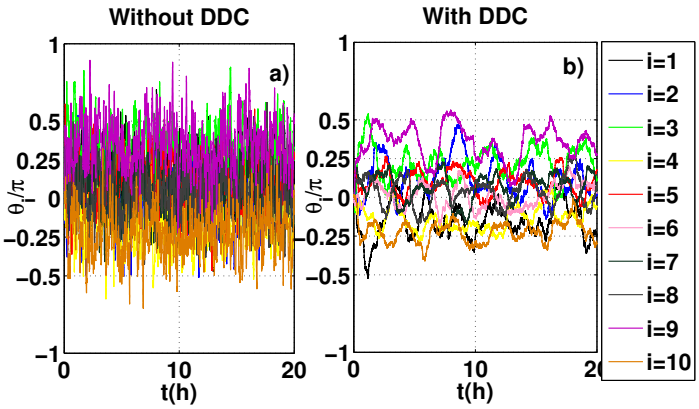

Figure 5.13: Time evolution of the phase at different nodes without (a) and with (b) DDC.

of the difference of phases between the nodes (6,4), (6,7), (5,9) or (8,9). Even if the failure is propagating, the strength of the disturbance is quickly absorbed across the network. By considering the case with DDC shown in Figure 5.18, one can observe two major differences: The size of the phase differences are largely reduced compared to the case without DDC.

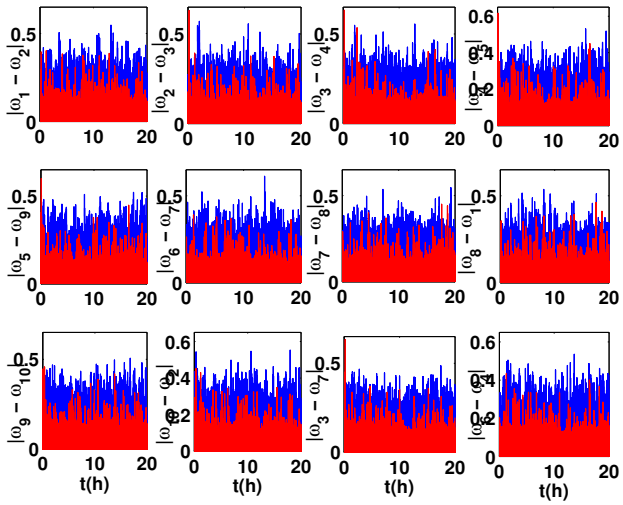

Figure 5.14: Time evolution of the frequency differences between two connected nodes without (blue) and with (red) DDC.

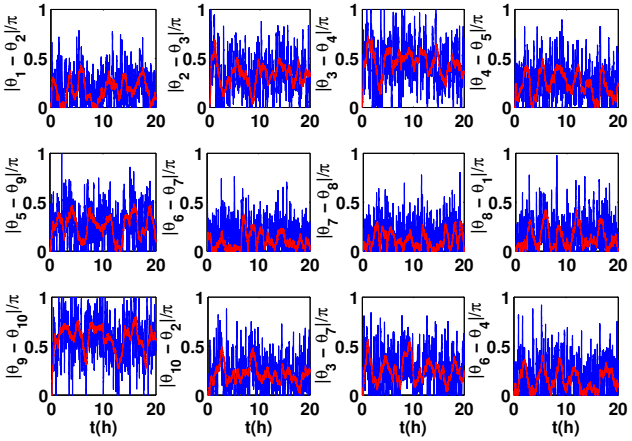

Figure 5.15: Time evolution of the phase differences between two connected nodes without (blue) and with (red) DDC.

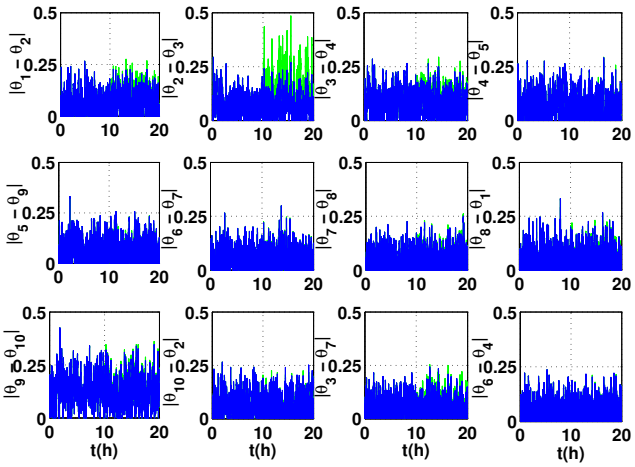

Figure 5.16: Illustration of the time evolution of the phase differences between the connected nodes without DDC, with perturbation (green) and without perturbation (blue).

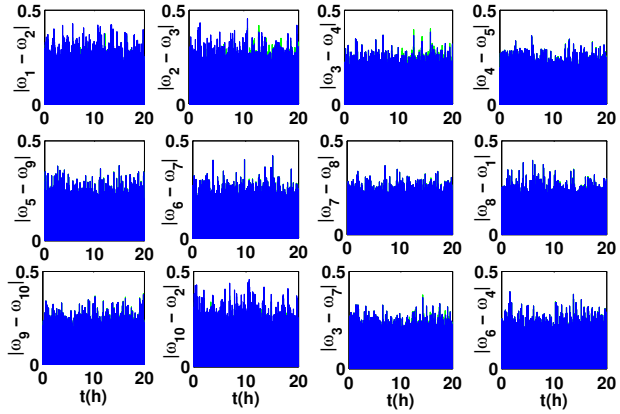

Figure 5.17: Illustration of the time evolution of the frequency differences between the connected nodes without DDC, with perturbation (green) and without perturbation (blue).

5.4

Conclusion

We have first studied the effects of frequency regulation on the stability of an elementary network considered as the connection of two power-grids,

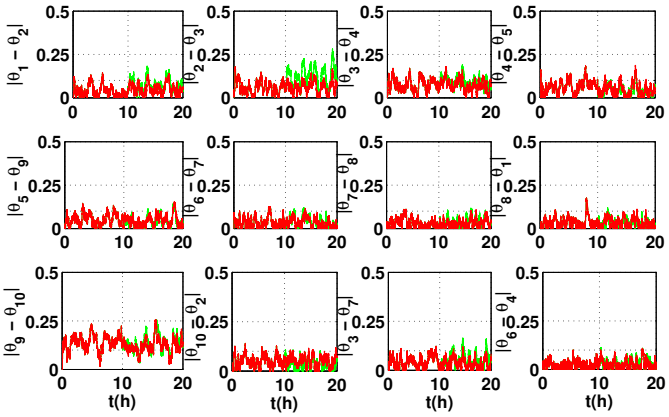

Figure 5.18: Illustration of the time evolution of the phase differences between the connected nodes with DDC, with perturbation (green) and without perturbation (red).

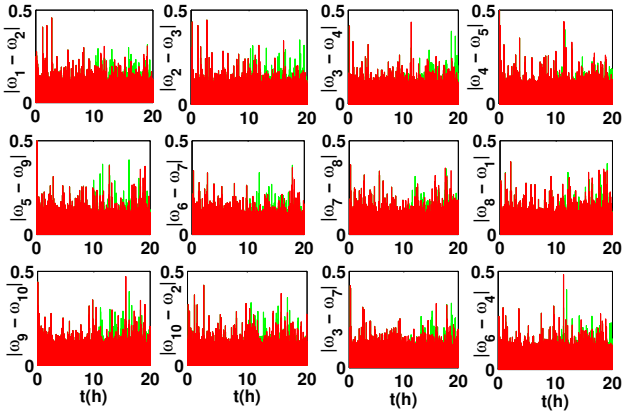

Figure 5.19: Illustration of the time evolution of the frequency differences between the connected nodes with DDC, with perturbation (green) and without perturbation (red).

where each power grid is composed by a generator powering loads which are modeled as a constant impedance. The basin of attraction of the whole system shows that the frequency regulator increases the basin of the synchronized steady state. The basin stability reveals also that the regulated system remains stable even for low line capacities while in absence of regulation the stability increases with the capacity of the line.
Furthermore, the consideration of fluctuating loads reveals that the DDC

stabilizes the frequency as well as the phase of all the nodes in the network. The extension of the study from an elementary network to a network of 10 nodes reveals that the network is robust against perturbations, as for instance the breaking of a specific line, when DDC is considered. The strength of the phase disturbance is damped faster as it moves away from the initial affected nodes with DDC.
The frequency differences between two connected nodes in absence of DDC is not affected by noise due to the action of the frequency regulation. But in presence of DDC it has been observed a deviation in the frequency differences due to the DDC constraints, which modifies the load pattern and consequently the frequency fluctuations.
Additional studies show that for a strong perturbation, DDC increases the time of propagation of the failure but does not avoid it completely. In other words, DDC gives extra time to react on the network in order to avoid a cascading failure and a blackout. This study can eventually be extended to different types of networks, and we think the general results will remain unchanged.

CHAPTER 6

How secondary control prevents Braess' paradox

Most of the generators in the electric grid are powered by fossil fuels and few of them use renewable energy sources. Its integration is addressed to reduce the emission of greenhouse gases, and at the same time to cover the overall increase of the electric demand. This integration has consequences such as their unpredictability, and their intermittency that we discussed in the previous chapters. Nevertheless, there are proposed solutions to face the demand increase. These solutions include the building of new generators (which are environmental and financial costly), the upgrade of line capacities, the extension and addition of new power transmission lines and the use of energy storage. The synchronization dynamics of electric network under some of these solutions have been studied principally by Witthaut and Timme [68, 121, 122], who found a particular counter intuitive behavior of a toy network. In fact, expecting an improvement of the network stability, they obtained the reverse results: the system lost its synchrony after a new line has been added or the capacity of a line has been upgraded. Such counter intuitive behavior is known as Braess paradox. These results have been obtained in a case of a particular network composed by 8 nodes (4 generators and 4 consumers), whose dynamics is governed by a 2nd order kuramoto model.
As presented in the previous chapters, considering frequency regulation makes the system resilient and robust against perturbations. Including frequency regulation, the model captures better the realistic dynamics of the electric network. In this chapter, we consider a frequency regulator model and investigate the possibility to identify Braess paradox in a resilient electric network [108]. The Chapter is structured as follows: the

electric network model will be proposed and its dynamics will be studied using perturbation methods in section 6.2. How the frequency regulator prevents or not Braess paradox will be investigated in different configurations in section 6.4.

6.1 Mathematical model

Most of today's electric power is generated by three phase synchronous generators, e.g. driven by steam or hydro turbines, which output an alternating current (AC) [4]. The electric power grid may then be modeled as an interconnected network consisting of nodes linked by power transmission lines (links). Each node can be interpreted as a local area including power generation and consumption with net mechanical power input P_i being negative for effective consumer regions, e.g. urban areas, and positive for effective generators. Let f_R be the reference frequency of the power grid (50Hz or 60Hz) and $\omega_R = 2\pi f_R$ be the reference angular velocity. The dynamics of a node or area, modeled as in the chapter 5 by the equation (5.4) is given by:

$$\dot{\theta}_i = \omega_i, \tag{6.1}$$

$$\dot{\omega}_i = -\alpha_i\omega_i + P_i - \sum_{j=1}^{n} K_{ij}\sin(\theta_i - \theta_j) + P_{ci}, \tag{6.2}$$

$$\tau_i\dot{P}_{ci} = -P_{ci} - [\beta_i\omega_i(t) + \gamma_i\theta_i], \tag{6.3}$$

where α_i plays the role of an effective damping constant. K_{ij} determines the capacity of a line, P_{ci} is the control power with time constant τ_i while β_i and γ_i give essentially the magnitude of the primary and secondary control respectively. Eqs. (6.1) and (6.2) have the form of the well-known 2nd-order Kuramoto model, which has been used for example in [41, 44] without control to describe the dynamics of the power grid as reported above. For the seek of simplicity, throughout this chapter, we set the parameter τ_i=0, meaning that the control acts instantaneously. This approximation does not affect the final steady state of the system, which we are mainly interested in, simplifying the model considerably. The time constant τ_i only changes the frequency of the oscillations during the transient dynamics. Thereby, we can solve Eq. (6.3) for P_{ci} and insert it into Eq. (6.2). In addition, since the damping α_i and primary control β_i play a similar dynamical role, we

absorb any contribution from β_i into α_i, effectively setting $\beta_i = 0$. With that, our equation of motion for each node reads

$$\begin{aligned} \dot{\theta}_i &= \omega_i, \\ \dot{\omega}_i &= -\alpha_i \omega_i - \gamma_i \theta_i + P_i - \sum_{j=1}^{n} K_{ij} \sin(\theta_i - \theta_j). \end{aligned} \tag{6.4}$$

The control term $-\gamma_i \theta_i$ has the same form than the integral control used in [120]. Alternative control schemes has been considered in [32, 45, 104, 118, 120]. Furthermore, we will initialize numerical simulations of the set of equations (6.4) using $\theta_i(0) = 0$ and $\omega_i(0) = 0$ for all nodes.

6.2

Steady state analysis and stability condition

The power grid is in a steady state when all rotatory machines are phase-locked, i.e, have the same frequency, which ideally is the reference frequency of $f_{\mathrm{R}} = 50$ Hz or 60 Hz [34]. This corresponds to the fixed point of (6.4) which is given by $\omega_i^* = 0$ and

$$\sum_{j=1}^{N} K_{ij} \sin(\theta_i^* - \theta_j^*) = P_i - \gamma_i \theta_i^*, \ \forall i \in 1, ..., N. \tag{6.5}$$

Without control, $\gamma_i = 0$, these algebraic equations do not always have a solution for the phases θ_i^*. As a trivial example, without enough transmission capacity, i.e, $\sum_{j=1}^{N} K_{ij} < P_i$ for finite power $P_i \neq 0$ there cannot be any fixed point. However, when control is included in all the nodes $\gamma_i > 0, \forall i$ then there is always at least one fixed point solution [120].

To derive the stability conditions of the synchronous state with respect to small perturbations, we linearize Eq. (6.4) around (θ_i^*, ω_i^*). We denote small perturbations around the fixed point as $\theta_i = \theta_i^* + \delta\theta_i$ and $\omega_i = \omega_i^* + \delta\omega_i$ and define $\mathbf{X_1}$ and $\mathbf{X_2}$, as the n-dimensional vectors of $\delta\theta_i$ and $\delta\omega_i$, respectively. Linearizing (6.4) yields

$$\begin{aligned} \dot{\mathbf{X}}_1 &= \mathbf{X_2}, \\ \dot{\mathbf{X}}_2 &= -(\mathbf{L} + \mathbf{\Gamma})\mathbf{X_1} - \mathbf{A}\mathbf{X_2}, \end{aligned} \tag{6.6}$$

where $\mathbf{\Gamma}$ and $\mathbf{A}$ are diagonal matrices with elements $\Gamma_{ii} = \gamma_i$ and $A_{ii} = \alpha_i$ respectively, representing the control and the damping matrix. Matrix

$\mathbf{L}$=(L_{ij}) is a Laplacian matrix of the network topology, defined as

$$L_{ij} = \begin{cases} -K_{ij}\cos(\theta_i^* - \theta_j^*), & i \neq j, \\ -\sum_{l\neq i}^{n} L_{il}, & i = j. \end{cases} \tag{6.7}$$

The Lyapunov exponents $\{\lambda_j\}$ of the dynamical system (6.6) are given by the eigenvalues of the Jacobian matrix

$$\mathbf{J} = \begin{bmatrix} \mathbf{0} & \mathbf{1} \\ -\mathbf{L} - \mathbf{\Gamma} & -\mathbf{A} \end{bmatrix}. \tag{6.8}$$

Without secondary control, i.e., $\gamma = 0$, there is a single zero Lyapunov exponent which arises because the stability is only defined up to an arbitrary phase shift, i.e., we could replace all phases by different ones by adding a constant everywhere $\theta_i \to \tilde{\theta}_i = \theta_i + \text{const.}$ [68]. In this case the synchronous state is stable if the real part of the other Lyapunov exponents is negative.

The inclusion of secondary control breaks the phase invariance and, as a consequence, for $\gamma > 0$, there is no generic zero Lyapunov exponent. Lyapunov exponents can only be zero at specific parameter values associated to bifurcation points. The synchronous state of the system is stable if and only if the real part of all Lyapunov exponents is negative.

In the case in which the damping and control parameters are the same for all nodes, namely $\alpha_i = \alpha$ and $\gamma_i = \gamma$ the stability of the synchronized state can be analyzed using the master stability function technique [85]. We diagonalize the Laplacian matrix $\mathbf{L}$ by substituting $\mathbf{Y_1} = \mathbf{M}^{-1}\mathbf{X_1}$, $\mathbf{Y_2} = \mathbf{M}^{-1}\mathbf{X_2}$, where $\mathbf{M}$ is the matrix composed of the eigenvectors of $\mathbf{L}$ such that $\mathbf{\Lambda} = \mathbf{MLM}^{-1}$ is the diagonalized matrix composed by the eigenvalues μ_j. We assume symmetric coupling $K_{ij} = K_{ji}$, thereby guaranteeing real eigenvalues μ_j. Eq. (6.6) can be rewritten as

$$\frac{\mathrm{d}}{\mathrm{d}t}\begin{bmatrix} Y_{1j} \\ Y_{2j} \end{bmatrix} = \begin{bmatrix} 0 & 1 \\ -\mu_j - \gamma & -\alpha \end{bmatrix}\begin{bmatrix} Y_{1j} \\ Y_{2j} \end{bmatrix}. \tag{6.9}$$

The Lyapunov exponents are given by:

$$\lambda_{j\pm} = -\frac{\alpha}{2} \pm \frac{1}{2}\sqrt{\alpha^2 - 4(\mu_j + \gamma)}. \tag{6.10}$$

Fig. 6.1 shows the dependence of the real part of Lyapunov exponents $\Re[\lambda_{j\pm}]$ with μ_j as given by Eq. (6.10). Without control, $\gamma = 0$, stability is guaranteed if all eigenvalues μ_j of the Laplacian matrix are positive,

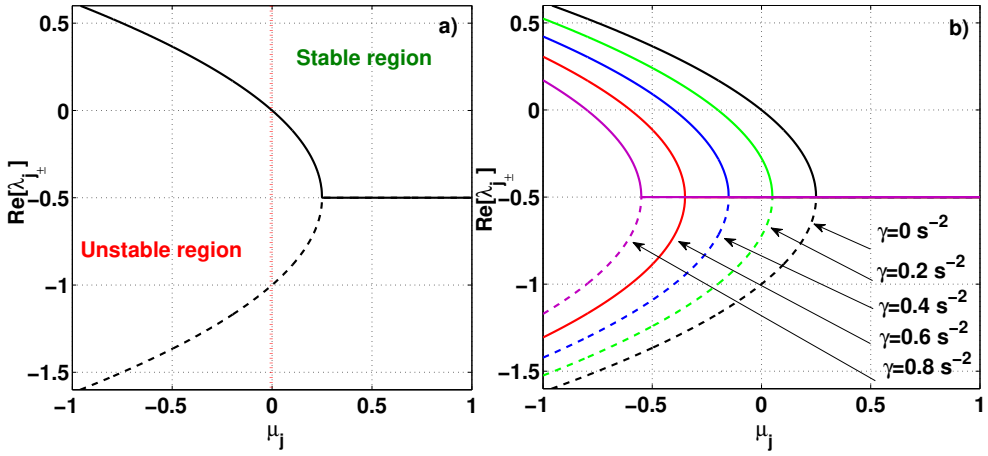

Figure 6.1: Secondary control extends the stable operation as a function of the topology (μ). We plot the real part of the largest eigenvalue λ_+ (continuous lines) and λ_- (dashed lines) as functions of the Laplacian eigenvalue μ, see Eq. (6.10). We assume that the control is homogeneous throughout the network, i.e., $\gamma_j = \gamma$. (a) Without control, $\gamma = 0$, the system becomes unstable as soon as the Laplacian eigenvalue μ becomes negative, as then $Re(\lambda) > 0$. Note that Eq. (6.10) starts having two solutions as soon as $\alpha^2 = 4(\mu+\gamma)$. (b) With increasing control, $\gamma > 0$, the region of stability also increases. The plots use a homogeneous damping value of $\alpha = 1$.

see Eq. (6.10) and [68, 80]. If however a given eigenvalue μ_j is negative, one of the corresponding eigenvalues $\lambda_{j\pm}$ is positive and the other one is negative; therefore, the synchronous state is unstable. With added secondary control, i.e., $\gamma > 0$, the region of stability increases, see Fig. 6.1, which holds for any number of nodes. Mathematically, the system is stable within the region defined by $\mu_j + \gamma > 0$, see also [80, 117].

The eigenvalues $\{\mu_j\}$ depend on the topology of the network. Changing the capacity of a line, adding additional lines or removing them will change the values of $\{\mu_j\}$ and, thus, that of $\{\lambda_j\}$, and may lead to instabilities. We label as λ^{m} the non-zero Lyapunov exponent with the largest real part and μ^{m} the corresponding eigenvalue of $\mathbf{L}$.

6.3

Two nodes system

Let us now investigate the elementary system consisting of two nodes, a generator ($P_1 > 0$) and a consumer ($P_2 < 0$) first without secondary control to then investigate the benefits of adding such control.

Uncontrolled two nodes system

Without control, $\gamma_1 = \gamma_2 = 0$, and assuming homogeneous damping $\alpha_1 = \alpha_2 = \alpha$, the dynamics is given by the following equations for the phase difference $\Delta\theta = \theta_1 - \theta_2$ and the frequency difference $\dot{\Delta\theta} = \omega_1 - \omega_2 = \Delta\omega$ with $\Delta P = P_1 - P_2$

$$\begin{aligned} \dot{\Delta\theta} &= \Delta\omega, \\ \dot{\Delta\omega} &= -\alpha\Delta\omega + \Delta P - 2K\sin(\Delta\theta), \end{aligned} \tag{6.11}$$

The system has a steady state if and only if $2K \geq \Delta P$, see also chapter 5. The physical reason for the absence of a fixed point for $2K < \Delta P$ is that the electric power flowing through a line cannot exceed the maximal capacity K.
For $2K > \Delta P$ the two steady states, T_1 and T_2, obtained from (6.11), and their respective eigenvalues are

$$T_1 : \begin{cases} \Delta\theta^* = \arcsin\left(\frac{\Delta P}{2K}\right), \Delta\omega^* = 0, \\ \lambda_\pm(T_1) = -\frac{\alpha}{2} \pm \sqrt{\frac{\alpha}{2}^2 - \sqrt{4K^2 - \Delta P^2}} \end{cases}, \tag{6.12}$$

$$T_2 : \begin{cases} \Delta\theta^* = \pi - \arcsin\left(\frac{\Delta P}{2K}\right), \Delta\omega^* = 0, \\ \lambda_\pm(T_2) = -\frac{\alpha}{2} \pm \sqrt{\frac{\alpha}{2}^2 + \sqrt{4K^2 - \Delta P^2}} \end{cases} . \tag{6.13}$$

The steady state T_1 is a stable fixed point since we assume the damping α to be positive. In contrast, the steady state T_2 is a saddle since its eigenvalue λ_+ is a positive real number.
For $2K = \Delta P$, T_1 and T_2 collide via a saddle node bifurcation on a cycle (SNIC), entering a limit cycle for $K < \frac{\Delta P}{2}$. Such limit cycles often cause large frequency deviations that would result in the shutdown of (parts of) the grid and are therefore undesirable [68]. But even for sufficient transmission capacity, i.e. $2K \geq \Delta P$, the grid enters a limit cycle if we have unbalanced power, $P_1 + P_2 \neq 0$ so that, from Eq. (6.4) the synchronous angular velocity is given as

$$\omega_{\text{syn}} = \frac{P_1 + P_2}{2\alpha}. \tag{6.14}$$

Hence, the grid is no longer at its reference frequency of $f_R = 50$ Hz or 60 Hz but below it for $P_1 + P_2 < 0$ and above it for $P_1 + P_2 > 0$. To restore the frequency to the reference, we apply our secondary controller in the next subsection.

Two nodes system with secondary control

Next, we consider the two nodes system where one node applies a secondary control, i.e., we set the control parameters $\gamma_1 = 0$ and $\gamma_2 = \gamma$ in the equation of motion (6.4). Then, the steady state of the controlled system is obtained as

$$\begin{aligned} \theta_1^* &= \tfrac{P_1+P_2}{\gamma} + \arcsin(\tfrac{P_1}{K}), \\ \theta_2^* &= \tfrac{P_1+P_2}{\gamma}, \\ \omega_1^* &= 0, \\ \omega_2^* &= 0. \end{aligned}$$

For $P_1 > K$, there is no steady state and the system approaches a limit cycle, as the power cannot be transferred via the line and node 1 is uncontrolled. For $P_1 < K$ however, there will be a fixed point, even if the power is unbalanced $P_1 + P_2 \neq 0$, in contrast to the uncontrolled system (Fig 6.2). While the uncontrolled system (solid lines) approaches a limit cycle with ω_{sync}, as obtained by Eq. (6.14), the controlled system is attracted to the fixed point, i.e. a stable operating state of the grid.

Next, we perform a stability analysis of the fixed point. Let $\mathbf{X}$=$(\delta\theta_1, \delta\theta_2, \delta\omega_1, \delta\omega_2)$ be a small perturbation of the fixed point. The equations of motion

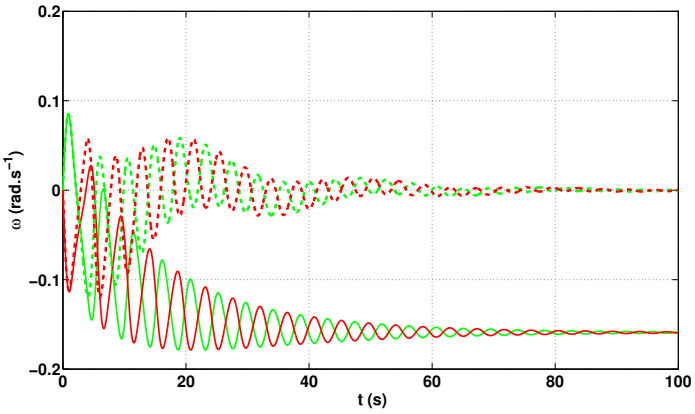

Figure 6.2: Including control restores the frequency back to the reference value. We plot the time evolution of the angular velocity deviations ω without control (solid lines) and when controlling one node (dashed lines). With control, the system returns to $\omega = 0$, i.e., the grid returns to its reference frequency f_R. Red and green curves represent the consumer and generator of a two node system respectively with parameters $\gamma = 0.1\ s^{-2}$, $\alpha = 0.1\ s^{-2}$, $K = 1.5\ s^{-2}$, $P_1 = 1\ s^{-2}$, $P_2 = -1.2\ s^{-2}$.

of these small perturbations are given by

$$\dot{\mathbf{X}}(t) = \mathbf{D} \cdot \mathbf{X}(t), \tag{6.15}$$

where the matrix D is defined as

$$\mathbf{D} = \begin{bmatrix} 0 & 0 & 1 & 0 \\ 0 & 0 & 0 & 1 \\ -K\cos(\theta_1^* - \theta_2^*) & K\cos(\theta_1^* - \theta_2^*) & -\alpha & 0 \\ K\cos(\theta_1^* - \theta_2^*) & -\gamma - K\cos(\theta_1^* - \theta_2^*) & 0 & -\alpha \end{bmatrix}. \tag{6.16}$$

The characteristic polynomial of matrix D is given as

$$\lambda^4 + a_1\lambda^3 + a_2\lambda^2 + a_3\lambda + a_4 = 0, \tag{6.17}$$

where the parameters a_1, a_2, a_3 and a_4 are given by

$$\begin{aligned} a_1 &= 2\alpha, \\ a_2 &= \alpha^2 + \gamma + 2a, \\ a_3 &= 2a\alpha + \alpha\gamma, \\ a_4 &= a\gamma, \\ a &= K\cos(\theta_1^* - \theta_2^*) = \sqrt{K^2 - P_1^2}. \end{aligned} \tag{6.18}$$

To analyze the stability of the full four dimensional system, we need to obtain an expression for the eigenvalues. Unfortunately, a fourth or higher order polynomial does not have an easy to analyze solution so that we apply the Routh Hurwitz (RH) criterion to determine the stability [124]. Applying then the RH criterion as in section 5.2, the system is stable if the parameter γ verifies the following inequality:

$$\alpha^2\gamma^2 + 2\alpha^4\gamma + 4a\alpha^2(a + \alpha^2) > 0, \tag{6.19}$$

which again is always true; hence, as long as there is non-zero control, $\gamma > 0$, the synchronous state is always stable, regardless of the value of the other parameters of the system, highlighting the potential of secondary control. Next, we shall investigate how secondary control interacts with changes of the network topology that lead to Braess' paradox in uncontrolled systems.

6.4

Braess' paradox prevented by secondary control

Adding lines to a transmission network is intuitively expected to improve its synchronization ability. However, adding certain lines instead causes the grid to lose its synchronous state. More general, the effect of adding edges to a network and thereby causing problems and a decrease in performance was first predicted in 1968 for traffic networks [14] and it is since known as Braess' paradox. It was observed in traffic systems in New York, USA [56], and Stuttgart, Germany [55], when closing a street made the traffic go faster.

In electric networks, Braess' paradox has been predicted in DC power flow [59], AC power flow [79] and recently in oscillator power grids [121, 122]. Building additional transmission capacity under specific conditions causes Braess' paradox and thereby the grid loses its fixed point and we observe a blackout. Fortunately, not every network is susceptible to Braess' paradox. Braess' paradox can be understood by considering the fixed point solutions as given by Eq. (6.5) without control ($\gamma_i = 0$). As discussed in sect. 6.2 the existence of fixed points is not guaranteed and in fact adding a line in a network can result in the equations to be overdetermined and therefore to have no solution. This can also be interpreted in the light of the critical coupling K_c of the grid [68]. The critical coupling is defined as the minimum value of K so that for a homogeneously coupled grid, i.e. $K_{ij} = Kk_{ij}$ with unweighted adjacency matrix $\mathbf{k}$, the algebraic equations (6.5) with $\gamma = 0$

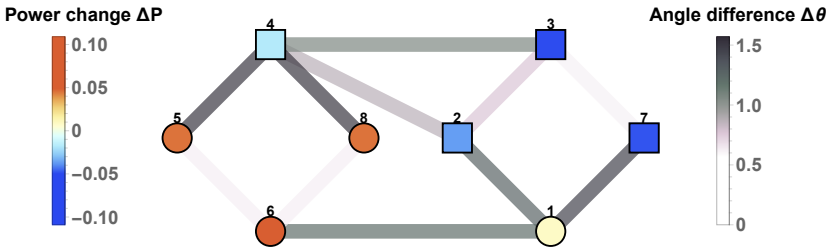

Figure 6.3: Controlling all nodes changes the power dispatch in the system and allows stable operation without Braess' paradox. We display the 8 node system susceptible to Braess' paradox with an added line $(2, 4)$. Including secondary control causes all nodes to adapt their power in the stationary state as $\Delta P_i^* = -\gamma_i \theta_i^*$. This results in consumers (circles) to consume less (red: positive power change), while generators (squares) generate less (blue: negative power change). Thereby, the system preserves its steady state even after including a line that causes an overload in the uncontrolled system. In addition, we note a very heterogeneous load of the lines (line color; darker colors indicate higher load). Specifically, the lines (4,5) and (4,8) are highly loaded, i.e., the phase difference $\Delta\theta_{4,5}^*$
becomes very large. Parameters used are $\alpha = 1\ s^{-1}$; $K = 1.03\ s^{-2}$, $\gamma = 0.1\ s^{-2}$.

have at least one solution. Thereby, K_c gives the minimum capacity necessary to synchronize the grid. Adding a line or capacity in an existing line effectively may increase the critical coupling K_c [121]. Increasing K_c means the fixed point can only be restored by increasing the capacity K for all lines. Besides, even if the fixed point solution exists after the network being modified, since its stability depends on the topology μ_i, it may become unstable.

To study the effect of Braess' paradox in more detail, we investigate an elementary example network composed of 8 nodes, where adding one additional transmission line or increasing the capacity of an existing line leads to a desynchronization of the network. The network is shown in Fig. 6.3 without the additional line $(2, 4)$, or in Fig. 1a in [122]. The grid is such that generation and consumption are not evenly distributed, for instance, generator node 4 is connected to consumer nodes 5 and 8 while generator node 3 is not connected to any consumer. All generators have power $P_i = 1\ s^{-2}$ and all consumers $P_i = -1\ s^{-2}$. All lines have the same capacity $K = 1.03\ s^{-2}$. In Fig. 6.4 we plot the time evolution of the phase of each node, with consumers in red and generators in green. As shown in panel a) after a short transient the original network enters a phase-locked state where all machines run stably in synchrony.

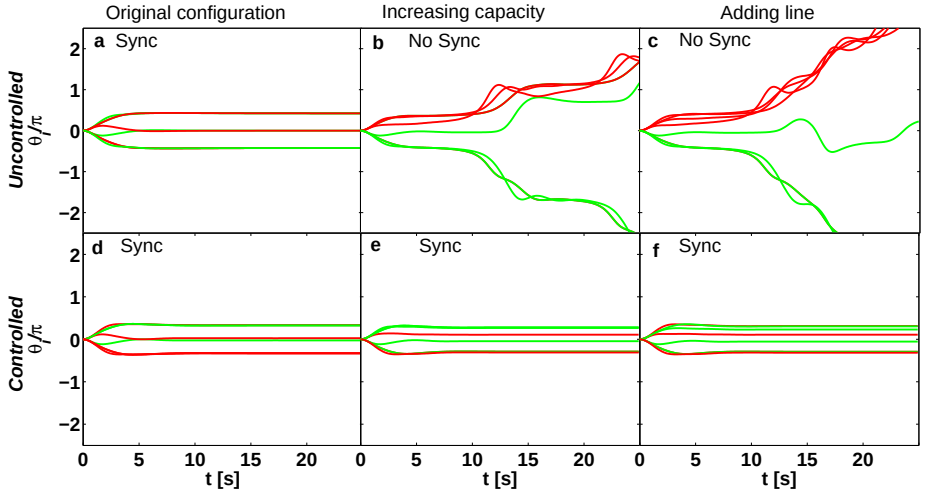

Figure 6.4: Secondary control stabilizes a network after increasing capacity or adding a link. Braess' paradox in power grids was observed when increasing the capacity of a line or adding an additional line caused the grid to lose its stable fixed point (panels a-c), see also [121]. In contrast, applying secondary control guarantees stability (panels d-f). We use the eight node system depicted in Fig. 6.3, only adding line $(2,4)$ for panels (c) and (f) and doubling the capacity of line $(3,4)$ in panels (b) and (e). Parameter are $\gamma = 0.1\ s^{-2}$, and $\alpha = 1\ s^{-1}$, $K = 1.03\ s^{-2}$ for all nodes and generator and consumer power set to $P_{gen} = 1\ s^{-2}$, $P_{con} = -1\ s^{-2}$, respectively. As in Fig. 6.2, red and green lines correspond to consumers and generators respectively.

The stationary power flux through line (i,j), F^*_{ij} is given by $F^*_{ij} = K_{i,j}\sin(\Delta\theta^*_{i,j})$ where $\Delta\theta^*_{i,j} = \theta^*_i - \theta^*_j$ is the stationary phase difference. Stationary phase differences can be obtained from the fixed point given by Eq. (6.5) with $\gamma = 0$, computed by Newton's method. As shown in Fig. 6.5 a) for the steady state of the original configuration ($\Delta K_{3,4} = 0$) lines $(3,2)$, $(3,7)$, $(6,5)$ and $(6,7)$ carry no load ($\Delta\theta_{i,j} = F^*_{i,j} = 0$) while for all the other lines $\Delta\theta_{i,j} = 0.41\pi$, $F^*_{i,j} = 1\ s^{-2}$. Thus the total power generated by 3 goes to 4 and from there it feeds the consumer nodes 5 and 8. Conversely, the power generated by 2 and 7 goes to 1, where half is consumed and half is feed to 6. The steady state can be seen as composed of two subgrids, one being the mirror of the other. Lets call subgrid $\mathcal{S}_A$ the one composed by nodes 3, 4, 5 and 8 and $\mathcal{S}_B$ the one composed by other nodes.

Consider an increase in the capacity of line $(3,4)$, connecting two generator nodes, by ΔK. From a dynamical point of view, the capacity

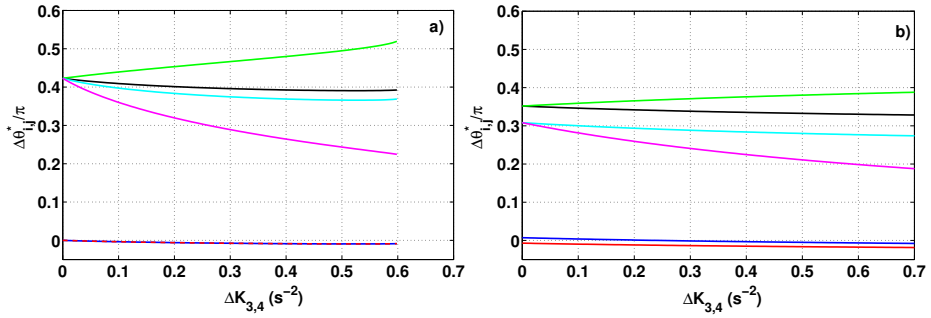

Figure 6.5: Stationary phase differences between nodes increasing the capacity of line $(3,4)$ of the grid shown in Fig. 6.3 (without line $(2,4)$) without control (panel a)) and with control in all nodes $\gamma = 0.1$ s^{-1} (panel b)). Colors correspond to the following lines: green to $(4,5)$ and $(4,8)$, cyan to $(1,6)$, magenta to $(3,4)$, blue to $(3,2)$ and $(3,7)$, red to $(6,5)$ and $(6,8)$, and black to $(2,1)$ and $(7,1)$. Without control beyond the critical added capacity $\Delta K_c \approx 0.6$ s^{-2} there is no longer any fixed point and thus the system goes to an desynchronized state. With control in all the nodes the synchronized state is always stable. $K_{i,j} = 1.03s^{-2}$ for all lines except the one with added capacity. Other parameters as in Fig. 6.4

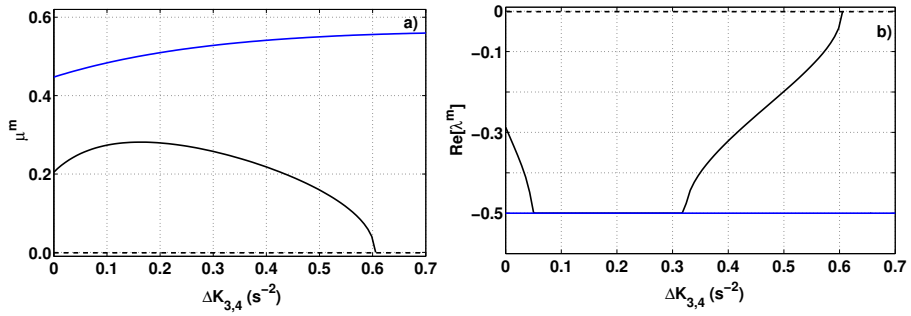

Figure 6.6: Stability of the synchronized solution as the capacity of line $(3,4)$ is increased. The real part of the largest non-zero Lyapunov exponent $\Re[\lambda^{\mathrm{m}}]$ is shown in b) while a) displays the corresponding Laplacian eigenvalues μ^{m}. Black lines correspond to the case without control ($\gamma = 0$) and blue lines to the case with control in all nodes ($\gamma = 0.1$ s^{-2}). Parameters as in Fig. 6.5.

increase translates into a larger coupling coefficient between nodes 3 and 4. As a consequence the phase difference between them decreases, as shown in 6.5 a) (magenta line). However this has a side effect: phase differences $\Delta\theta^*_{4,5} = \Delta\theta^*_{4,8}$ increase (green line) as does the power flow on lines $(4,5)$ and $(4,8)$, $F^*_{4,5} = F^*_{4,8} > 1\ s^{-2}$. The power arriving from 4 to 5 and 8 is slightly larger than their consumption, thus the leftover power is fed to 6 and $\Delta\theta^*_{6,5} = \Delta\theta^*_{6,8}$ (red line) are no longer 0. They are slightly negative signaling a weak flow towards 6. Node 6 no longer gets all the power from 1 and $\Delta\theta^*_{1,6}$ decreases (cyan line). The flow send to 1 by generators 2 and 7 is also reduced, meaning that phases $\Delta\theta^*_{2,1} = \Delta\theta^*_{7,1}$ slightly decrease (black line). Finally since now 2 and 7 feed less power to 1 the leftover power is send to 3 and $\Delta\theta^*_{3,2} = \Delta\theta^*_{3,7}$ (blue line) are no longer 0, rather slightly negative corresponding to a weak flow towards 3. Thus the increase of capacity has induced a weak power flow between the two subgrids. Furthermore, it has broken the mirror symmetry between the subgrids. Comparing the flows with the original ones, the difference can be seen as a weak overall counterclockwise flow. The counterclockwise direction has been set by that of the flow in the line whose capacity has been increased. For the lines in which the original flow was in opposite direction than this induced overall flow the effect of the added capacity is beneficial since the flow is actually reduced. However, lines $(4,5)$ and $(4,8)$, for which the original flow has the same direction than the induced overall flow, are now threaten since their capacity has not been upgraded and now they have to carry a larger load. Eventually lines $(4,5)$ and $(4,8)$ reach the maximum power they can deliver and at $\Delta K_c \sim 0.6 s^{-2}$ the system does no longer has a fixed point.

Fig. 6.6 shows the real part of the largest non-zero Lyapunov exponent $\Re[\lambda^{\mathrm{m}}]$ and the corresponding eigenvalue of the Laplacian matrix μ^{m} (black lines). For the small added capacity the overall effect is positive: μ^{m} increases and thus $\Re(\lambda^{\mathrm{m}})$ decreases and therefore the stability of the synchronized solution is improved as intuitively expected. For $\Delta K_{3,4} = 0.05\ \mathrm{s}^{-2}$, μ^{m} reaches $1/4$ so that λ^{m} becomes complex and $\Re(\lambda^{\mathrm{m}})$ remains clamped at $-1/2$ which is the most negative value it can take. As capacity is further increased μ^{m} reaches a maxima at $\Delta K = 0.16\ \mathrm{s}^{-2}$ and then decreases. For $\Delta K_{3,4} = 0.32\ \mathrm{s}^{-2}$, $\mu^{\mathrm{m}} < 1/4$ and $\Re(\lambda^{\mathrm{m}})$ starts to increase. Finally at ΔK_c, $\mu^{\mathrm{m}} = 0$ and $\Re(\lambda^{\mathrm{m}}) = 0$. Thus the fixed point is stable while it exists and at ΔK_c the system undergoes a saddle node bifurcation which signals the Braess' paradox for this system. For $\Delta K_{3,4} > \Delta K_c$ the system enters a desynchronized regime, as shown in Fig. 6.4b) and [121].

Similar effects can be triggered by an increase of the capacity of line $(1,6)$ (in this case the weak overall flow is clockwise overloading lines $(2,1)$ and $(7,1)$ and the synchronized state disappears at $\Delta K_c \approx 0.6$) or by

the addition of a new line. Consider the addition of a line connecting nodes $(2, 4)$ as shown in Fig. 6.3. For the new topology there is no fixed point and the grid desynchronizes as shown in Fig. 6.4c) and [121].

Is Braess' paradox still present after adding secondary control? Let us consider the same 8 node network and the same cases as before but now with control in all the nodes $\gamma_i = \gamma > 0$. As shown in Fig. 6.4 e) and f) controlling the network guarantees a stable state even after doubling the capacity of line $(3, 4)$ or adding a new line $(2, 4)$, thereby preventing Braess' paradox.

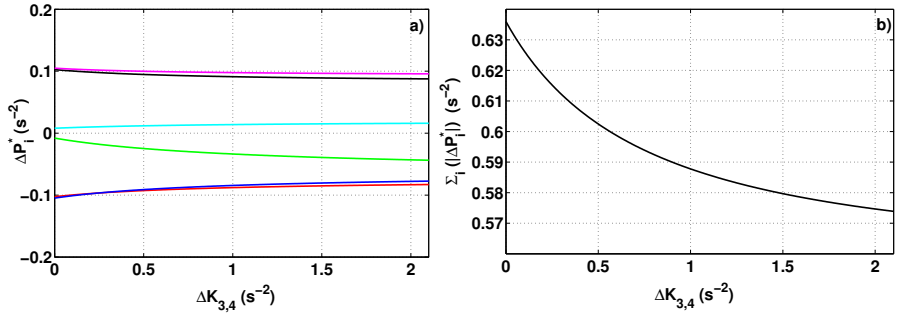

Figure 6.7: Change in power in the stationary regime induced by applying control in all the nodes $\gamma = 0.1$. Colors correspond to the following nodes: cyan to 1, red to 2 and 7, blue to 3, green to 4, black to 5 and 8 and magenta to 6. Control leads to a positive power change in consumers and negative in generators. Parameters as in Fig. 6.5.

As indicated in Sect. 6.2 when control is included in all the nodes there is always a fixed point solution. Even if the transmission capacity K_{ij} is insufficient or would normally cause Braess' paradox, the term $-\gamma_i\theta_i^*$ in Eq. (6.5) balances both sides of the equation and guarantees a solution. In fact

$$\Delta P_i^* = -\gamma_i\theta_i^* \tag{6.20}$$

is the power provided by the secondary control in the stationary regime. The effective power generated/consumed at each node in the stationary regime is given by

$$P_i^{\text{eff}} = P_i + \Delta P_i^*. \tag{6.21}$$

Thereby, we do not need to increase the capacity of all lines because the control reduces the total power flow in the system.

We illustrate this for a 2 node system with $\gamma_1 = \gamma_2 = \gamma$. The critical coupling is then given as

$$K_c^{\text{New}} = K_c - \gamma\theta, \tag{6.22}$$

i.e. the controller reduces the load on the lines, enabling the fixed point with lower capacity. Following the same argumentation, secondary control also cures Braess' paradox which would otherwise require an increase of the transmission capacity.

To better understand how the controller stabilizes the network, we plot in Fig. 6.7 a) the stationary change of power with respect to the nominal values ΔP_i^* as the capacity of line $(3,4)$ increases. Consider first the original network, $\Delta K_{3,4} = 0$. Control changes the effective power of each node. With control, generators have negative and consumers positive power change, i.e., consumption is reduced ($P_1^{\text{eff}} = -0.99\ \text{s}^{-2}$, $P_5^{\text{eff}} = P_8^{\text{eff}} = -0.897\ \text{s}^{-2}$, $P_6^{\text{eff}} = -0.895\ \text{s}^{-2}$) as well as generation ($P_4^{\text{eff}} = 0.99\ \text{s}^{-2}$, $P_2^{\text{eff}} = P_7^{\text{eff}} = 0.897\ \text{s}^{-2}$, $P_3^{\text{eff}} = 0.895\ \text{s}^{-2}$). As a consequence the power flow through the loaded lines is reduced and phase differences are smaller than in the uncontrolled case: $\Delta\theta_{4,5}^* = \Delta\theta_{4,8}^* = \Delta\theta_{2,1}^* = \Delta\theta_{7,1}^* = 0.35\pi$, $\Delta_{3,4} = \Delta_{1,6} = 0.31\pi$. Furthermore control induces a (small) flow between the two subgrids: $\Delta\theta_{6,5}^* = \Delta\theta_{6,8}^* = -0.01\pi$, $\Delta\theta_{3,2}^* = \Delta\theta_{3,7}^* = 0.01\pi$. This steady state is more robust in front of perturbations than the uncontrolled case for a double reason: first, the range for which $\Re(\lambda^{\text{m}})$ is negative now extends to negative values of μ^{m} as shown in Fig. 6.1 b). Second, as shown in Fig. 6.6, for this steady state $\mu^{\text{m}} = 0.447$ which is in fact larger than that of the steady state without control. As a consequence $\Re[\lambda^{\text{m}}] = -1/2$ which is way below the value for the uncontrolled case and is the most negative value it can take.

As capacity is added in line $(3,4)$, $\Delta\theta_{3,4}^*$ decreases as expected magenta line in Fig. 6.5 b), thus control gradually decreases the effective power of node 4 while increasing that of the other generators so that effective power in the different generator nodes becomes more similar as shown in Fig. 6.7. In the same way control gradually decreases the consumption of node 1 while increasing the consumption of the other nodes. Although the phase differences $\Delta\theta_{4,5}^* = \Delta\theta_{4,8}^*$ increase, lines $(4,5)$ and $(4,8)$ never get overloaded. As shown in Fig. 6.6, blue lines, as capacity is added the μ^{m} keeps increasing and $\Re[\lambda^{\text{m}}]$ remains clamped $-1/2$, signaling maximum stability. Therefore the synchronized steady state is always stable, curing Braess' paradox.

One may question whether curing the paradox has been done at the expense of increasing the amount power that secondary control has to provide. If it were so, increasing line capacity would have a negative impact on control, and its cost, and thus it can be seen as a Braess' paradox occurring on the control power rather than in the power flow. To analyze this we consider the sum of the absolute value of the stationary power provided by the control systems, $\sum_i |\Delta P_i^*|$, which can be seen as an indicator of the

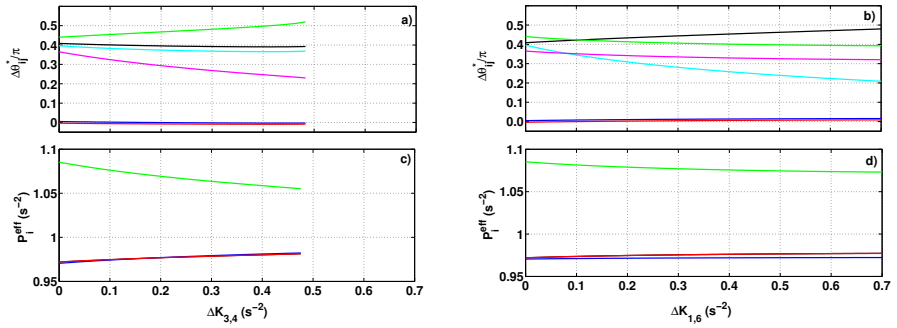

Figure 6.8: Effectiveness of control only in generators in curing Braess' paradox depends on the topology. Here we plot the stationary phase differences (panels a) and b)) and the effective power of the generators (panels c) and d) when increasing the capacity of lines $(3,4)$ (panels a) and c)) or $(1,6)$ in (panels b) and d)), for the grid shown in Fig. 6.3 without line $(2,4)$. When increasing the capacity of line $(3,4)$ instability takes place earlier that in the case without control (compare the green line with that of Fig. 6.5 a)). On the contrary, when adding capacity to line $(1,6)$ the control prevents the failure of the network. Parameters and color codes for the phase differences as in Fig. 6.5. Color codes for effective power as in Fig. 6.7

overall cost of control. As shown in Fig. 6.5, as $\Delta K_{3,4}$ increases the overall cost, $\sum_i |\Delta P_i^*|$, does not increases, on the contrary, it decreases. This means that with control in all nodes a line capacity increase is beneficial, not only for stability but also in decreasing the overall cost of control, and thus Braess paradox is completely avoided.

For the case of adding line $(2,4)$ with control applied to all nodes we plot the change of power ΔP_i^* in Fig. 6.3. As before, generators have negative and consumers positive power change i.e., the total consumption and the total generation are decreased with respect to the uncontrolled case.

6.5 Control only in generators

So far, we assumed that we control all nodes in the network. Consumer nodes, however, may have limited generation capacity and therefore limited control capability. Therefore, let us now assume that secondary control is only available at the nodes with positive power generation (generators), as usual in today's power grids [66]. Consumption is fixed and

so it must be the total generation, thus control can only redistribute the effective power delivered by the generators among them. In this case the effectiveness of the control depends strongly on the topology, e.g. which line is getting upgraded. We consider two cases.

First, we increase the capacity of line $(3,4)$ by $\Delta K_{3,4}$, which without control eventually leads to Braess' Paradox (Fig. 6.4b). Adding control in generators only does not help to improve the situation. In fact, as shown in Fig. 6.8 a) the phase difference $\Delta\theta^*_{4,5} = \Delta\theta^*_{4,8}$ increases faster with $\Delta K_{3,4}$ and the fixed point disappears at $\Delta K_c \sim 0.49 s^{-2}$, before than without control. So, controlling only the generators does not prevent Braess' paradox in this case. The fact that the instability takes place before than the uncontrolled case can be understood as follows. Consider the original grid. Since node 4 has to feed two consumer nodes, control increases the effective power of 4 up to 1.09, while it decreases that of the other generators to 0.97 as shown in Fig. 6.8 c). The total generation power in subgrid $\mathcal{S}_A$ is 2.06 while that in subgrid $\mathcal{S}_B$ is 1.94. Since consumers have a fixed power a small net flux has to go from subgrid $\mathcal{S}_A$ to $\mathcal{S}_B$. This is done through lines $(6,5)$ and $(6,7)$ which now carry a small flux towards 6 ($\Delta\theta^*_{6,5} = \Delta\theta^*_{6,8} < 0$ and through lines $(3,2)$, $(3,7)$ which carry flux towards 2 and 7 ($\Delta\theta^*_{3,2} = \Delta\theta^*_{3,7} > 0$). As a consequence the phase difference $\theta^*_{4,5} = \Delta\theta^*_{4,8} = 0.44\pi$ and the fluxes $F^*_{4,5} = F^*_{4,8} = 1.012$ s^{-1} are larger than in the uncontrolled case. Adding additional capacity in line $(3,4)$ leads to a reduction of the effective power in generator 4 and an increase of that of the others so that the overall net flow from subgrid $\mathcal{S}_A$ to $\mathcal{S}_B$ decreases. However the added capacity breaks the symmetry and in fact the flow through $(6,5)$ and $(6,8)$ actually increases while that through $(3,2)$, $(3,7)$ decreases (which can even reverse). This can be understood as the overlapping of a flow balancing the subgrids for the original network and a weak counterclockwise flow induced by the added capacity. To account for the increasing flux going through $(6,5)$ and $(6,8)$, the flux through lines $(4,5)$ and $(4,7)$, which were already quite loaded, has also to increase. Thus with control only in generators the $\Delta\theta^*_{4,5}$ and $\Delta\theta^*_{4,8}$ is larger than without control and thus instability takes place at a smaller value of ΔK_c

Nevertheless, the oscillatory regime reached after the instability is somehow different in the cases with and without control. As shown in Fig. 6.9a). With control most of the nodes remain synchronized at the reference frequency and only two nodes show phase slips at a slow time scale. On the contrary, without control all nodes rotate showing phase slips at a much faster rate (compare with Fig. 6.4b) for the same $\Delta K_{3,4}$ noting the different time scale of both figures).

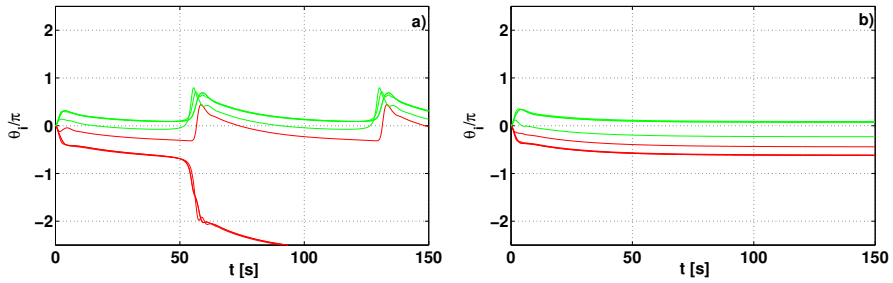

Figure 6.9: Controlling generators does not reliably prevent Braess' paradox [108]. We show the time evolution of the phases of the nodes for the grid as shown in Fig. 6.3 but without line $(2,4)$ after increasing the capacity of one line, specifically (a): $\Delta K_{3,4} = 1.0s^{-2}$ or (b) $\Delta K_{1,6} = 1.0s^{-2}$. When adding capacity to line $(3,4)$, the control on the generators cannot prevent a loss of the fixed point (panel a). However, the angles do not diverge as drastically as in an uncontrolled case (compare Fig. 6.4 b). Contrary, applying control only on the generators fully prevents Braess' paradox, when line $(1,6)$ is modified. Parameters as in Fig. 6.4.

Next, we increase the capacity of line $(1,6)$, connecting two consumer nodes, by $\Delta K_{1,6}$. As discussed in Sect. 6.4 without control, increasing $\Delta K_{1,6}$ lines $(2,1)$ and $(7,1)$ get overloaded until the system becomes unstable at $\Delta K_c \sim 0.6s^{-2}$ leading to Braess' paradox. Applying control exclusively to generator nodes does indeed help in this case. The range of existence of the fixed point is extended to any value of $\Delta K_{1,6}$ preventing the paradox completely, see Fig. 6.9. Let's analyze why here the synchronous state is stabilized while this was not the case when increasing the capacity of line $(3,4)$. Consider $\Delta K_{1,6} = 0$: the phase differences and the effective power delivered by each generator are the same in both cases as shown in Fig. 6.8. The phase difference for lines $(2,1)$ and $(7,1)$ (black) is smaller than that of lines $(4,5)$ and $(4,8)$ (green). This is because, with respect to the case without control, control in generators increases $\Delta\theta^*_{4,5}$ and $\Delta\theta^*_{4,8}$ while it decreases $\Delta\theta^*_{2,1} = \Delta\theta^*_{7,1}$. In this situation, adding extra capacity in line $(1,6)$ will increase the $\Delta\theta^*_{2,1} = \Delta\theta^*_{7,1}$ and thus the flux carried on lines $(2,1)$ and $(7,1)$. However the added capacity will, as before, reduce the overall net flow from subgrid $\mathcal{S}_A$ to $\mathcal{S}_B$ slowing down the growth of the phase differences $\Delta\theta^*_{2,1} = \Delta\theta^*_{7,1}$. The aftermath is that lines $(2,1)$ and $(7,1)$ do not get saturated in this case and Braess paradox is avoided.

6.6

Conclusion

Concluding, we have studied a simple secondary control algorithm that successfully restores the grid frequency of an unbalanced power and may prevent Braess' paradox.

Secondary control, when applied to all nodes, improves the stability of the grid, regardless of topology, and even allows stable operation for mismatched power [58, 66, 123]. While primary control stabilizes the frequency, secondary control restores the frequency to the reference value and always guarantees the existence of a stable fixed point. We have systematically computed the fixed point stability of the power grid with secondary control as a function of both the network topology and the control action. Control improves stability increasing the range of network topologies for which the synchronized steady state is stable. Thereby, we have extended previous stability analysis of uncontrolled systems [80] or systems including secondary control restricted to balanced power [32].

Secondary control in all nodes also prevents the loss of the operational state via Braess' paradox. As shown by Witthaut and Timme [121, 122], the addition of certain transmission lines may lead to a loss of the operational state of the power grid. Using primary control only [68], does not suffice to prevent Braess' paradox. In contrast, we have now demonstrated that secondary control prevents the desynchronization in networks prone to Braess' paradox if all nodes, i.e., consumers and generators alike, are controlled (Figs. 6.3 and 6.4). The control reduces the total amount of net power generated and consumed at each node of the grid guaranteeing that the transmitted power does not exceed the transmission capacity. Thereby, it offers a trade-off between grid extension and investments in control, assuming some amount of local generation is possible. Once secondary control is implemented in all nodes, subsequent line capacity increases are beneficial, both for stability and also in decreasing the overall power delivered by control and thus its cost, fully avoiding Braess' paradox.

In today's grid, secondary control is implemented only in power plants. Thus nodes with generation much larger than consumption, i.e., generator nodes, have a large control capability while nodes in which consumption is larger than generation, consumer nodes, have very little, if any, control capability. If control does only takes place at generator nodes, it can only redistribute the effective power delivered by the generators among them and as a consequence its efficiency strongly depends on the grid topology.

We have observed that if the capacity of a line connecting two generator nodes is increased, the control does not prevent Braess' paradox. On the contrary, in the case of increasing the capacity of a line connecting two consumer nodes, secondary control is capable of redistributing the power flow so that lines are not overloaded and the paradox is avoided.

Concluding, using secondary control on all nodes in a network improves its stability and robustness with respect to dynamical and topological perturbations. If control is mainly available in generator nodes only the effectiveness of the control depends strongly on the topology of the network. This stresses the importance of involving consumers, e.g. via demand control schemes or local generation (prosumers) in future grids [38, 93, 94]. One could also consider alternative options to provide secondary control at the consumer side, e.g. by using distributed storage or back-up generation. Finally, further research is necessary to extend our results, e.g., to alternative control mechanisms. One example is to allow $\tau > 0$ in Eq. (6.3), i.e., making the power provided by each node explicitly time-dependent.

CHAPTER 7

Integration of DDC in a model for the complex dynamics in electric power system blackouts

In the previous chapters, we focused on the dynamics and control of the electric network, considered as a number of interconnected ac synchronous machines. Such network has been characterized by its angle, frequency and voltage, whose stability is imperative for the stable operation of the network and its synchronization. In this chapter, a electric network composed by generators and consumers (nodes) connected by transmission lines through which dc current flows is considered. Under this configuration, the angle and frequency dynamics of the generators are neglected, assuming them to be quasi-constant in the system. Such a network is then defined by the power generated, the power consumed and the voltage at each substation. In This setting, failures of the power system can be triggered by a failure of a line or the failure of a generation. In a network the failure of a line can cause the overloading of another ones, creating a cascade that propagates along the network causing a blackout.

The propagation of failures also called cascading failures, is known as the usual mechanism responsible for large blackouts of the electric transmission network system. There are several examples around the world of blackouts triggered by cascading failures. These examples include the November 1965 blackout in the Northeast of the US and the north of Canada, which left more than 800 thousands of people without electricity, the August 1996 blackout in Northwestern America that disconnected 7.5 million customers [31], the August 2003 blackout in the northeastern America, which affected

about 50 million people and the September 2003 Italian blackout, which disconnected 57 million people[88]. Electric blackouts in all the cases have enormous consequences affecting social life, security, health and human activities. The great importance of the electric network for the society encourages the understanding and the analysis of blackouts [21].

To study blackouts, Ian Dobson *et al* [30] constructed a model, mainly based on available blackouts data, and the use of some statistical techniques, Physical laws and Engineering methods to understand the process leading to blackouts. To be validated, the constructed model is compared to available blackouts data from the NERC (North Electrical Reliability Council) for the case of the North American blackouts. Indeed, the data analysis of the North America blackouts had shown that the failure data representing the scale of blackouts, has a power law characteristic [31, 71], whose signature characterizes a dynamical system close to a critical point. Self-Organized Criticality (SOC) has then been suggested as one possible principle governing this dynamics [7]. The idea behind the SOC is that the operation and evolution of any system is defined by two variables: a fast and a slow variable [71]. Furthermore, at certain condition verified by these variables, the system reaches a critical state, in which any perturbation might provoke catastrophic interruptions of the system. Several SOC based models of blackouts have been proposed in the literature [7, 30, 71, 106]. That includes: the hidden failure model [21], the OPA (ORNL-PSerc-Alaska) model [30], Manchester model based on load shedding and ac power [71], blackout models based on OPF (Optimal Power Flow), etc. [71]. In this chapter, we will introduce the OPA model which is a simple SOC based blackout model, using the idealized dc optimal power flow analysis. This model can easily be adjusted or modified due to its structure and its simplicity [30]. So, we propose in the second section a modified OPA model which includes Dynamic Demand Control. We afterwards investigate the effects of DDC on the network.

7.1

OPA model

The original OPA model of blackouts in transmission power system was established in [20, 30]. It is a simple blackout model considering two timescales, a fast and a slow dynamics [30, 71]. The fast dynamics, which occur in time scale of minutes to hours, reproduce the cascading failures resulting to load shedding, generation dispatch and line overloads, which

cause blackouts. The slow dynamics, which occur on time scale of days to years, simulate the uniform daily load growth, line improvements, generation limits upgrades, maintenances of defective electric components etc. That is done to prevent a future failure which could happen in the fast dynamical process [30]. In this section, we define and characterize the power transmission network and its associated variables, and we describe the original OPA model afterwards.

Transmission network

We consider in this study the power transmission network showed in Fig. 7.1, which is assumed undirected and composed by $n = n_L + n_G + n_P$ nodes, where n_L, n_G and n_P represent respectively the number of consumers, generators and prosumers which are consumers with local generation. n represents the total number of nodes of the network. In the present

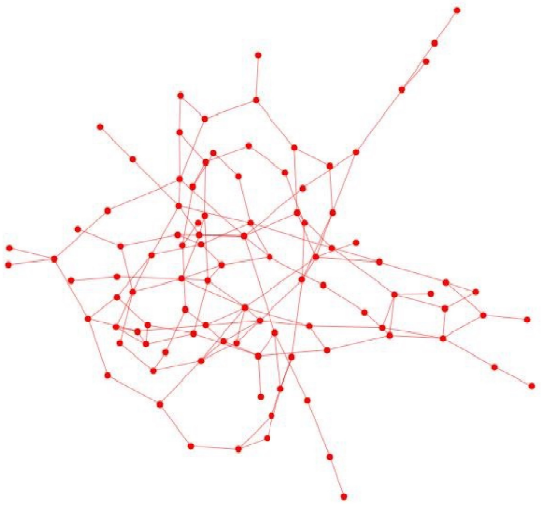

Figure 7.1: Electric network of 100 nodes and 151 links, composed by $n_G = 0$ generators, $n_L = 81$ consumers and $n_P = 19$ prosumers, all connected by transmission lines.

network $n = 100$ nodes, composed by $n_L = 81$ consumers, $n_G = 0$ generator and $n_P = 19$ prosumers connected to each other via transmission lines.

Each node i is characterized by a degree k_i, which is defined as the number of lines connected to that node i. It is expressed by $k_i = \sum_j a_{ij}$, where a_{ij} represents the elements of the adjacency matrix. a_{ij} takes the value 1 if the node i is connected to the node j and 0 otherwise. The network is also characterized by the average of k_i for all node, and it is expressed by $< k >= \frac{1}{n}\sum_i k_i$=3.03. In Fig. 7.2, we plot the degree distribution $P(k)$ of the network, defined as the fraction of nodes in the network with degree k. It is mathematically expressed by: $P(k) = \frac{N_k}{n}$, where N_k represents the number of node with degree k among the n nodes that composed the network. Here a node of the network is electrically characterized by the

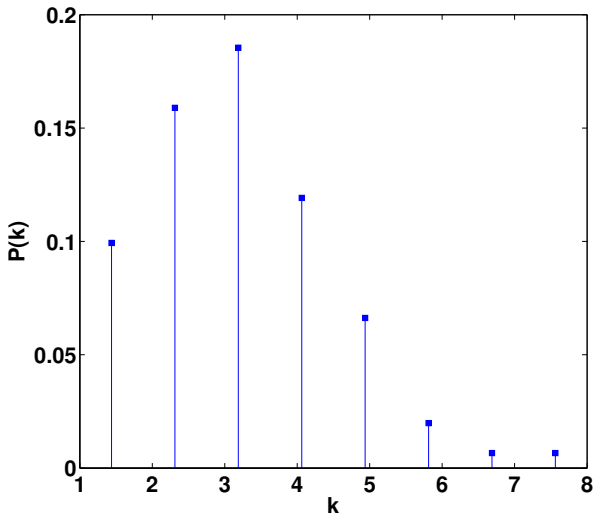

Figure 7.2: Degree distribution $P(k)$ of the network.

following parameters:

- P_i is the instantaneous real power injected at bus i (i=1, ..., n). P_i is negative for consumer nodes and positive for generator nodes. The maximal generator power is defined by P_i^{max}.
- F_{ij} defines the instantaneous power flow on line (i, j), and F_{ij}^{max} its maximal power flow (i, j=1, m, m is the number of lines).
- V_i defines the voltage at the terminal of the node i.
- z_{ij}, defines the impedance of the line (i, j).

The stable operation of the transmission requires the system to verify the equality and inequality constraints:

1. The load power is negative: $P_j \leq 0$, with $j \in \mathbb{L}$ (representing the set of the load)
2. $0 \leq P_i \leq P_i^{max}$, the generated power should be lower than the maximum generator power, with $i \in \mathbb{G}$ (representing the set of generators)
3. $|F_{ij}| \leq F_{ij}^{max}$, the power flowing on a line should be lower than the maximal capacity of the line.
4. $\sum_i P_i = 0$, the power must be balanced in the network. $i \in \mathbb{L} \cup \mathbb{G}$

Furthermore, each transmission line is assumed to be lossless and modeled as an inductance including inductance of any equipment in the line such as transformers; meaning that a failure on this equipment is modeled as a failure of the line [30].

Implementation of the model

We review here the implementation of the OPA model, whose details can be found in [20, 30, 31]. It can be used for any type of electrical network, except in the case of an isolated network. OPA model is a SOC based model, which evolves in two timescales, being the slow and fast dynamics represented into the diagram given in Fig. 7.3 [20]. The slow timescale dynamic indicated in blue in Fig. 7.3, represents the global increase of demand, the building of new generation units (meaning here the increase of the generation limit) and the improvement of the network components. It starts with a daily initialization of the variables of the system as follows:

- All the loads are increased by a factor $\bar{\lambda}$, representing the secular daily increase of load. $\bar{\lambda}$ is chosen based on the past rate of electricity growth, which corresponds to the 2% annual demand growth [30]. That increase in load on day d, is done through the following mathematical expression:

$$P_i(d) = \bar{\lambda} P_i(d-1), \tag{7.1}$$

  i=1, ..., $n_L + n_P$.
  The maximum generator power is also increased at the same rate following the increase in load, and it is given by:

$$P_i^{max}(d) = \bar{\lambda} P_i^{max}(d-1), \tag{7.2}$$

  i=1, ..., n_P.

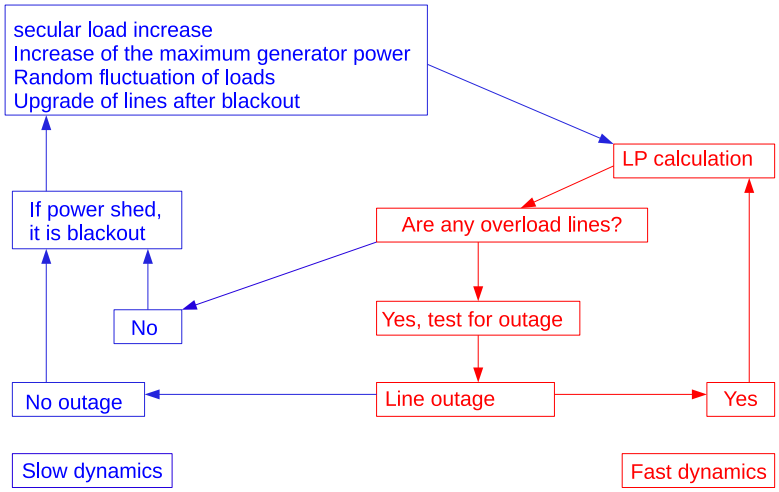

Figure 7.3: Schematic representation of the OPA model algorithm, with LP meaning linear programing.

- The random fluctuating loads, representing the daily fluctuations in power demand, are modeled by multiplying all load powers by a random number [20]. Here we assume the daily average power demand to be constant.
- In response to outages and blackouts (we consider a blackout when the ratio of load shed (load unserved) to total load is larger than 10^{-5}) that may occur in the network, the outaged lines and the overloaded lines during the blackout on the previous day, are fixed and upgraded by multiplying their previous capacity by a constant parameter μ as follows:

$$F_{ij}^{max}(d) = \mu F_{ij}^{max}(d-1). \tag{7.3}$$

The figure 7.4 shows the time evolution of the demand (in black) and power generation limit P_i^{max} (in red) for a single day. One observes that the generation limit follows the demand and it is always above, such that there is always sufficient resources to supply the loads.

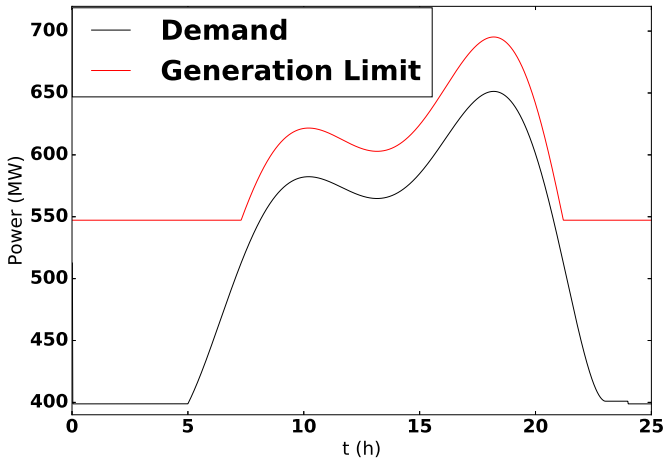

Figure 7.4: Daily variation of the demand and generation limit

On the other hand, the fast dynamics indicated in red in Fig. 7.3, reproduces the cascading failures resulting to load shedding, generation dispatch and line overloads, which cause blackouts. It starts with the Linear programing (LP) calculation, including linearized dc optimal power flow analysis, which consists on the determination of the variables (voltage angle, current flow, injected power) of the system according to certain criteria previously enumerated. One additional and obvious criterion is the minimization of the generation cost, which is defined in Eq. (7.4), where C_i is the cost of the generated electricity assuming that all the generators run at the same cost. W defines the penalty cost faced by the electricity utilities when there is a power shed. That calculation starts with the choice of initial conditions verifying the LP problem, without line overloads and power shed. The power shed defines the energy unserved to the customers.

$$Cost = \sum_{generator} C_i P_i(t) - W \sum_{Loads} P_j(t). \tag{7.4}$$

This LP problem is solved numerically using the simplex solver. A full description and the details of the resolution methods used can be found in [20, 30, 110]. As it is reported in [31], the system can reach a solution of the Linear program that requires load sheding or tends to overload one or more lines, which can trigger a cascade failure.
After the first step (secular increase of power and improvement of the network), the LP problem is solved and solutions are found. If the solutions

lead to some overloaded lines, and if the affected lines outage with a certain probability, then their impedances are increased by multiplying them by a large number and reducing the maximum line capacity by dividing it by another large number. This is done to avoid any isolation of node or group of nodes in the network. The LP calculation is repeated until either no overloaded line is found or there is no lines outage. When this is fulfilled, we move to the slow dynamics and we check if there is any power sheds greater that 10^{-5}. In the case of power sheds of that order, the system is considered to face a blackout and the simulation ends for the day.
The dynamics of the system depend then on the following parameters: the mean load daily growth factor $\bar{\lambda}$, the probability that a line accidentally outage, the probability of overloaded line outage and the line improvement factor μ among others. The main system state of the power system is defined by the averaged value over time of the fractional line overloads M or $< M_{ij} >$. The fractional overload M_{ij}

$$M_{ij} = \frac{F_{ij}}{F_{ij}^{max}}, \tag{7.5}$$

measures the stress of the line. Mainly, it gives an information on how close each line works to its maximal capacity. Its average value describes the daily pattern of loading in the system [20], and it is computed when the system reaches a stationary state. Once the system reaches the stationary dynamics, recorded time series of the system can be analyzed.

7.2

Power bursts and dynamic demand control in the OPA model

The OPA model has the advantage that it can be applied to a variety of networks of different sizes and structures. That includes ring, tree, square and hexagonal networks [20].
DDC is an algorithm conceived to manage the electricity in response to a proxy (instantaneous frequency or electricity price [94]). To be able to include in the OPA model instantaneous responses of demand, it is primordial to consider in all the network time scales shorter than a hour, which is the smallest time scale in the original OPA model. The timescale of a minute is chosen in this work, and a one day simulation will be done in 1440 steps of a minute. Hence, the daily variation of the demand must be incorporated into the new model as it is shown in figure 7.4. The typical

power demand profile (in black in figure 7.4) profile during a single day has two peaks of consumption, the first occurring in the morning, represents commercial/industrial consumption and the second one which happens in the early night represents domestic/home consumption. It is important to notice that these peaks vary from season to season or with the weather and with the geographic location. The generation limit (in blue in figure 7.4) in the other hand, increases following the demand consumption to ensure the availability of the power at any time. We aim in this section to observe the effects of control in this model. To achieve that objective, we will propose a dynamical load including sudden random consumption that will represent random power bursts in the system, that will be added on the top of the daily load variation. The control as in the ac network, will act to avoid the random bursts to create instability in the network. How the bursts are induced in the system is explained in the next subsection.

Power bursts

As it has already been explained, each load has a shape shown in Fig. 7.4, representing the daily variation of the demand with an average value which could change randomly, to represent the day to day change of demand. On the top of that daily variation, we introduce the power bursts in the following way:
Every minute, a number of nodes of the network are randomly selected, with a probability p_3 to have a power burst of random value, such that the power at the selected node becomes

$$P_i(t) = P_0 + \xi(t), \tag{7.6}$$

where P_0 represents the averaged power in that node and $\xi(t)$ represents the power bursts. The power bursts transform the system into a stochastic system, where the process behind the bursts is Markovian, as the one described in chapter 3. The set of power bursts generated has a half Gaussian distribution, whose probability density function is given by:

$$PDF = \sqrt{\frac{2}{\sigma^2_{burst}\pi}} e^{-\frac{(x-\mu^*)^2}{2\sigma^2_{burst}}}, \tag{7.7}$$

where $x \geq 0$ represents a Gaussian random number, $E[x] = \mu^* + \frac{\sigma_{burst}\sqrt{2}}{\sqrt{\pi}}$ and $Var(x) = \sigma^2_{burst}\left(1 - \frac{2}{\pi}\right)$ the mean and the variance of the half gaussian distribution respectively. μ^* and σ^2_{burst} are the mean and the variance of the gaussian distribution respectively.

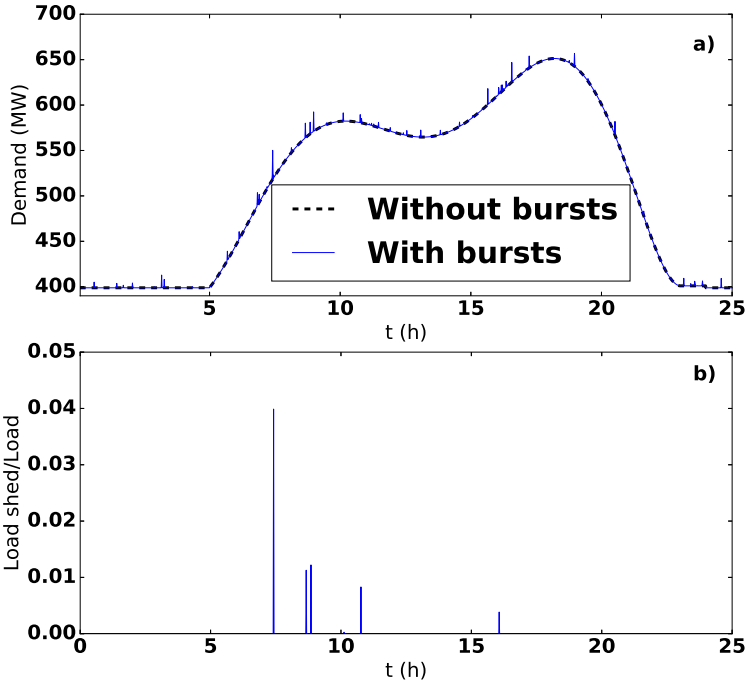

Figure 7.5: Daily variation of the demand (a) and the power shed (b), for $\bar{\lambda}$=1., σ^2_{burst}=0.3, μ=1. The rest of the parameters are given in the table 7.1

The figure 7.5 a), shows the daily variation of the power demand with bursts (solid blue lines) and without bursts (dashed black lines). Some fluctuations corresponding to the bursts are observed on the top of the demand daily pattern. These power bursts can represent different unpredicted power loads or some sudden switchings on of group of devices in the system. The magnitude of the power bursts randomly assigned to the selected nodes is controlled by the variance of the distribution σ^2_{burst}. Increasing this value, stresses more the network and decreasing it releases the system. Figure 7.5 b) shows the load shed defined as the power unserved to consumers. The dashed black lines representing the system without bursts and for this case there are no blackouts, because in this proposed simplified OPA model, blackouts are induced only by the power bursts. The solid blue lines in Fig. 7.5 b) represent the power shed obtained with bursts in the system. The frequency of blackouts and the distribution of the size of blackout strongly depend on the variance of the power burst as it is shown in figure 7.6 and figure 7.7.

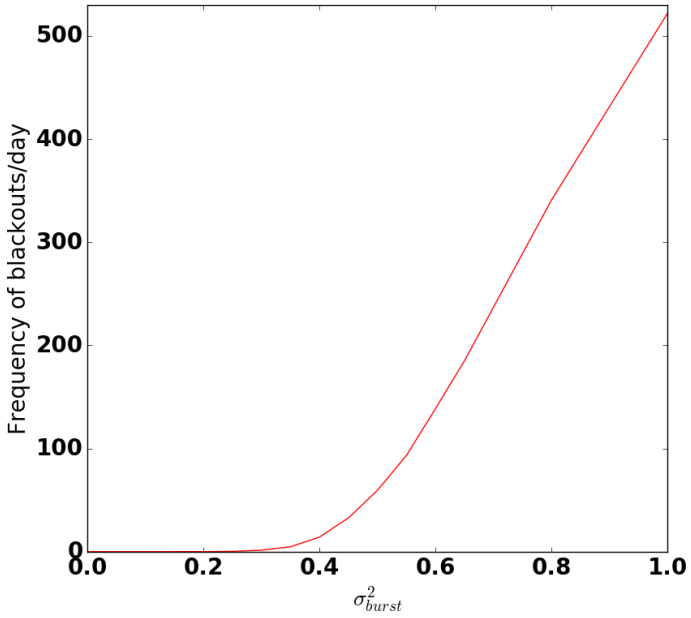

Figure 7.6: Frequency of blackouts per day increases with $\sigma^2{}_{burst}$. This plot is obtained for $\bar{\lambda}$=1., μ=1.0, and the rest of the parameter values as given in table 7.1

Indeed, Fig. 7.6 shows how the frequency of blackouts per day increases with the variance of the power bursts. According to the data from NERC and analyzed in [20, 30], in average the US electric network has faced about one blackout every thirteen days (0.07 blackout/day). That corresponds here in to $\sigma^2_{burst} \approx 0.3$. For very large frequency of blackouts, the system needs to be controlled, and some devices should be turned off to reduce the stress on the network.

On the other hand Fig. 7.7 gives the tail distribution or the complementary cumulative distribution function (ccdf) of the size of blackouts times the frequency of blackouts for different values of $\sigma^2{}_{burst}$. This allows us to directly compare these probabilities. This figure shows how the ccdf increases with the variance, meaning that for large value of the variance, there is a larger probability of having blackouts of any size. Then, the choice of a good value of the variance is determinant for the analysis of the system and its comparison with the real situation. As it has been mentioned above, respect to the 0.07 blackout/day observed with the data from the NERC, $\sigma^2_{burst} \approx 0.3$ remains the adequate value to use for reasonable size and frequency of blackouts. Nevertheless, larger values

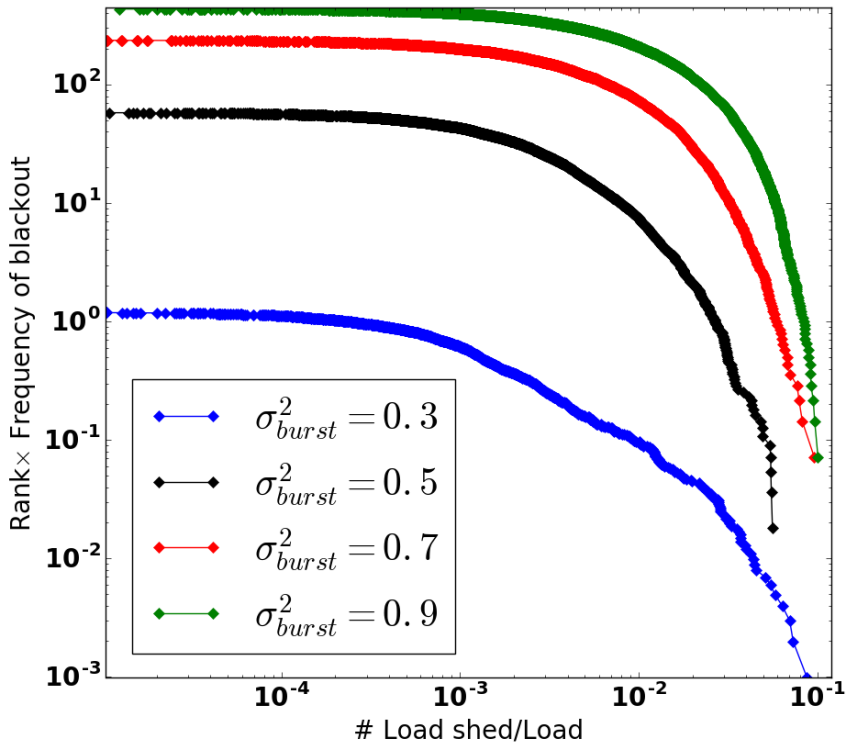

Figure 7.7: Complementary cumulative distribution function (ccdf) of the size of blackouts for different values of the variance $\sigma^2{}_{burst}$, with $\bar{\lambda}$=1., μ=1.0, and the rest of the parameter values as given in table 7.1

of the variance remain also good for the study since they create large power fluctuations that we aim to control through the dynamic demand control in order to reduce the number and size of blackouts hitting the network.

Dynamic demand control in the OPA model

As it has been applied in previous chapters in the case of an ac network, dynamically controlled loads respond instantaneously to a proxy signal, by turning on or off according to the control policies. With the assumption of constant frequency, one could use in this case the electricity price as incentive to control the electric

consumption. As it is well known, the electricity is more expensive during the peaks of consumptions around 10 AM-2 PM for the morning peak and around 7 PM- 10 PM for the night peak. One could use these periods to control the load, by defining a power threshold above which the sudden loads are controlled. That would have the effect to transfer the consumption to later times. The control is then performed as follows:
It is defined two power levels PL_1 (the control threshold), representing the power above which the power bursts are delayed and PL_2 (the recovery threshold), which represents the power under which the delayed power bursts are recovered with a certain probability p_4. This randomization in the recovery has been shown in chapter 4, to be necessary to avoid the synchronized responses which can induce large demand peaks, hence frequency peaks in the system. Depending of the objectives of the electric utilities, the power thresholds can whether be constant or variable. Indeed, considering PL_1 constant and below the highest demand peaks would delay the unpredicted electric consumption (power bursts) a certain time, until these are recovered during the period of low consumption (when the demand is below PL_2). This particular case corresponds to the Time-Of-Use (TOU) demand response program. As mentioned before, one can consider the threshold variable and following the daily demand variation, such that during all day, some large power bursts are delayed but not for a long period of time. Such consideration does not shift the consumption from a period of time to another as it does with the previous configuration, but redistributes the power bursts during all the day. In the next section, we show some results obtained considering the constant power thresholds. The other case will be considered in future work.

7.3

Results

For this first preliminary studies, we assume that the power demand as well as the generation limit do not evolve in the time ($\bar{\lambda}$= 1). The only random variation of the load is included in the power bursts, making the power bursts be the only source of fluctuations in the system. The transmission lines outage resulting from an external cause such are weather or accident are neglected. The rest of the parameters are reported in Tab. 7.1. Fig. 7.8 a) shows a day variation of the demand without control (solid black lines), with control but, without recovery (solid blue lines) and with control and recovery (solid red lines) obtained with the same stochastic realization. The control and recovery power thresholds PL_1 and PL_2, considered constant are represented respectively by the green and yellow solid lines. At the beginning of the day, when the power consumed is below PL_1,

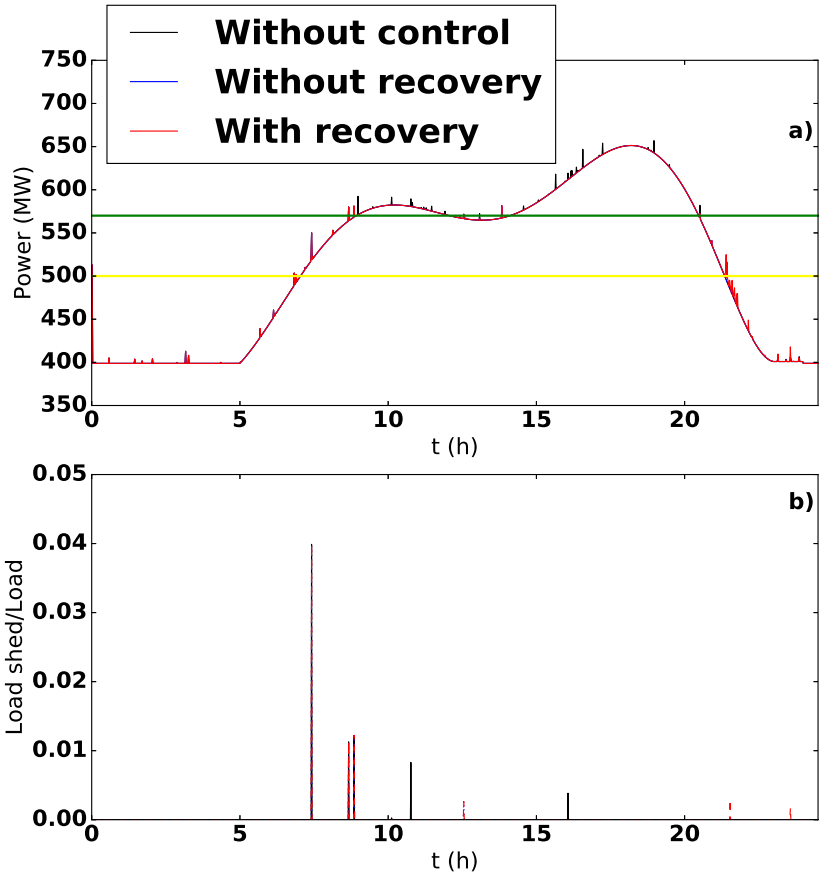

Figure 7.8: Time evolution of the demand (a) and the load shed (b), without control (in black), without recovery (in blue) and with recovery (in red),for $\bar{\lambda}$=1., μ=1.0. The rest of the parameters are given in the table 7.1

users can turn on their devices without any restriction, which produces some power sheds as shown in Fig. 7.8 b), which for those induce blackouts in the system. Once the total demand surpasses PL_1, the bursts are delayed. That is noticeable on the red and blue solid lines which do not have any peaks comparing to the solid black lines. These delayed bursts are recovered once the total power goes below PL_2 depending on the probability p_4. The recovery of the pending power bursts induce blackouts in the system, observable by the power shed in figure 7.8 b).

Furthermore, one can observe in figure 7.9 the frequency of blackouts times the ccdf of size of blackouts for different configurations including the case without control (solid black lines), without recovery (solid blue lines) and with recovery (solid red lines) obtained for different values of the recovery threshold PL_2 and for $\sigma^2_{burst} = 0.5$. This variance has been chosen to induce in the system larger number of blackouts comparing to a realistic case, which has about 0.07 blackout/day. Without recovery (solid blue lines), the control basically impedes random switchings on above PL_1 fixed at 570 MW. As a consequence, the control reduced from about 59 blackouts/day without control (solid black lines) to about 12 blackouts/day. This represents about 80% of reduction of blackouts initially induced in the network. In fact, this result is obvious in the sense that the consumers did not consume what they planed to consume and therefore the system remains underloaded. Thus the recovery of pending energy is allowed once the total load in the system is less than the threshold for recovery PL_2. It is observed

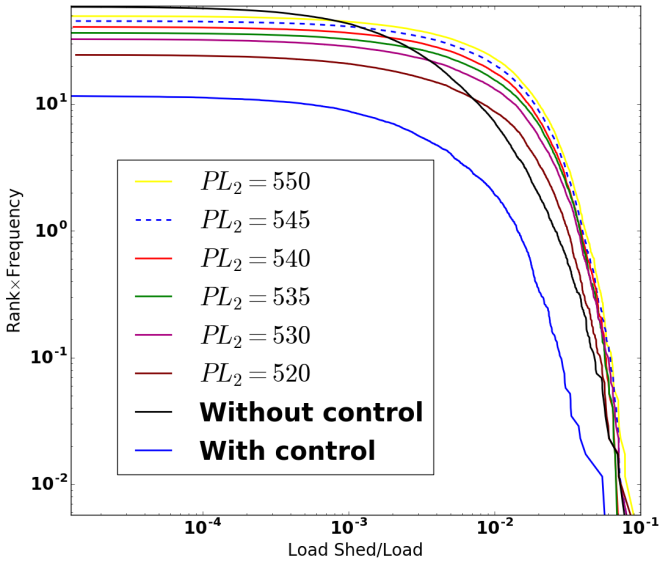

Figure 7.9: rank times the frequency of blackouts, obtained for $\sigma^2_{burst} = 0.5$ as a function of the blackout sizes.

in figure 7.9 that as PL_2 increases, the frequency of the blackouts increases, as well as the largest blackout size. For all the cases studied, the fall-off with the size of blackouts observed in figure 7.9 are close to a power law characteristics, basically as the one recorded by the NERC of the energy unserved in North American

blackouts from 1984 to 1998 [30]. The role of power threshold for recovering is very important in such system, and its choice should be done in consequence. In fact, Fig. 7.10 shows the frequency of blackouts versus the threshold PL_2 for a fixed value of $p_3 = 0.08$. One notices that the frequency of blackout is increasing with PL_2. Indeed, for small value of PL_2 the system has enough capacity or generation to handle any sudden increase in demand as it can be observed in Fig. 7.4 (regarding the gap between the demand (solid black lines) and the generation limit (solid red lines)). When PL_2 is close to the generation limit, the system does not have enough capacity to supply a large demand (recovery of pending power bursts) and the system becomes more vulnerable and any sudden increase in demand induces blackouts. A way to solve this problem, could be to increase the generation limit, at the time of recovery by the energy saved earlier during the control. Such consideration will be done in future works. It is well

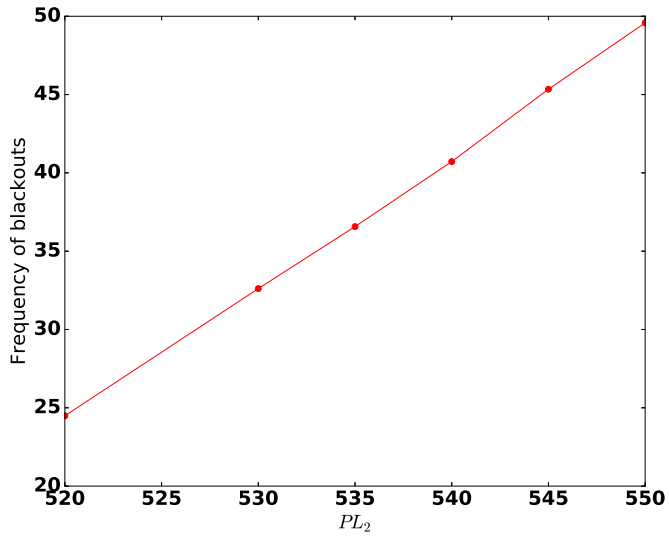

Figure 7.10: Frequency of blackouts versus the recovery power threshold, for $\sigma^2_{burst} = 0.5$ and the rest of the parameters as given in the table 7.1

known that most of the blackouts in the system are due to the frustrations of the transmissions lines which in some cases overload and break down. As consequence the power is redistributed through other paths and that redistribution can lead to another failure which will leave unserved a part of the network, generating then a blackout. In fact, how blackouts and stressed lines are related is presented in Fig. 7.11. Indeed, Fig. 7.11 a) shows the time evolution of the line average fractional overloads, characteristic of the state of the system with

(solid blue lines) and without (solid black lines) DDC. This figure shows that the system is in the stationary regime. In this state, the average fractional load of the network is about 0.5, which means in another words that in average the power flowing through the lines is at 50% of the capacity of the lines. In Fig. 7.11 b), it is plotted the corresponding daily fractional loading of the system without (black dots) and with control (without recovery (blue dots) and with recovery (red dots). One can observe a period of time where the system is less loaded in presence of control, comparing to the case without control. These regions correspond to the period of time where the control is acting. One can further observe

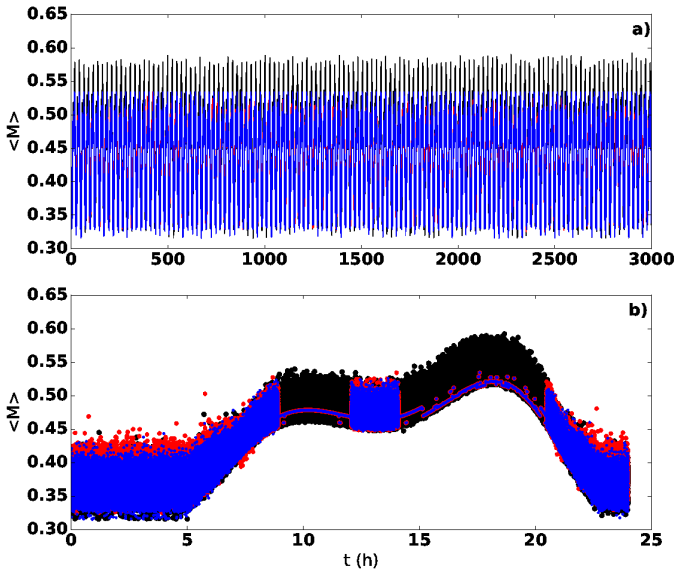

Figure 7.11: The control reduces the stress in the transmission lines. Time evolution of the network loading a) and daily fractional loading b), for $\sigma^2_{burst} = 0.5$ and the rest of the parameters as given in the table 7.1. The black, blue and red colors represent the case without control, without recovery and with recovery respectively.

that the lines of the system without recovery are less loaded than the one with recovery. At this stationary state, we can compute the other variables of the system and statistically analyze the system and then make a comparison between the system without control, the system with control but without recovery of delayed bursts and finally the system with control and recovery of pending bursts. In figure 7.12, we present the complementary cumulative distribution function of overloaded lines considering the cases without control, without recovery and with

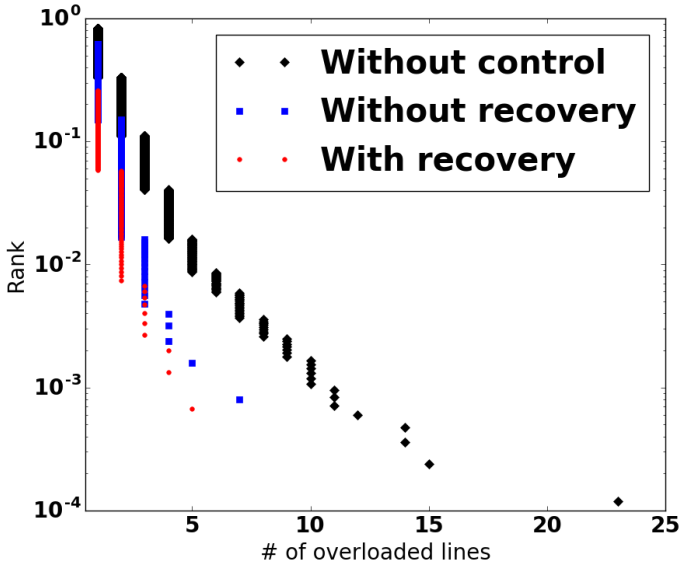

Figure 7.12: complementary cumulative probability times the frequency of overloaded lines obtained for $\sigma^2_{burst} = 0.5$ and the rest of the parameters as given in the table 7.1

recovery for PL_2= 530, p_4= 0.08 and $\sigma^2_{burst} = 0.5$. One observes that without control all lines are susceptible to fall down or to break (black dots), and the number considerably decreases with control. The maximal number of lines overloaded without control is about 24 lines, which is reduced to about 5 lines while applying the control. So as in the case of frequency of blackouts it is observed that the number of lines susceptible to outage is reduced for about 80% while controlling the network. This somehow justify the fact that most of the blackouts occurring in the system are due to the lack of lines capacity.

To emphasize these results, Fig. 7.13 b), shows the distribution of the blackout during the day for all the compared cases. In general small and medium size of blackouts seem to appear at every period of the day without control, while large blackouts (when Load shed/total load is larger than 0.01) are observed during the consumption peaks. In fact, since in the peaks of consumption the lines are loaded and close to their maximal capacity such that the induction of power bursts overload them that justifies the large number of susceptible lines reported in figure 7.12. On the other hand, these blackouts present in the peaks of consumption, are suppressed in presence of control. The recovery of pending

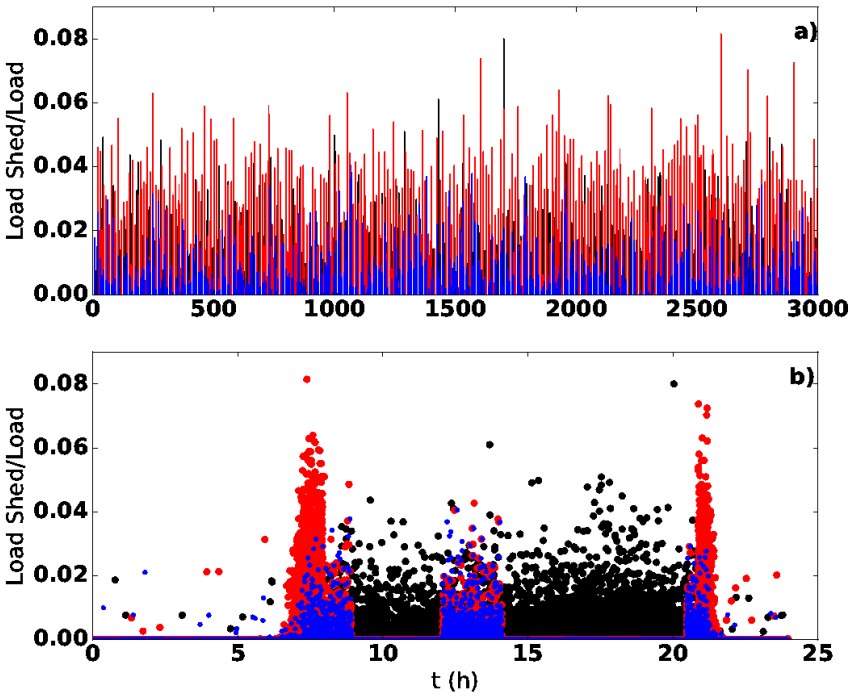

Figure 7.13: Time evolution (a) and daily distribution (b) of the blackout. ${\sigma^2}_{burst}$=0.5 $\bar{\lambda}$=1., μ=1.0, and the rest of the parameter values as given in table 7.1. The black, blue and red colors represent the case without control, without recovery and with recovery respectively.

tasks is turn induces blackouts in the system when the recovery threshold is close to the generation limit, when the system is stressed.

7.4

Conclusion

Throughout this chapter we have proposed a simplified OPA model to analyze and understand the blackout dynamics in a toy network composed by a hundred nodes. Such a system, under some assumptions and approximations such as the

Table 7.1: Value of the parameters used in the model

Parameters	Value	Observations
p_0	0	Probability of weather event in a minute
p_1	0.0	Probability of failure of an overloaded line
p_3	1.10^{-3}	Probability of a burst of demand
p_4	2.10^{-2}	Probability of recover a delayed burst
$\bar{\lambda}$	1.	Rate of increasing demand per minute
PL_1	570 (MW)	Control threshold
PL_2	530 (MW)	Recovery threshold
μ	1.	Rate of increasing current limit
Z_{max}	1000	Rate of decreasing the inductance of outage lines
${\sigma^2}_{burst}$	0.5	power bursts variance

constant average power in all the nodes, no improvement of line capacities do not lead to blackouts in a normal operation. Power burst fluctuations modeling a sudden increase in demand induce power sheds in the network, hence blackouts occur. Most of them appeared as a consequence of overload lines as it as been presented in figure 7.12. We observe as trivial result that the frequency of blackouts increases with the variance of the power bursts distribution as well with the recovery threshold. Nevertheless, the application of DDC in this stochastic network has shown similar results as those obtained with the ac network controlling the frequency of the power grid. In fact, we observed that the control reduced by 80% the number of blackouts and the number of vulnerable lines compared to the case without control. The recovery of pending tasks induces blackouts, whose size and number vary regarding the gap between the generation limit and the recovery threshold. Indeed, the number and the size of the blackouts increase when the recovery threshold gets close to the generation limit. In all the studied cases, the complementary cumulative distribution function has a fall-off close to a power law characteristic.

As future work, one could investigate the full OPA model integrating the DDC, in which the complex interaction between the fast and slow dynamics, the stochasticity and the DDC is expected to produce rich and complex behaviors in the network. In such systems infer some results or any type of correlation between variables may not be simple and probably impossible to do. In fact according to the original OPA model, the more the network is stressed, the more it is upgraded (improvement of the line capacities, increase of the generation limits for example) and consequently probably it is more robust. Naively, one could guess that the incorporation of DDC avoids the network to be upgraded and therefore weakens the lines, inducing outages and probably blackouts in the controlled network.

CHAPTER 8

Conclusions and outlook

8.1

Overall concluding remarks

The need to reduce emissions into the atmosphere of greenhouse gases such as Carbone dioxide (CO_2), methane, nitrous oxide, fluorinated gases, etc., in order to limit the global warming is a task which requests the action of every polluting infrastructure. This pollution is made mostly by the burning of fossil fuels such as coal, gas and oil, especially in the electric power system, which burns these fossil fuels in power plants to cope with the growing electricity demand. Thus, as one of the most polluting infrastructure, the electric power system offers at the same time the possibility to reduce or even suppress its pollution. This can be done by, in the one hand, the replacement of dirty power plants (using fossil fuels) by cleaner ones using renewable energy sources (wind, solar, hydro power plants), and on the other by the possibility to control the electric consumption in the demand side (demand-side management) and by encouraging customers to use the electricity in a smart way (energy efficiency).
In ac power grids the fluctuations in demand or generation translates into frequency fluctuations, thus the frequency is a readily available variable from which one can infer the status of the power grid. Controlling the electric system avoids some probable blackouts which could occur due to an electric component failure, overloaded lines or frequency and voltage instabilities. Nowadays, control is performed by adjusting the production to the fluctuating demand, thus the lions share of the responsibility lies on the generation side. The objective of this dissertation is on one hand, to contribute to the conception of algorithms and protocols in which part of the control takes place on the demand side, namely in

residential houses, industries, offices, shopping centers, etc, and , on the other, to investigate the impacts of these algorithms on the dynamics of the electric grid. To this aim we have proposed an electric consumption environment which models the dynamics of producers (using the swing equation together with the primary and secondary control for generator dynamics) and consumers (introducing a stochastic demand model in which devices turn on and off randomly). We have checked that this electric consumption environment is capable of reproducing statistical properties of the frequency fluctuations measured experimentally. In particular the characterization of the demand model has been done by comparing the resulting frequency power spectrum with the one recorded from the Balearic's electric system. These are the results obtained in the first chapter, primordial for the application of demand side management.
Second, we have proposed an algorithm for controlling the switchings of devices according to the frequency of the grid. From numerical simulations, we have observed that the control acts by reducing the frequency peaks and keeping the system permanently balanced. On the other hand, the recovery of pending tasks resulting from the restrictions applied by the control leads to the generation of new and rare frequency peaks, bigger than those observed without control. Even if this peaks are very rare, they can trigger a power outage or blackout. The suppression of these frequency peaks is possible by the introduction of interaction among devices, in such a way that despite of the state of the frequency a device can switch on or off if another device in the same cluster have performed an opposite operation in a small time window. The idea of this scheme is not to directly help in restoring the frequency to its nominal value but rather to minimize fast variations in the consumed power at a cluster level allowing for the control in the power plants to react and stabilize the frequency. Besides the peak suppression, the device-device interactions reduce the frequency fluctuations as compared with the uncontrolled power system, keeping the number of pending tasks very low.
The extension of the control from a single power system to a network has been done in chapter 5 and the control has been found to be important for the frequency and phase synchronizations. Furthermore, the control of the frequency through secondary control, enhances the synchronization of the network. On the other side, in the toy network considered, which is composed by 4 generation and 4 consumption nodes, we observe that an improvement of the network, for instance by adding a new line or increasing a line capacity, induces instability in the network. This counterintuitive behavior or response of the network is known as Braess's paradox. In this thesis, we have shown that Braess's paradox can be fully avoided if control is applied to all generation and consumption nodes, while if control is applied only to generation nodes, as it is now done in practice, then effectivity of the control to avoid the paradox is limited and depends on the network topology.

Finally, we have applied DDC to the ORNL-PSerc-Alaska (OPA) model, which is a simple SOC based blackout model using the idealized dc optimal power flow analysis and considering two timescales (fast and slow dynamics), in order to investigate its effects on the statistic of blackouts. This application have consisted in defining power limits above which the devices could not be turned on, and below which the pending tasks could be recovered. We have not considered the switching-off of devices in this case because having too much power available does not stress the network, hence does not cause blackouts. This is due to the fact the OPA model considers dc grids, while in ac grids, too much available mechanical power induces an increase of the frequency, which can go above its admissible value if the power is not extracted from the grid. We have obtained a reduction of the small- and mid-size blackouts observed by computing the cumulative probability distribution of blackout sizes, which shows a power law distribution. We have also observed an increase of the probability of large size blackouts with the recovery of the pending energy. DDC in OPA model effectively acts like the Time of Use (ToU) demand response program by shifting the consumption from peak time where the consumption is maximal to valley time where it is smaller. The advantage of DDC is that the shifting of the operation time is done in an automatic way not requiring the end-user to manually change or reprogram the operation of electrical devices. The recovery of pending tasks in this valley time favors the appearance of blackouts of different sizes, including sizes larger than the case without control. In the ToU, the electric utility has programmed the available power necessary to cover the demand at the valley time, thus, avoiding the stress of the network and even blackouts. For the model studied, both recovering and control threshold are taken constant. The more the recovery threshold is close to the generation limit, the more the network is susceptible to face blackouts, including blackouts of size larger than the uncontrolled case.

8.2

Future works

In this thesis, the electric model neglects the voltage dynamics and assumes that the voltage is kept constant independently of the frequency. To complete the study, we will include in our future work voltage dynamics as well as the automatic voltage regulator associated. Such consideration of voltage dynamics have been done recently in [18, 64, 95, 96]. One could also study the interaction between the frequency and voltage controller in an electric model considering the voltage dynamics.

We also considered that the smart devices have the same power and have only two possible states (on and off). To extend this study we will consider diversity in power consumptions of devices and also include a standby state, where a device has a smaller power. Considering diversity in such system better reflects the reality, where some devices have priority over others. The prioritized devices can then have lower probability to turn off and higher probability for recovering pending tasks.

DDC has been applied here to a single generator grid and to a toy network. In our future work, we will apply the previous study to different networks and we will study the existence or not of Braess' paradox in a network with fluctuating demand and in which DDC is considered.

Regarding the fluctuations, we considered all along this thesis that it is included in the demand side. In addition to it, we will consider in our future work other sources of fluctuations. This can be done including different types of generators, namely turbines, wind farms and solar panels whose outputs are fluctuating. The modeling of such networks could be interesting despite of the complexity carried by the equations governing the dynamics of these generators. On the top of this network DDC could be included.

The OPA model used in this thesis, neglects the global increase of about 2% of the demand. It would be interesting to consider that parameter in the model, since it is a part not negligible of the slow dynamics. In addition, the shape of the control and recovery power thresholds can be taken similar to the demand instead to have them constant allowing faster recovery of pending tasks.

Bibliography

[1] Albadi, M. H. and El-Saadany, E. F. (2007). Demand response in electricity markets: An overview. In *Power Engineering Society General Meeting, 2007. IEEE*, pages 1–5. IEEE. [Cited on page 17]

[2] Albadi, M. H. and El-Saadany, E. F. (2008). A summary of demand response in electricity markets. *Electric power systems research*, 78(11):1989–1996. [Cited on page 17]

[3] Alsac, O. and Stott, B. (1974). Optimal load flow with steady-state security. *IEEE transactions on power apparatus and systems*, (3):745–751. [Cited on page 12]

[4] Anderson, P. M. and Fouad, A. A. (2008). *Power System Control and Stability*. John Wiley & Sons. [Cited on page 100]

[5] Anvari, M., Lohmann, G., Wächter, M., Milan, P., Lorenz, E., Heinemann, D., Tabar, M. R. R., and Peinke, J. (2016). Short term fluctuations of wind and solar power systems. *New Journal of Physics*, 18(6):063027. [Cited on page 35]

[6] Arghir, C., Jouini, T., and Dörfler, F. (2018). Grid-forming control for power converters based on matching of synchronous machines. *Automatica*, 95:273–282. [Cited on pages 9 and 13]

[7] Bak, P., Tang, C., and Wiesenfeld, K. (1987). Self-organized criticality: An explanation of the 1/f noise. *Physical review letters*, 59(4):381. [Cited on page 120]

[8] Beaudin, M. and Zareipour, H. (2017). Home energy management systems: A review of modelling and complexity. In *Energy Solutions to Combat Global Warming*, pages 753–793. Springer. [Cited on page 19]

[9] Bergen, A. (1986). Power systems analysis. [Cited on pages 12, 15, 25, 74, 79, 90, and 93]

[10] Berizzi, A. (2004). The italian 2003 blackout. In *Power engineering society general meeting, 2004. IEEE*, pages 1673–1679. IEEE. [Cited on page 92]

[11] Bevrani, H. and Raisch, J. (2017). On virtual inertia application in power grid frequency control. *Energy Procedia*, 141:681–688. [Cited on pages 9 and 13]

[12] Bhatt, U., Newman, D. E., Carreras, B. A., and Dobson, I. (2005). Understanding the effect of risk aversion on risk. In *System Sciences, 2005. HICSS'05. Proceedings of the 38th Annual Hawaii International Conference on*, pages 64b–64b. IEEE. [Cited on pages 20 and 54]

[13] Bhowmik, S., Tomsovic, K., and Bose, A. (2004). Communication models for third party load frequency control. *IEEE Transactions on Power Systems*, 19(1):543–548. [Cited on page 15]

[14] Braess, D. (1968). Über ein paradoxon aus der verkehrsplanung. *Mathematical Methods of Operations Research*, 12(1):258–268. [Cited on page 107]

[15] Brummitt, C. D., Hines, P. D. H., Dobson, I., Moore, C., and D'Souza, R. M. (2013). Transdisciplinary electric power grid science. *Proceedings of the National Academy of Sciences*, 110(30):12159. [Cited on page 20]

[16] Buesseler, K., Aoyama, M., and Fukasawa, M. (2011). Impacts of the fukushima nuclear power plants on marine radioactivity. *Environmental science & technology*, 45(23):9931–9935. [Cited on page 2]

[17] Buldyrev, S. V., Parshani, R., Paul, G., Stanley, H. E., and Havlin, S. (2010). Catastrophic cascade of failures in interdependent networks. *Nature*, 464(7291):1025–1028. [Cited on page 74]

[18] Calabria, M., Schumacher, W., Guerrero, J. M., Vasquez, J. C., and Zhao, X. (2015). Stability analysis and design of the improved droop controller on a voltage source inverter. In *2015 IEEE 6th International Symposium on PEDG*, pages 1–9. IEEE. [Cited on page 141]

[19] Carpentier, J. (1962). Contribution a l'etude du dispatching economique. *Bulletin de la Societe Francaise des Electriciens*, 3(1):431–447. [Cited on page 12]

[20] Carreras, B. A., Lynch, V. E., Sachtjen, M., Dobson, I., and Newman, D. E. (2001). Modeling blackout dynamics in power transmission networks with simple structure. In *System Sciences, 2001. Proceedings of the 34th Annual Hawaii*

International Conference on, pages 719–727. IEEE. [Cited on pages 120, 123, 124, 125, 126, and 129]

[21] Chen, J., Thorp, J. S., and Dobson, I. (2005). Cascading dynamics and mitigation assessment in power system disturbances via a hidden failure model. *International Journal of Electrical Power & Energy Systems*, 27(4):318–326. [Cited on page 120]

[22] Clark, A., Alomair, B., Bushnell, L., and Poovendran, R. (2016). *Submodularity in dynamics and control of networked systems*. Springer. [Cited on page 90]

[23] Cornelius, S. P., Kath, W. L., and Motter, A. E. (2013). Realistic control of network dynamics. *Nature communications*, 4:1942. [Cited on pages 74 and 75]

[24] Corwin, J. L. and Miles, W. T. (1978). Impact assessment of the 1977 new york city blackout. final report. Technical report, System Control, Inc., Arlington, VA (USA). [Cited on page 1]

[25] Cuffe, P. (2017). A comparison of malicious interdiction strategies against electrical networks. *IEEE Journal on Emerging and Selected Topics in Circuits and Systems*, 7(2):205–217. [Cited on page 54]

[26] Dahms, T., Hövel, P., and Schöll, E. (2007). Control of unstable steady states by extended time-delayed feedback. *Physical Review E*, 76(5):056201. [Cited on page 74]

[27] Davito, B., Tai, H., and Uhlaner, R. (2010). The smart grid and the promise of demand-side management. *McKinsey on Smart Grid*, 3:8–44. [Cited on pages 3 and 18]

[28] Dehghanpour, K. and Afsharnia, S. (2015). Electrical demand side contribution to frequency control in power systems: a review on technical aspects. *Renewable and Sustainable Energy Reviews*, 41:1267–1276. [Cited on page 17]

[29] Dobson, I. (2015). Cascading network failure in power grid blackouts. *Encyclopedia of Systems and Control*, pages 105–108. [Cited on pages 20 and 92]

[30] Dobson, I., Carreras, B., Lynch, V., and Newman, D. (2001). An initial model for complex dynamics in electric power system blackouts. In *hicss*, page 2017. IEEE. [Cited on pages 20, 120, 121, 123, 125, 129, and 134]

[31] Dobson, I., Carreras, B. A., Lynch, V. E., and Newman, D. E. (2007). Complex systems analysis of series of blackouts: Cascading failure, critical points, and self-organization. *Chaos: An Interdisciplinary Journal of Nonlinear Science*, 17(2):026103. [Cited on pages 119, 120, 123, and 125]

[32] Dongmo, E. D., Colet, P., and Woafo, P. (2017). Power grid enhanced resilience using proportional and derivative control with delayed feedback. *The European Physical Journal B*, 90(1):6. [Cited on pages 101 and 117]

[33] Dörfler, F. and Bullo, F. (2014). Synchronization in complex networks of phase oscillators: A survey. *Automatica*, 50(6):1539–1564. [Cited on page 75]

[34] Dörfler, F., Chertkov, M., and Bullo, F. (2013). Synchronization in Complex Oscillator Networks and Smart Grids. *Proceedings of the National Academy of Sciences*, 110(6):2005–2010. [Cited on pages 75, 90, and 101]

[35] Dörfler, F., Simpson-Porco, J. W., and Bullo, F. (2016). Breaking the hierarchy: Distributed control and economic optimality in microgrids. *IEEE Transactions on Control of Network Systems*, 3(3):241–253. [Cited on page 74]

[36] D'Arco, S., Suul, J. A., and Fosso, O. B. (2015). Small-signal modeling and parametric sensitivity of a virtual synchronous machine in islanded operation. *International Journal of Electrical Power & Energy Systems*, 72:3–15. [Cited on page 13]

[37] Egea-Alvarez, A., Beerten, J., Van Hertem, D., and Gomis-Bellmunt, O. (2015). Hierarchical power control of multiterminal hvdc grids. *Electric Power Systems Research*, 121:207–215. [Cited on page 14]

[38] Fang, X., Misra, S., Xue, G., and Yang, D. (2012). Smart Grids - The new and improved Power Grid: A Survey. *Communications Surveys & Tutorials, IEEE*, 14(4):944–980. [Cited on page 118]

[39] Faruqui, A. (2007). Pricing programs: time-of-use and real time. *Encyclopedia of Energy Engineering*. [Cited on page 18]

[40] Filatrella, G., Nielsen, A. H., and Pedersen, N. F. (2008a). Analysis of a power grid using a kuramoto-like model. *The European Physical Journal B-Condensed Matter and Complex Systems*, 61(4):485–491. [Cited on page 77]

[41] Filatrella, G., Nielsen, A. H., and Pedersen, N. F. (2008b). Analysis of a Power Grid using a Kuramoto-like Model. *The European Physical Journal B*, 61(4):485–491. [Cited on page 100]

[42] Geidl, M. and Andersson, G. (2007). Optimal power flow of multiple energy carriers. *IEEE Transactions on Power Systems*, 22(1):145–155. [Cited on page 12]

[43] Gellings, C. W. and Chamberlin, J. (1988). Demand-side management. [Cited on page 17]

[44] Grzybowski, J., Macau, E., and Yoneyama, T. (2016). On synchronization in power-grids modelled as networks of second-order kuramoto oscillators. *Chaos: An Interdisciplinary Journal of Nonlinear Science*, 26(11):113113. [Cited on pages 74, 77, and 100]

[45] Hammid, A. T., Hojabri, M., Sulaiman, M. H., Abdalla, A. N., and Kadhim, A. A. (2016). Load frequency control for hydropower plants using pid controller. *Journal of Telecommunication, Electronic and Computer Engineering (JTEC)*, 8(10):47–51. [Cited on page 101]

[46] Hamon, C. (2012). *On frequency control schemes in power systems with large amounts of wind power*. PhD thesis, KTH Royal Institute of Technology. [Cited on page 26]

[47] Hines, P., Blumsack, S., Sanchez, E. C., and Barrows, C. (2010). The topological and electrical structure of power grids. In *System Sciences (HICSS), 2010 43rd Hawaii International Conference on*, pages 1–10. IEEE. [Cited on page 92]

[48] Huneault, M. and Galiana, F. (1991). A survey of the optimal power flow literature. *IEEE transactions on Power Systems*, 6(2):762–770. [Cited on page 12]

[49] Imperato, P. J. (2016). Public health concerns associated with the new york city blackout of 1977. *Journal of community health*, 41(4):707–716. [Cited on page 1]

[50] Jan, M., Janusz, W., and James, R. (2008). Power system dynamics: Stability and control. *John Wily and Sons*. [Cited on page 25]

[51] Johnson, C. W. (2007). Analysing the causes of the italian and swiss blackout, 28 th september 2003. In *Proceedings of the twelfth Australian workshop on Safety critical systems and software and safety-related programmable systems-Volume 86*, pages 21–30. Australian Computer Society, Inc. [Cited on page 92]

[52] Kassakian, J., Schmalensee, R., Desgroseilliers, G., Heidel, T., Afridi, K., Farid, A., Grochow, J., Hogan, W., Jacoby, H., Kirtley, J., et al. (2011). Mi of technology, the future of the electric grid: An interdisciplinary mit study. [Cited on page 13]

[53] Kii, M., Sakamoto, K., Hangai, Y., and Doi, K. (2014). The effects of critical peak pricing for electricity demand management on home-based trip generation. *IATSS research*, 37(2):89–97. [Cited on page 18]

[54] Klinshov, V. V., Nekorkin, V. I., and Kurths, J. (2015). Stability threshold approach for complex dynamical systems. *New Journal of Physics*, 18(1):013004. [Cited on page 74]

[55] Knödel, W. (2013). *Graphentheoretische methoden und ihre anwendungen*, volume 13. Springer-Verlag. [Cited on page 107]

[56] Kolata, G. (1990). What if they closed 42d street and nobody noticed? The New York Times, URL: http://www.nytimes.com/1990/12/25/health/what-if-they-closed-42d-street-and-nobody-noticed.html. [Cited on page 107]

[57] Krause, S. M., Börries, S., and Bornholdt, S. (2015). Econophysics of adaptive power markets: When a market does not dampen fluctuations but amplifies them. *Physical Review E*, 92(1):012815. [Cited on page 50]

[58] Kundur, P., Balu, N. J., and Lauby, M. G. (1994). *Power system stability and control*, volume 7. McGraw-hill New York. [Cited on pages 25 and 117]

[59] Labavić, D., Suciu, R., Meyer-Ortmanns, H., and Kettemann, S. (2014). Long-range response to transmission line disturbances in dc electricity grids. *The European Physical Journal Special Topics*, 223(12):2517–2525. [Cited on page 107]

[60] Li, X., Hui, D., and Lai, X. (2013). Battery energy storage station (bess)-based smoothing control of photovoltaic (pv) and wind power generation fluctuations. *IEEE Transactions on Sustainable Energy*, 4(2):464–473. [Cited on page 35]

[61] Li-Xin, Y. and Xiao-Jun, L. (2012). The synchronization of complex networks via impulsive control. In *Computer Science & Service System (CSSS), 2012 International Conference on*, pages 1969–1971. IEEE. [Cited on page 75]

[62] Luo, F., Ranzi, G., Dong, Z., and Murata, J. (2017). Natural aggregation approach based home energy manage system with user satisfaction modelling. In *IOP Conference Series: Earth and Environmental Science*, volume 73, page 012005. [Cited on page 19]

[63] Luo, F., Zhao, J., Dong, Z. Y., Tong, X., Chen, Y., Yang, H., and Zhang, H. (2016). Optimal dispatch of air conditioner loads in southern china region by direct load control. *IEEE Transactions on Smart Grid*, 7(1):439–450. [Cited on page 19]

[64] Ma, J., Sun, Y., Yuan, X., Kurths, J., and Zhan, M. (2016). Dynamics and collapse in a power system model with voltage variation: The damping effect. *PloS one*, 11(11):e0165943. [Cited on pages 87, 88, and 141]

[65] Maas, G., Bial, M., and Fijalkowski, J. (2007). Final report-system disturbance on 4 november 2006. *Union for the Coordination of Transmission of Electricity in Europe, Tech. Rep.* [Cited on page 1]

[66] Machowski, J., Bialek, J., and Bumby, J. (2011). *Power System Dynamics: Stability and Control*. John Wiley & Sons. [Cited on pages 114 and 117]

[67] Manik, D., Rohden, M., Ronellenfitsch, H., Zhang, X., Hallerberg, S., Witthaut, D., and Timme, M. (2016). Network susceptibilities: theory and applications. *arXiv preprint arXiv:1609.04310*. [Cited on page 74]

[68] Manik, D., Witthaut, D., Schäfer, B., Matthiae, M., Sorge, A., Rohden, M., Katifori, E., and Timme, M. (2014a). Supply Networks: Instabilities without Overload. *The European Physical Journal Special Topics*, 223(12):2527–2547. [Cited on pages 74, 99, 102, 104, 105, 107, and 117]

[69] Manik, D., Witthaut, D., Schäfer, B., Matthiae, M., Sorge, A., Rohden, M., Katifori, E., and Timme, M. (2014b). Supply networks: Instabilities without overload. *The European Physical Journal Special Topics*, 223(12):2527–2547. [Cited on pages 77 and 79]

[70] Matthewman, S. and Byrd, H. (2014). Blackouts: a sociology of electrical power failure. [Cited on page 1]

[71] Mei, S., Xue, A., and Zhang, X. (2008). On power system blackout modeling and analysis based on self-organized criticality. *Science in China Series E: Technological Sciences*, 51(2):209–219. [Cited on page 120]

[72] Menck, P. J., Heitzig, J., Kurths, J., and Schellnhuber, H. J. (2014). How Dead Ends undermine Power Grid Stability. *Nature Communications*, 5(3969). [Cited on pages 74 and 79]

[73] Menck, P. J., Heitzig, J., Marwan, N., and Kurths, J. (2013). How Basin Stability Complements the Linear-stability Paradigm. *Nature Physics*, 9(2):89–92. [Cited on page 87]

[74] Milano, F., Dörfler, F., Hug, G., Hill, D. J., and Verbič, G. (2018). Foundations and challenges of low-inertia systems. In *2018 Power Systems Computation Conference (PSCC)*, pages 1–25. IEEE. [Cited on page 9]

[75] Modi, N., Yan, R., et al. (2016). Low inertia power systems: Frequency response challenges and a possible solution. In *Power Engineering Conference (AUPEC), 2016 Australasian Universities*, pages 1–6. IEEE. [Cited on page 13]

[76] Moghadam, M. R. V., Ma, R. T., and Zhang, R. (2013). Distributed frequency control via demand response in smart grids. In *Acoustics, Speech and Signal Processing (ICASSP), 2013 IEEE International Conference on*, pages 5233–5237. IEEE. [Cited on page 19]

[77] Moghadam, M. R. V., Ma, R. T., and Zhang, R. (2014). Distributed frequency control in smart grids via randomized demand response. *IEEE Transactions on Smart Grid*, 5(6):2798–2809. [Cited on page 28]

[78] Mohsenian-Rad, A.-H., Wong, V. W., Jatskevich, J., Schober, R., and Leon-Garcia, A. (2010). Autonomous demand-side management based on game-theoretic energy consumption scheduling for the future smart grid. *IEEE transactions on Smart Grid*, 1(3):320–331. [Cited on pages 19 and 50]

[79] Motter, A. E. and Lai, Y.-C. (2002). Cascade-based attacks on complex networks. *Physical Review E*, 66(6):065102. [Cited on pages 74, 75, and 107]

[80] Motter, A. E., Myers, S. A., Anghel, M., and Nishikawa, T. (2013). Spontaneous Synchrony in Power-grid Networks. *Nature Physics*, 9(3):191–197. [Cited on pages 74, 75, 104, and 117]

[81] Nagata, M., Fujiwara, N., Tanaka, G., Suzuki, H., Kohda, E., and Aihara, K. (2014). Node-wise robustness against fluctuations of power consumption in power grids. *The European Physical Journal Special Topics*, 223(12):2549–2559. [Cited on page 35]

[82] Nishikawa, T. and Motter, A. E. (2015). Comparative analysis of existing models for power-grid synchronization. *New Journal of Physics*, 17(1):015012. [Cited on page 23]

[83] Noman, N. and Iba, H. (2008). Differential evolution for economic load dispatch problems. *Electric Power Systems Research*, 78(8):1322–1331. [Cited on page 12]

[84] on Climate Change, I. P. (2015). *Climate change 2014: mitigation of climate change*, volume 3. Cambridge University Press. [Cited on page 2]

[85] Pecora, L. M. and Carroll, T. L. (1998). Master stability functions for synchronized coupled systems. *Phys. Rev. Lett.*, 80(10):2109–2112. [Cited on page 102]

[86] Pedrasa, M. A. A., Spooner, T. D., and MacGill, I. F. (2010). Coordinated scheduling of residential distributed energy resources to optimize smart home energy services. *IEEE Transactions on Smart Grid*, 1(2):134–143. [Cited on page 19]

[87] Poolla, B. K., Groß, D., and Dörfler, F. (2018). Placement and implementation of grid-forming and grid-following virtual inertia. *arXiv preprint arXiv:1807.01942*. [Cited on pages 9 and 13]

[88] Pourbeik, P., Kundur, P. S., and Taylor, C. W. (2006). The anatomy of a power grid blackout-root causes and dynamics of recent major blackouts. *IEEE Power and Energy Magazine*, 4(5):22–29. [Cited on page 120]

[89] Rahimi, F. and Ipakchi, A. (2010). Demand response as a market resource under the smart grid paradigm. *IEEE Transactions on Smart Grid*, 1(1):82–88. [Cited on page 17]

[90] Saadat, H. (2002). Power systems analysis, ser. [Cited on pages 4, 15, 24, 25, 26, 27, 50, and 76]

[91] Saebi, J., Taheri, H., Mohammadi, J., and Nayer, S. S. (2010). Demand bidding/buyback modeling and its impact on market clearing price. In *Energy Conference and Exhibition (EnergyCon), 2010 IEEE International*, pages 791–796. IEEE. [Cited on page 18]

[92] Schäfer, B., Beck, C., Aihara, K., Witthaut, D., , and Timme, M. (2017). Heavy tails, superstatistics and scaling of power grid frequency fluctuations. *ArXiv: XYZ, submitted to Nature Energy*. [Cited on page 35]

[93] Schäfer, B., Grabow, C., Auer, S., Kurths, J., Witthaut, D., and Timme, M. (2016). Taming instabilities in power grid networks by decentralized control. *The European Physical Journal Special Topics*, 225(3):569–582. [Cited on page 118]

[94] Schäfer, B., Matthiae, M., Timme, M., and Witthaut, D. (2015). Decentral Smart Grid Control. *New Journal of Physics*, 17(1):015002. [Cited on pages 17, 118, and 126]

[95] Schmietendorf, K., Peinke, J., Friedrich, R., and Kamps, O. (2014). Self-organized synchronization and voltage stability in networks of synchronous machines. *Euroean Physical Journal Special Topics*, 223(12):2577–2592. [Cited on page 141]

[96] Schmietendorf, K., Peinke, J., and Kamps, O. (2016). On the stability and quality of power grids subjected to intermittent feed-in. *arXiv preprint arXiv:1611.08235*. [Cited on page 141]

[97] Schröder, M., Chakraborty, S., Witthaut, D., Nagler, J., and Timme, M. (2016). Interaction control to synchronize non-synchronizable networks. *Scientific reports*, 6:37142. [Cited on page 74]

[98] Schultz, P., Heitzig, J., and Kurths, J. (2014). Detours around basin stability in power networks. *New Journal of Physics*, 16(12):125001. [Cited on pages 87 and 88]

[99] Schultz, P., Heitzig, J., and Kurths, J. (2016). A random growth model for power grids and other spatially embedded infrastructure networks. *arXiv preprint arXiv:1602.02562*. [Cited on page 88]

[100] Short, J. A., Infield, D. G., and Freris, L. L. (2007). Stabilization of Grid Frequency through Dynamic Demand Control. *IEEE Transactions on Power Systems*, 22(3):1284–1293. [Cited on pages 19, 23, 50, and 74]

[101] Short, M. and Dawood, M. (2014). Networking infrastructures for micro grids part i: Discussion and proposal. In *Proceedings of the International Conference on Green Technology and Sustainable Development*. [Cited on page 15]

[102] Shu, H., Yang, W., Chai, C. C., and Yu, R. (2014). Demand response based on voluntary time-dependent pricing scheme. *APSIPA Transactions on Signal and Information Processing*, 3. [Cited on page 17]

[103] Siano, P. (2014). Demand response and smart grids—a survey. *Renewable and Sustainable Energy Reviews*, 30:461–478. [Cited on page 17]

[104] Simpson-Porco, J. W., Dörfler, F., and Bullo, F. (2012). Droop-controlled inverters are kuramoto oscillators. *IFAC Proceedings Volumes*, 45(26):264–269. [Cited on page 101]

[105] Skardal, P. S. and Arenas, A. (2015). Control of coupled oscillator networks with application to microgrid technologies. *Science advances*, 1(7):e1500339. [Cited on page 75]

[106] Song, J., Cotilla-Sanchez, E., Ghanavati, G., and Hines, P. D. (2016). Dynamic modeling of cascading failure in power systems. *IEEE Transactions on Power Systems*, 31(3):2085–2095. [Cited on page 120]

[107] Tchuisseu, E. B. T., Gomila, D., and Colet, P. (2018a). Reduction of power grid fluctuations by communication between smart devices. *arXiv preprint arXiv:1805.07432*. [Cited on pages 20, 60, 71, and 89]

[108] Tchuisseu, E. B. T., Gomila, D., Colet, P., Witthaut, D., Timme, M., and Schäfer, B. (2018b). Curing braess' paradox by secondary control in power grids. *New Journal of Physics*, 20(8):083005. [Cited on pages 20, 99, and 116]

[109] Tchuisseu, E. T., Gomila, D., Brunner, D., and Colet, P. (2017). Effects of dynamic-demand-control appliances on the power grid frequency. *Physical Review E*, 96(2):022302. [Cited on pages 18, 19, 20, 39, 47, 49, 69, 70, 89, and 91]

[110] Teukolsky, S. A., Flannery, B. P., Press, W., and Vetterling, W. (1992). Numerical recipes in c. *SMR*, 693:1. [Cited on page 125]

[111] Toral, R. and Colet, P. (2014). *Stochastic numerical methods: an introduction for students and scientists*. John Wiley & Sons. [Cited on pages 34, 37, 40, and 42]

[112] Torres, M. and Lopes, L. A. (2013). A virtual synchronous machine to support dynamic frequency control in a mini-grid that operates in frequency droop mode. *Energy and Power Engineering*, 5(03):259. [Cited on pages 9 and 14]

[113] Turker, H., Bacha, S., Chatroux, D., and Hably, A. (2012). Modelling of system components for vehicle-to-grid (v2g) and vehicle-to-home (v2h) applications with plug-in hybrid electric vehicles (phevs). In *Innovative Smart Grid Technologies (ISGT), 2012 IEEE PES*, pages 1–8. IEEE. [Cited on page 9]

[114] Ullah, M., Javaid, N., Khan, I., Mahmood, A., and Farooq, M. (2013). Residential energy consumption controlling techniques to enable autonomous demand side management in future smart grid communications. In *Broadband and Wireless Computing, Communication and Applications (BWCCA), 2013 Eighth International Conference on*, pages 545–550. IEEE. [Cited on page 17]

[115] U.S. Department of Energy (2016). Eia-411: Coordinated bulk power supply and demand program report. [Cited on page 2]

[116] Van der Vleuten, E. and Lagendijk, V. (2010). Transnational infrastructure vulnerability: The historical shaping of the 2006 european "blackout". *Energy Policy*, 38(4):2042–2052. [Cited on page 1]

[117] Wang, B., Suzuki, H., and Aihara, K. (2016a). Enhancing synchronization stability in a multi-area power grid. *Scientific reports*, 6:26596. [Cited on pages 75 and 104]

[118] Wang, C., Grebogi, C., and Baptista, M. S. (2016b). Control and prediction for blackouts caused by frequency collapse in smart grids. *Chaos: An Interdisciplinary Journal of Nonlinear Science*, 26(9):093119. [Cited on page 101]

[119] Wang, H., Meng, K., Dong, Z. Y., Xu, Z., Luo, F., and Wong, K. P. (2015). Efficient real-time residential energy management through milp based rolling horizon optimization. In *Power & Energy Society General Meeting, 2015 IEEE*, pages 1–6. IEEE. [Cited on page 19]

[120] Weitenberg, E., Jiang, Y., Zhao, C., Mallada, E., De Persis, C., and Dörfler, F. (2017). Robust decentralized secondary frequency control in power systems: Merits and trade-offs. *arXiv preprint arXiv:1711.07332*. [Cited on page 101]

[121] Witthaut, D. and Timme, M. (2012). Braess's Paradox in Oscillator Networks, Desynchronization and Power Outage. *New Journal of Physics*, 14(8):083036. [Cited on pages 99, 107, 108, 109, 111, 112, and 117]

[122] Witthaut, D. and Timme, M. (2013). Nonlocal failures in complex supply networks by single link additions. *The European Physical Journal B*, 86(9):1–12. [Cited on pages 99, 107, 108, and 117]

[123] Wood, A. J., Wollenberg, B. F., and Sheblé, G. B. (2013). *Power Generation, Operation and Control*. John Wiley & Sons, New York. [Cited on page 117]

[124] Xie, L. (2011). A criterion for hurwitz polynomials and its applications. *International Journal of Modern Education and Computer Science*, 3(1):38. [Cited on pages 32 and 107]